EXPERIMENTAL DETERMINATION OF HEAT AND MASS TRANSFER IN DESICCANT MATRICES

by

TODD BRYANT JEKEL

A dissertation submitted in partial fulfillment

of the requirements for the degree of

Doctor of Philosophy

(Mechanical Engineering)

at the

UNIVERSITY OF WISCONSIN—MADISON

1997

EXPERIMENTAL DETERMINATION OF HEAT AND MASS TRANSFER IN DESICCANT MATRICES

Todd Bryant Jekel

Under the supervision of Professor J.W. Mitchell

At the University of Wisconsin—Madison

A single-blow experiment was designed and implemented that measured the heat and mass transfer in a commercially available aluminum matrix of triangular passages with a polymer desiccant coating. The experimental procedure used a step in inlet humidity ratio and measured the outlet temperature and humidity response as a function of time.

The experimental conditions were numerically simulated with a finite-difference method. The numerical results were significantly different than the experimental data. For the step increase in humidity, using the fully-developed value of heat transfer coefficient for laminar flow in triangular passages with adiabatic boundary condition and an overall Lewis number of unity, the simulated temperature rise is nearly 2.5 times larger than the experiment. The experiment exhibited a small mass transfer rate early in the adsorption process, resulting in a small temperature rise in the outlet temperature. Similar analysis on the step decrease in humidity showed that the first wave was in good agreement and temperature drop was only approximately 10% larger, but the second wave was sharper than the experimental results.

Increasing the mass transfer resistance did not explain the discrepancies between simulation and experiment. A decreased mass transfer coefficient represented the low mass transfer rate early in the adsorption experiment, but failed to represent the mass transfer rate early in the desorption experiment.

The simulation of experimental conditions for adsorption proved to be very sensi-

tive to isotherm shape at low relative humidities. Since no isotherm data was available between 0% and 33% for the polymer desiccant, the isotherm was not well defined in the that region. A reduction in water capacity in the low relative humidity region of the isotherm lowered the maximum temperature rise during the adsorption experiment. The simulation of the desorption experiment was very sensitive to the high relative humidity region of the isotherm. It was concluded that the sensitivity to the isotherm was the major contribution to the lack of agreement between the experiment and the simulation.

Approved:

John W. Mitchell 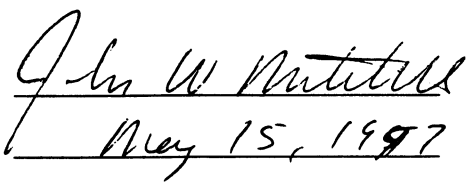

Date May 15, 1997

Acknowledgements

From this day forward, when I read a paper in any engineering journal describing an experiment, I will read it with immense respect. Experimentation is the most exhilirating and frustrating thing I have ever done. Nothing compares to the reality of an experiment when things go well! And nothing compares to the reality of an experiment when things don't go well. I wish I had a dollar for every time I was *sure* that this was the reason for the difference between reality and virtual reality (simulation).

First and foremost, I would like to thank my wife, Lisa. She supported me through my schooling both emotionally and financially. I will be forever in debt for the opportunity you gave me to get this degree. Thanks to my children, Sam and Johanna. Watching you grow up has been a source of joy. Thanks also to my parents, for their support, patience and understanding. Thanks to my parents-in-law, Jack and Shirley, for the countless cookouts and babysitting.

Thanks to Professors John Mitchell, Sandy Klein, and Bill Beckman for their years of advising and questions. Without their help, this would have been impossible. The support and encouragement were much appreciated.

Thanks also to Shirley for all the help with paperwork, forms, room reservations, etc. Thanks to Jeff Thornton (former) and Nate Blair (current TRNSYS engineer) for assistance with computers, etc.

Through the years, I have met a lot of great people at the Solar Energy Lab,

people that will be lifelong friends (assuming that my picking on them hasn't totally alienated them). Thanks to all the students (too many to list) that have helped me in the completion of this degree. The comraderie and support between students at the Lab was one of the reasons I chose Wisconsin, and throughout the many years and students it has remained a constant.

Thanks also to John Robinson for the use of experimental equipment and the staff in the Mechanical Engineering shop for helping me create the experimental test section.

Thanks also to Joe Lacey, an experimental wealth of knowledge, and the ME 370 TAs during my TAing stint.

Contents

List of Tables

List of Figures

Chapter 1

Introduction

Solid desiccants dehumidify moist air by adsorbing water on the surface [Ruthven, 1984]. This process is called physical adsorption. The adsorbed water molecules accumulate on the surface of the desiccant and form a layer that has properties similar to liquid water. Adsorption, unlike condensation, occurs at temperatures above the dew point. As water vapor is adsorbed, thermal energy is liberated. This thermal energy, called the heat of adsorption, is on the same order of magnitude as the heat of condensation.

In the 1950's, Pennington [1955] proposed the use of cooling cycles that were driven by adsorption and low-grade thermal energy. Since then, many desiccant air-conditioning systems have been studied and the similar conclusions have been reached: the required equipment is large and the first cost is too high to compete with a conventional vapor compression system. The desiccant dehumidifier must be large to meet the dehumidification load because the coefficients for heat and mass transfer are small.

Desiccant dehumidification is an attractive concept because it does not use an ozone depleting, global warming refrigerant and it can reduce the on-peak electricity demand [Pesaran et al., 1993]. The on-peak electricity is reduced because the com-

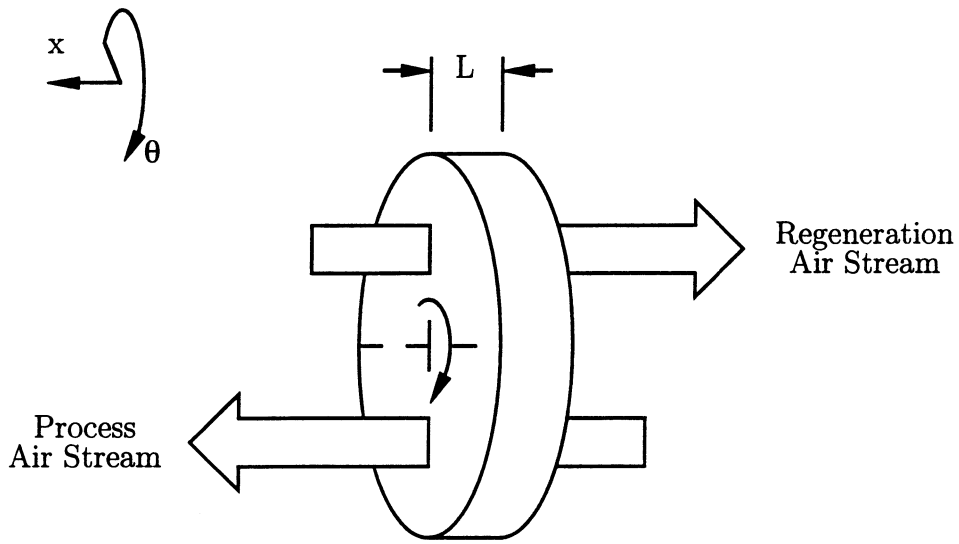

Figure 1.1: Schematic of a rotary desiccant dehumidifier or enthalpy exchanger.

pressor of a conventional vapor compression refrigeration cycle requires much more power than the fan power required to pass air through the desiccant dehumidifier.

Figure 1.1 shows a schematic of a rotary desiccant dehumidifier or enthalpy exchanger. The matrix is being both continuously processed (dehumidifying) and regenerated. The purpose of a desiccant dehumidifier is a primary component in a system designed to condition a space. An enthalpy exchanger is a device used with conventional systems to recover energy (both sensible and latent) from the exhaust air stream. The rotation speed of an enthalpy exchanger is much faster than a desiccant dehumidifier.

The regeneration heat that the desiccant dehumidifier requires in order to continuously dehumidify the process air can be delivered by a solar collector array, process waste heat, or a gas furnace. The regeneration heat is usually supplied at 60-100°C; however, higher regeneration temperatures can dramatically increase the performance and decrease the size of the dehumidifier.

1.1 Desiccant Air-Conditioning Systems

Desiccant air-conditioning systems require heat to regenerate the desiccant and cooling and humidification to prepare the desiccant outlet air flow for delivery to the space. The art of desiccant air-conditioning is in the arrangement of these competing needs. This section provides an introduction to desiccant air-conditioning systems and the technologies available to improve system performance.

1.1.1 Basic Desiccant Systems

The most basic desiccant air-conditioning system is the Pennington [1955] or ventilation cycle as shown in Figure 1.2. The exhaust air from the space is used to cool the supply stream and regenerate the desiccant. The supply air is taken directly from the ambient. The supply air stream is dehumidified by the desiccant, cooled by sensible heat exchange with the exhaust air stream, and evaporatively cooled to the supply state. The performance of the ventilation cycle has been researched extensively [Jurinak, 1984; Kang, 1989] The indicators for system performance are the Coefficient of Performance (COP) and the cooling capacity. The COP is defined as the amount of cooling capacity that the air-conditioning system delivers to the space divided by the amount of heat that must be added to regenerate the desiccant dehumidifier. The COPs that investigators have found range from 0.5 to 1.4 [Pesaran et. al., 1993]. The COPs vary over a wide range because performance is a strong function of the sensible heat exchanger effectiveness. Kang [1989] determined that the COP for a balanced flow system with infinite transfer coefficients was 1.62 at ARI conditions (Room: 26.7°C dry bulb, 19.4°C wet bulb; Ambient: 35°C dry bulb, 23.9°C wet bulb). For non-infinite transfer coefficients the COP was reduced to 1.04 with a cooling effect of 15.54 kJ/kg and a regeneration temperature of 70.64°C. The non-idealities in this analysis were an effectiveness of the heat exchanger of 0.95, an efficiency of the evap-

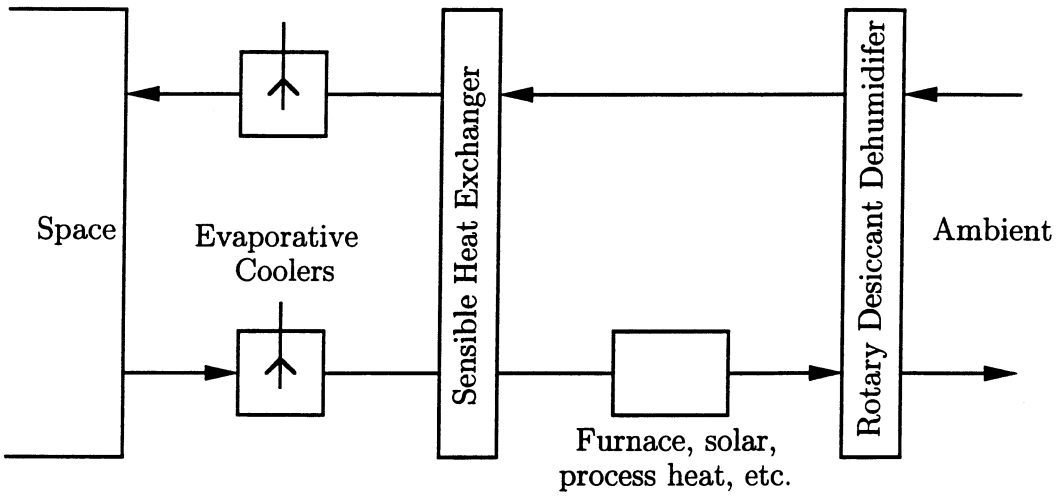

Figure 1.2: Ventilation cycle schematic.

orative coolers based on the adiabatic saturation temperature of 0.95 and a Number of Transfer Units (Ntu) for the desiccant dehumidifier of approximately 20.

The recirculation cycle differs from the ventilation cycle in that the supply air is entirely or partly taken from the return air from the space. The regeneration stream has the same mass flow rate as the process stream and is taken directly from the ambient. The recirculation cycle with no fresh air flow rate is shown in Figure 1.3. The performance of the recirculation cycle is similar to the ventilation cycle. The COPs range from 0.5 to 0.78 [Jurinak, 1984]. Using Kang's analysis [1989] and the same values to model the non-idealities as the ventilation cycle, the COP of the recirculation cycle with no fresh air flow rate was 0.70 with a cooling effect of 16.63 kJ/kg and a regeneration temperature of 70°C. Therefore, for the same regeneration temperature the recirculation cycle had a greater cooling effect but a lower COP.

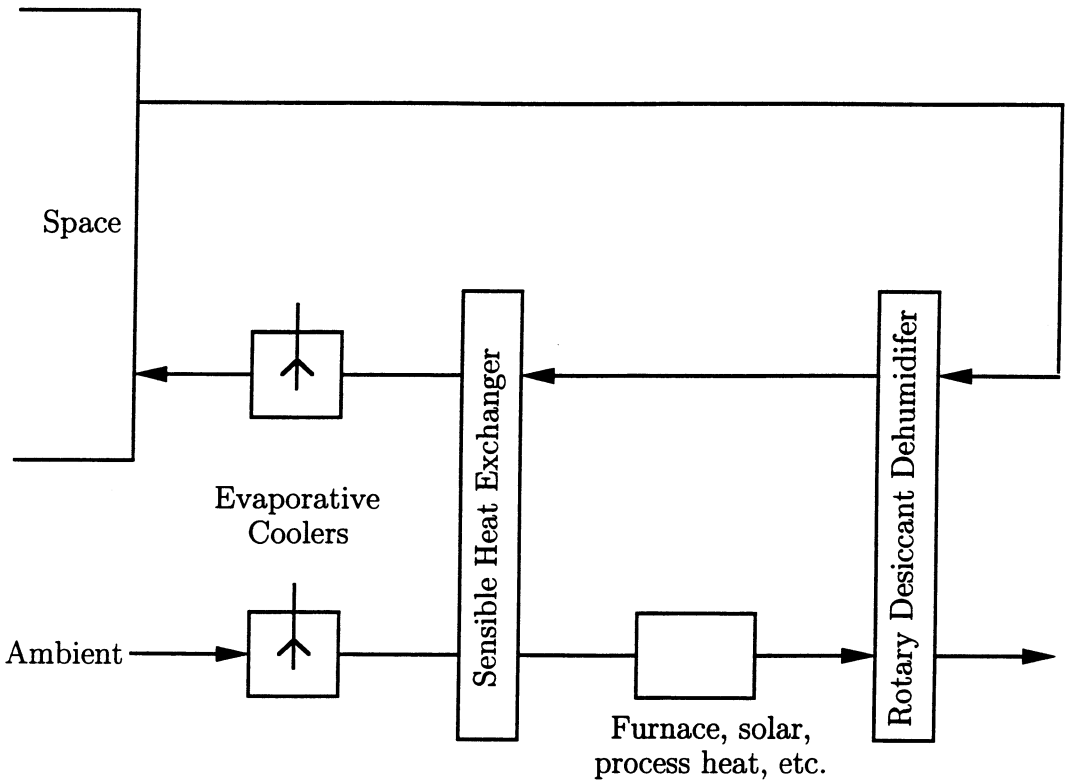

Figure 1.3: Recirculation cycle schematic.

1.1.2 Advanced Desiccant Systems

In an effort to increase the performance of the basic systems, systems that utilize improved components have been developed. Maclaine-cross [1985] and Kang [1989] proposed and analyzed systems that incorporate a finned coil and cooling tower instead of the direct evaporative coolers that have COPs greater than 2. Waugamann [1993] proposed and analyzed a system that utilizes one direct evaporative cooler and one indirect evaporative cooler that has a COP of 1.6.

The SENS cycle was developed by Maclaine-cross [1985] and is shown in Figure 1.4. The COP of this cycle is much higher than the ventilation and recirculation cycles. The SENS cycle uses two heat exchangers and a finned coil and cooling tower.

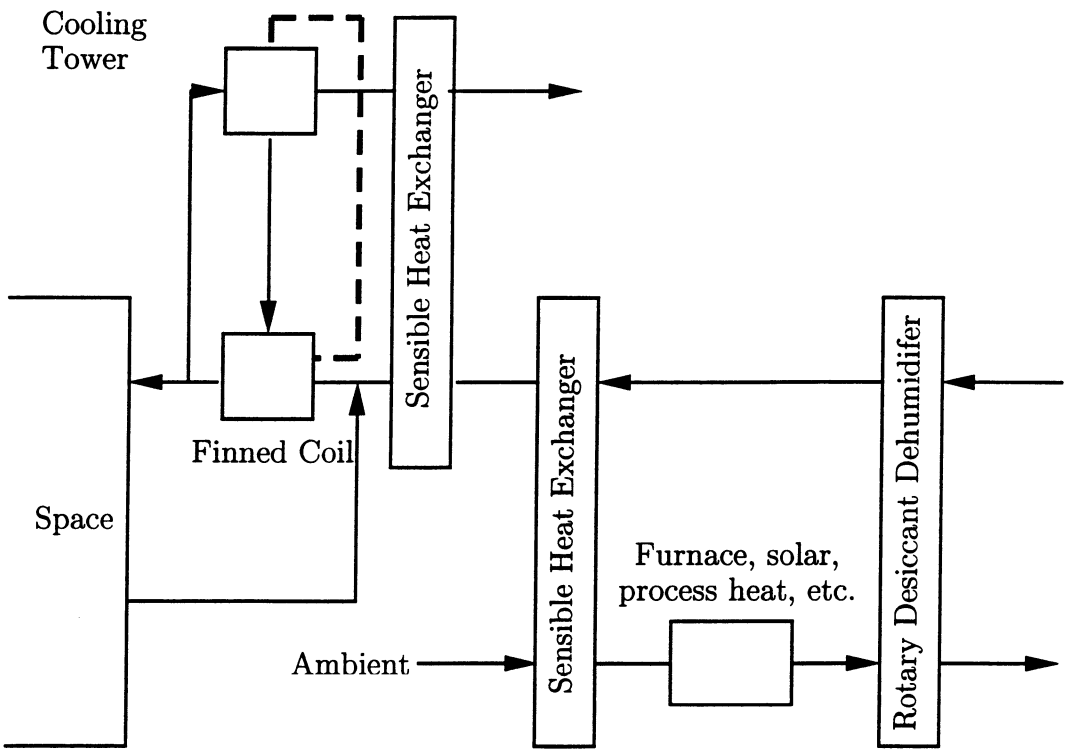

Figure 1.4: The SENS cycle schematic.

Maclaine-cross reports an ideal (infinite transfer coefficients, no latent load) COP of 5.8 at ARI conditions. Kang [1989] reports a COP of 2.58, a cooling effect of 29.02 kJ/kg, and a regeneration temperature of 67°C with non-ideal components and a 20% latent load at ARI conditions. The non-idealities are Ntus for the heat exchanger, finned coil heat exchanger, cooling tower and desiccant dehumidifier of 9.0. The flow rates were chosen to give good performance at ARI conditions [Kang, 1989].

The REVERS cycle is a simplification of the SENS cycle [Kang, 1989]. The simplification is the elimination of one of the heat exchangers and a redirection of flows. The REVERS cycle is shown in Figure 1.5. The resulting COP, cooling effect, and regeneration temperature are 2.41, 25.3 kJ/kg, and 64.9°C respectively [Kang, 1989]. The REVERS cycle has a lower COP but a higher cooling effect for a lower

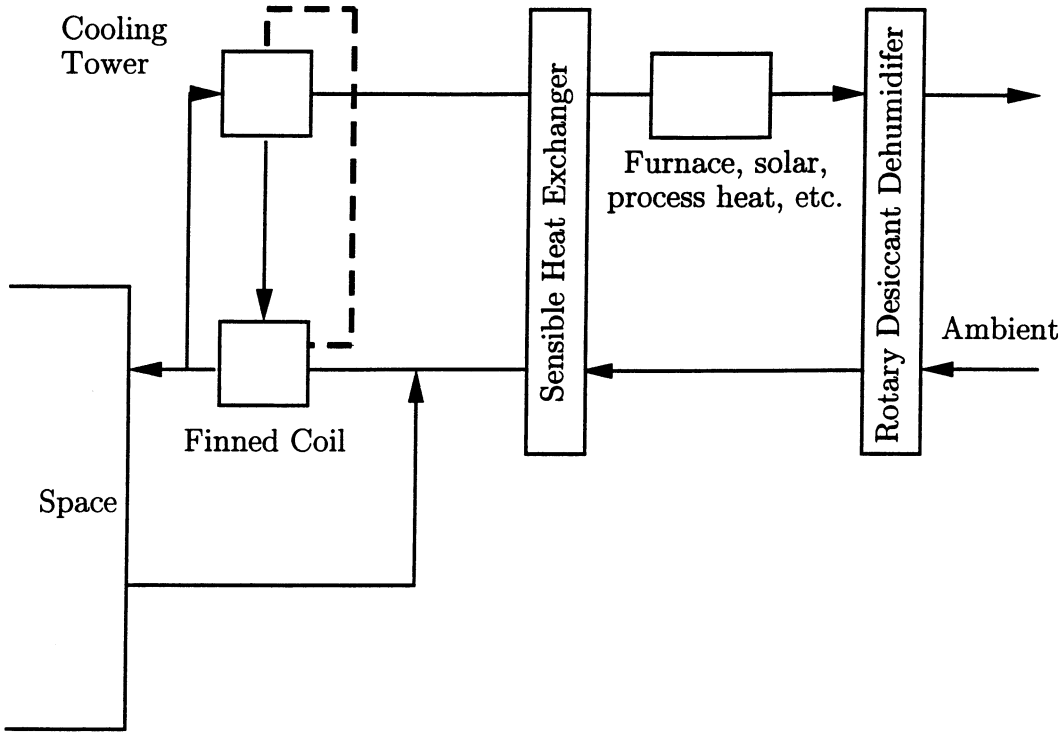

Figure 1.5: The REVERS cycle schematic.

regeneration temperature. The non-idealities were identical to those used for the SENS cycle.

The DINC cycle [Waugamann, 1993] shown in Figure 1.6 uses an indirect evaporative cooler in place of a direct evaporative cooler in the ventilation and recirculation cycles. Waugamann predicts a COP of 1.6 at ARI conditions. The DINC cycle provides the benefit of an increased COP, but does not require the expensive components (cooling tower and finned coil) that the SENS and REVERS cycles require.

1.1.3 Improved Operational Concepts for Basic Cycles

Advanced systems that utilize better components is one way of increasing the performance of desiccant dehumidification, for example, using a cooling tower and finned

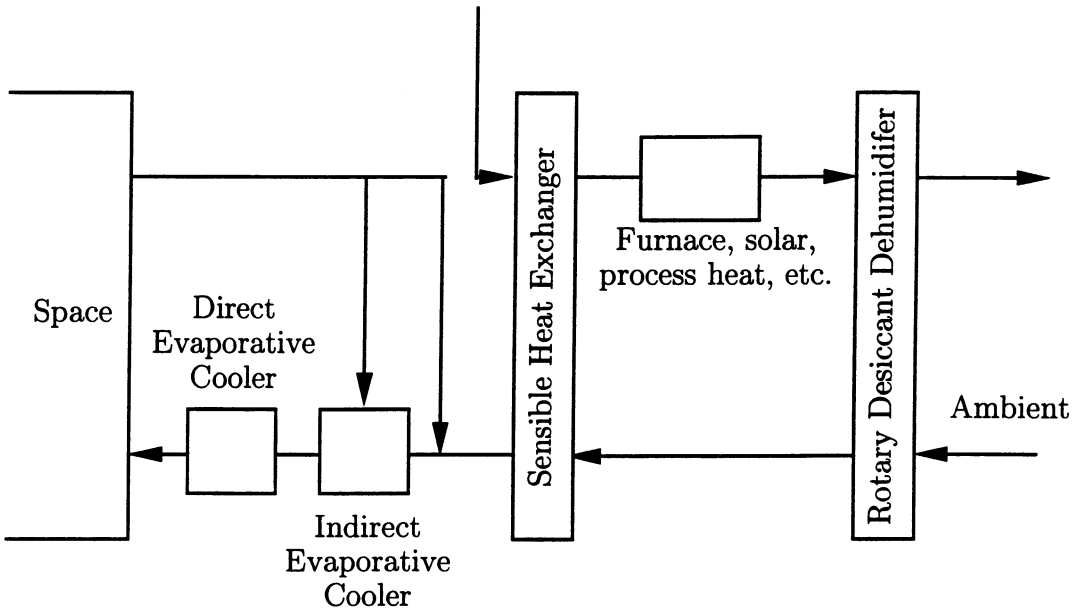

Figure 1.6: The DINC cycle schematic.

coil instead of the evaporative coolers in the ventilation cycle; another is to improve the way the cycles with the basic components work by utilizing improved concepts for desiccant dehumidification. Improving the basic systems is attractive because that the advanced systems have a greater number of components or more expensive components than the basic cycles.

Staged Regeneration

Staged regeneration reduces the amount of heat needed to regenerate the desiccant by first regenerating part of the desiccant with unheated (i.e. no solar or gas heating) air and then finishing the regeneration process with solar or gas heated air. Collier [1991] predicted that staged regeneration can increase the COP of the ventilation cycle from 0.76 to 1.0. The fraction of heated regeneration air was 50%. Desiccant dehumidifiers with higher heat capacity showed less dramatic improvements with

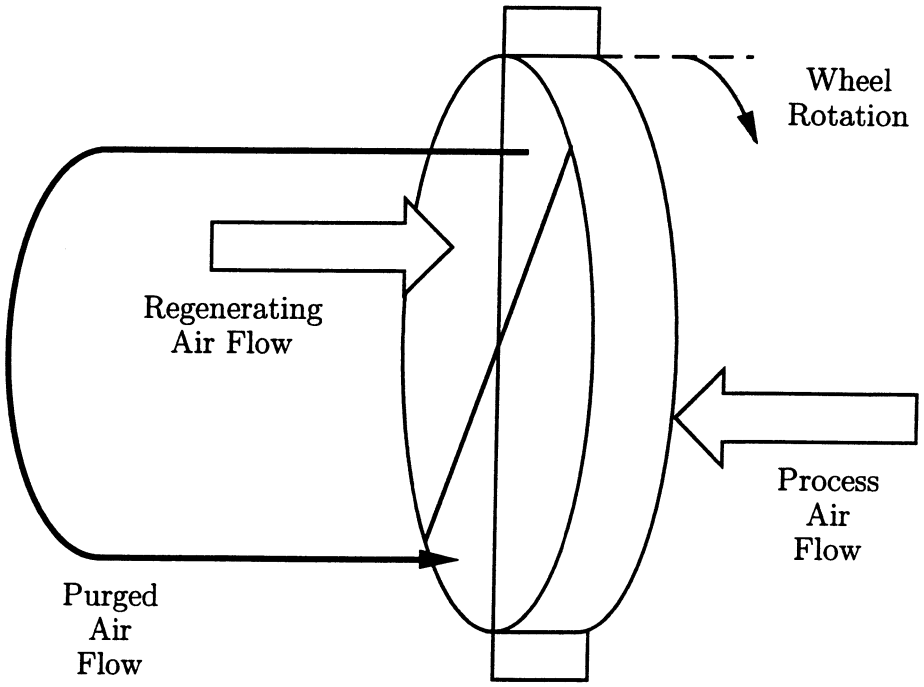

Figure 1.7: Air Flow Paths for Rotary Desiccant Dehumidifier with Purged flow.

staged regeneration [Collier, 1991].

Purged Flow

At the beginning of the processing period the outlet of the first 10-20% of the rotation of the dehumidifier is hot and humid [Jurinak, 1984]. The removal of this air reduces the average outlet humidity ratio of the processing period. In addition, if this purged flow is then used to regenerate the desiccant the heat needed to regenerate the desiccant can be reduced. Figure 1.7 shows the flow of air through a desiccant dehumidifier operation with purged flow. Purged flow increased the dehumidification capacity of a silica gel wheel 4% for a low thermal capacitance matrix and 8% for a high thermal capacitance matrix [Jurinak, 1984].

Cross Cooling

The performance of a silica gel dehumidifier can be improved by removing the heat that is generated during the adsorption process [Mei, 1983]. The amount of dehumidification capacity is increased because the equilibrium amount of water the desiccant can adsorb decreases with increased temperature. Mei showed that for a constant regeneration temperature the COP increases with the amount of moisture cycled in the adsorption/desorption process. Cross cooling the experimental setup increased the amount of moisture cycled from 0.05 to 0.08 kg water/kg silica for a cross cooling flow rate of 150% of the process flow. For a regeneration temperature of 63-66°C, the resulting COP changed from 0.2 to about 0.35 for the experimental setup.

Majumdar and Worek [1988] explored the performance of a cooled-bed desiccant dehumidifier operating in recirculation mode with varying indoor and outdoor conditions and regeneration temperature. The results showed that the indoor and regeneration temperature and outdoor humidity ratio affect the COP more than the outdoor temperature and indoor humidity ratio and that low temperature heat (i.e. 50°C) can provide cooling.

1.1.4 Desiccant Air-Conditioning System Summary

Desiccant dehumidification systems are a viable alternative to vapor compression air-conditioning machines [Jurinak et. al., 1984]. The advantages of desiccant air-conditioning systems lie in the elimination of the vapor compression cycle. First, the potentially harmful refrigerant is eliminated, and second, the on-peak electric peak and demand are reduced. The result is an air-conditioning system that saves the operator money from reduced electricity demand rates and consumption. The reduced electric usage is offset by heat from a solar collector, waste heat from another process, or heat from a gas furnace.

The disadvantages of desiccant air-conditioning lie in the equipment. A simple desiccant air-conditioning system involves a rotary desiccant wheel, a thermally large heat exchanger, two evaporative coolers and a gas furnace or solar collector array. These components lead to a large capital investment compared to conventional air-conditioning systems. In addition to its cost, the rotary desiccant wheel is large to compensate for the low transfer coefficients.

Basic systems reduce electric demand and energy despite COPs less than 1 at ARI conditions. Advanced systems and methods not only accomplish the reduction of electrical energy and demand but also increase the COP of the system to more effectively compete with conventional systems. The state-of-the-art advanced systems have COPs greater than 2 at ARI conditions.

Advanced concepts also increase the performance of desiccant systems. Staged regeneration reduces the regeneration heat by only heating a portion of the regeneration air stream. Purged flow expels the hot, moist air that initially comes out of the dehumidifier after regeneration, this is recirculated into the regeneration stream to reduce the regeneration heat. Cross cooling involves introducing a cool air stream that passes through the desiccant dehumidifier to reduce the heating of the process stream from the liberation of heat in the adsorption process; therefore, cross cooling is limited to switched bed applications.

Regardless of the simplicity or complexity of the desiccant air-conditioning cycle and its operational control, the performance of the desiccant dehumidifier is critical to the cycle performance.

1.2 Basic Concepts and Experimentation

Desiccants and desiccant air-conditioning systems have been extensively researched in the past 30-40 years. Many numerical studies and experiments to determine the

performance of the desiccant and the system have been done. The literature that is most applicable to the current project are studies to determine the heat and mass transfer coefficients and methods for solution of the governing partial differential equations.

1.2.1 Desiccant Equilibrium Properties

Desiccant equilibrium properties define the performance of the desiccant dehumidifier. Many models for the description of the adsorption and desorption of adsorbate on a desiccant have been proposed. The test of the models is how well they represent the isotherms that are acquired by static sorption experiments. Static sorption experiments determine the amount of moisture that the desiccant can hold when in contact with moist air at a given temperature and relative humidity. Exposed to a range of relative humidities at the same temperature, the resulting amount of water contained in the desiccant is an isotherm. Several isotherms contain all the information that is needed to predict desiccant performance; that is, the equilibrium humidity ratio of the air in contact with the desiccant and the heat of adsorption. Many references are available on adsorption properties and processes [Ruthven, 1984].

The models for representation of the equilibrium isotherm range from the very simple to very complex. However, with today's computer capabilities, a simple model is not a priority.

1.2.2 Methods of Solution of Governing Equations

The performance of a desiccant dehumidifier or enthalpy exchanger requires solution of a system of partial differential equations that includes the conservation of mass and energy and rate equations that define the heat and mass transfer.

$$\dot{m}\frac{\partial w}{\partial x} + \frac{M}{L}\frac{\partial W}{\partial \theta} = 0 \tag{1.1}$$

$$\dot{m}\frac{\partial i}{\partial x} + \frac{M}{L}\frac{\partial I}{\partial \theta} = 0 \tag{1.2}$$

$$\dot{m}\frac{\partial w}{\partial x} = \frac{h_m A}{L}\left(w_{eq}\left(T, W\right) - w\right) \tag{1.3}$$

$$\dot{m}\frac{\partial i}{\partial x} = \frac{h_t A}{L}\left(T - t\right) + i_{wv}\frac{h_m A}{L}\left(w_{eq}\left(T, W\right) - w\right) \tag{1.4}$$

where the coordinate nomenclature is given in Figure 1.1, M, T, W and I are the mass, temperature, water content and enthalpy of the desiccant material respectively, $\dot{m}$, t, w and i are the mass flow rate, temperature, humidity ratio and enthalpy of the moist air, h_t and h_m are the overall heat and mass transfer coefficients respectively, i_{wv} is the enthalpy of water vapor, and w_{eq} is the humidity ratio of the air if it were in equilibrium with the desiccant.

Solution to the conservation and rate equations has be done by using an analogy with heat transfer or with more general finite difference or finite element methods.

Analogy with Heat Transfer

Maclaine-cross [1972], Close and Banks [1972] developed a method of transforming the system of coupled hyperbolic non-linear partial differential equations into a system of uncoupled hyperbolic partial differential equations by assuming that mass transfer is analogous to heat transfer. In order to perform the transformation, several assumptions were required: 1. Axial conduction and diffusion were neglected, 2. constant inlet and initial boundary conditions, and 3) infinite heat and mass transfer coefficients.

The transformed equations are:

$$\frac{\partial F_i}{\partial z} + \lambda_i \frac{\partial F_i}{\partial \tau} = 0 \qquad i = 1, 2 \tag{1.5}$$

F_1 and F_2, which are called the combined potentials for heat and mass transfer, are state properties of the desiccant-fluid system. These potentials pass through the

desiccant like waves with speed λ_i. The result of this transformation is a set of equations for heat and mass transfer in a rotary desiccant dehumidifier that are the same form as the equations for a rotary sensible heat exchanger. Lines of constant F_1 and F_2 for silica gel resemble lines of constant moist air enthalpy and relative humidity respectively on psychrometric coordinates. The combined potentials and wave speed correspond to temperature and the ratio of the heat capacities of the matrix and humid air respectively [Van Den Bulck, 1983; Klein, 1988]. The following assumptions are utilized in uncoupling the equations:

$$\frac{\partial F_{i,f}}{\partial i_f} = \frac{\partial F_{i,m}}{\partial i_f} \qquad Le_o = \frac{Ntu_t}{Ntu_m} = 1 \tag{1.6}$$

where Le_o is called the overall Lewis number and the Ntus for heat and mass transfer respectively are defined as follows:

$$Ntu_t = \frac{h_t A}{\dot{m} c_{p,f}} \qquad Ntu_m = \frac{h_m A}{\dot{m}} \tag{1.7}$$

The first assumption is equivalent to saying that the combined potentials are linear functions of the moist air enthalpy and relative humidity of the air in contact with the desiccant [Jurinak, 1982]. The second assumption means that the Ntu_m for mass transfer is equal to the Ntu_t for heat transfer. Both assumptions are true for systems with infinite transfer coefficients (i.e. equilibrium performance) but are only approximations for systems with finite transfer coefficients.

Waves of temperature and humidity ratio travel together through the desiccant matrix, but the combined potentials travel at distinctly different speeds. Since the combined potentials change independently, the equilibrium performance of a desiccant dehumidifier can be determined quickly and easily by the intersection point method. The intersection point is the minimum humidity ratio plateau in the processing period and corresponds to the intersection of the constant F_1 potential that passes through

the processing state and the constant F_2 potential that passes through the regenerating state. However, solution to the performance of the non-ideal (i.e. finite transfer coefficients) desiccant dehumidifier is more difficult because the F_i potentials cannot be analytically determined and therefore a curve fit of the combined potentials is needed to solve the equations [Jurinak, 1982].

Finite Difference Methods

Finite-difference methods for solution to the governing equations are the most practical way to solve for the performance of a desiccant dehumidifier with non-infinite heat and mass transfer coefficients. Unlike the combined potentials derived by Banks and Close [1971] that require the ratio of the number of transfer units for heat and mass transfer to be unity, there are no limits on the value of this ratio for finite-difference methods. Unfortunately, the methods are complex and computationally intense.

Maclaine-cross [1974] developed a finite-difference method that used a second order representation of the governing equations. Second order accuracy is achieved by performing a Taylor's series expansion around the center of the element. The finite-difference equations are solved implicitly. The program MOSHMX [Maclaine-cross, 1974] uses this finite-difference formulation. MOSHMX utilizes algorithms for determination of time and space step sizes and extrapolates the results to zero grid size. MOSHMX solves for the periodic steady-state of the dehumidifier given the inlet process and regeneration states and the time of each period.

Zheng and Worek [1993] presented a finite-difference formulation that has high-order accuracy, is numerically implicit, and is unconditionally stable. The finite-difference formulation of the governing equations utilize a central-difference scheme with average values used at the midpoint of the nodes in time and space. The starting scheme is formulated identically except a backward difference scheme is used.

This isotherm is linearized by performing a first order Taylor series expansion. The resulting grid size for this finite difference method required 5 steps in space and 20 steps in time compared to 100 steps in space and 2000 steps in time for an explicit method [Zheng and Worek, 1993]. The authors conclude a considerable computer time reduction compared to explicit numerical methods.

1.2.3 Numerical Performance Evaluation

Numerical simulations of desiccant dehumidification are relatively easy to accomplish using finite difference or finite element methods. Therefore, a large number of numerical parametric studies have been done to determine the effect of desiccant properties (i.e. isotherm shape, total moisture content, and matrix thermal capacitance) and the heat and mass transfer coefficients [Collier et al., 1990; Collier and Cohen, 1991; Epstein and Grolmes, 1985; Farooq and Ruthven, 1991; Jurinak, 1982; Zheng and Worek, 1993; Mei, Chen, Lavan, Collier, Meckler, 1992]. The influence of these properties on performance are discussed below.

Desiccant Properties Choice

Much discussion has resulted from the proposal of optimum desiccant properties, that is, total desiccant water content, heat of adsorption and isotherm shape. Questions of advantages of addition of inert material to the matrix to increase the thermal capacity of the matrix have also been debated.

The isotherm shape of a desiccant has been qualified by Brunauer [1945]. Figure 2.2 shows the five isotherm types defined by Brunauer. Briefly, a Brunauer Type I isotherm shape shows considerable water capacity except at very low relative humidities. Conversely, a Brunauer Type III isotherm shape shows low water capacity except at very high relative humidities.

Jurinak [1982] varied the isotherm shape to determine the optimum isotherm shape. The heats of adsorption were assumed to be typical for the isotherm shape. The results showed that the Type I was the best for adsorption; that is, for the same process and regeneration states the dehumidification capacity is greater than the other four Brunauer types or a linear isotherm.

Collier et al. [1990] showed that the moderate Type I was the best choice for systems with staged regeneration and the nearly linear isotherm was the best choice without staged regeneration. Farooq and Ruthven [1991] did a numerical study of a fixed bed desiccant dehumidifier subjected to cyclic operating conditions. The conclusion was that there is a large range of acceptable isotherm shapes.

Zheng et. al. [1993] determined that the moderate Type I was the best isotherm shape. The Type I also had the longest cycle time and therefore the lowest rotation speed and least carryover. Zheng measured the dehumidification performance as the average minimum outlet humidity ratio.

The moderate Type I isotherm shape is the optimum isotherm for adsorption processes (i.e. provides the most dehumidification); however, the optimum is very flat and a wide range of isotherm shapes (from moderately Type I to linear) provide adequate dehumidification performance.

The total water content of the desiccant is the amount of water that the desiccant can adsorb when in contact with saturated air. The maximum amount varies for different desiccants; for example, molecular sieves usually have a maximum in the range of 0.2-0.3 kg water/kg dry desiccant and silica gel has a range of 0.35-0.5 kg water/kg dry desiccant for microporous and up to 1.0 kg water/kg dry desiccant for macroporous silica gel [Jurinak, 1984].

Jurinak [1984] studied the effect of total water content and concluded that increasing the amount adsorbed increased the cooling performance; however, the effect

of doubling the total water adsorbed was easier accomplished by a small change in the isotherm shape from linear to Type I. Jurinak measured the performance of the desiccant as the equilibrium intersection point compared to the intersection of the constant relative humidity and constant enthalpy lines for the process and regeneration states.

Collier et al. [1990] found that the COP and capacity decreased for decreased total water content without staged regeneration. The nominal desiccant was Type I with a total water content of 0.4 kg/kg. The COP and capacity were reduced 2% and 4% for a reduction of total water content to 0.25 kg/kg. The COP and capacity were reduced 6% and 10% for a reduction of total water content to 0.15 kg/kg. Collier [1990] found that for a dehumidifier with staged regeneration the COP was unaffected by reduction of total water content, but the capacity was decreased by 15% for a reduction of total water content from 0.4 to 0.08 kg water/kg dry desiccant.

Zheng et. al. [1993] concluded that changing the total water content of the desiccant matrix from 0.1 to 0.4 kg water/kg dry desiccant produced nearly the same performance when operated at the optimum cycle time (i.e. the time that corresponds to the time averaged minimum outlet humidity ratio). However, the performance of a dehumidifier with a high maximum water content exhibited less sensitivity to cycle time. The only difference was that lower total water content reduced the cycle times. However, as the cycle time decreases the amount of carryover between the process and regeneration streams increases thus decreasing performance.

The total water content of the desiccant matrix effects the rotation speed of the rotary dehumidifier more than the dehumidification capacity when operated at the optimum cycle time. A reduction in the total water content increases the rotation speed of the dehumidifier.

Jurinak [1982] concluded that increased thermal capacitance decreased the capacity of the desiccant dehumidifier. Increased thermal capacitance also increased the

cycle time. Collier and Cohen's [1991] analysis agrees with Jurinak's, but also stated that the waves associated with heat and mass transfer in desiccant dehumidification "smeared" together for high thermal capacitance. Although the capacity of the dehumidifier decreased, the COP increased because the desiccant retains the regeneration energy and transfers it to the process stream thus providing higher preheat temperatures out of the sensible heat exchanger. However, this benefit is only realized with high sensible heat exchanger effectiveness ($> 94\%$) [Collier and Cohen, 1991].

Heat and Mass Transfer Coefficients

The effect of the heat and mass transfer coefficients on the performance of a desiccant dehumidifier is simple. The performance (i.e. COP and capacity) increases with increasing transfer coefficients. Equivalently, for the same dehumidification load the dehumidifier size is reduced with increasing transfer coefficients.

1.2.4 Experimental System Performance Evaluation

Löf et al. [1988] studied an American Solar King Energymaster desiccant cooling unit operated in ventilation mode. The desiccant material on the rotary desiccant dehumidifier matrix was lithium chloride. The system was regenerated using heat from a evacuated tube solar collector array and storage tank with water as the working fluid. The space (residential building) was temperature controlled to be 22°C. The results showed that a thermal COP of 1 can be exceeded with this system, and for every unit of solar energy incident on the collector array a half of a unit of cooling can be delivered with solar heated water temperatures of 50-65°C.

Krishna and Murthy [1989] studied a cylindrical honeycomb matrix of 0.2 mm paper board impregnated with silica gel. The matrix was held together with a fiber-reinforced plastic drum. The dehumidifier was operated continuously, i.e. regen-

erating half of the matrix while the other half was processing air. The range of regeneration temperature was 60-75°C, the range of rotational speeds was 4-12 rotations per hour, and the range of process stream velocity was 1.4-2.2 m/s. The results show an optimum rotation speed for maximum water adsorbed for constant process and regeneration air stream velocities and regeneration temperature. A ratio of velocity of process to regeneration air stream of 1.3 produced the maximum amount of moisture adsorbed for a given rotation speed and regeneration temperature.

Prasad and Kumar [1984] considered three desiccant materials.: calcium chloride, copper sulfate and silica gel. Silica gel was determined to be the best of the three because the calcium chloride and copper sulfate had lower dehumidification and regeneration. The silica gel proved to be the most stable under cyclic conditions.

1.2.5 Experimental Transfer Coefficient Determination

Schultz [1987] performed rotary steady state experiments on silica gel-coated tape that was spiral wound into a parallel plate matrix. The overall heat and mass transfer units were determined from comparison of high rotational speed experiments and a finite-difference code MOSHMX [Maclaine-Cross, 1974]. The results were used to predict the performance at medium rotational speeds with good agreement and confirmed the use of overall transfer coefficients. The overall Lewis number was in the range 1 to 1.2.

Bullock and Threlkeld [1966] performed single-blow adsorption experiments on silica gel that was initially dried by hot, dry air, cooled with cool, dry air and then subject to a humid air stream at the same temperature. Using overall heat and mass transfer coefficients developed by Hougen and Marshall [1947], the authors obtained good agreement between experiment and numerical simulation. They concluded that the agreement between experiment and simulation did not justify further refinements

in the mathematical model to include intra-particle properties due to the lack of knowledge of these properties and their non-uniformity within the matrix.

Van Den Bulck [1987, 1990] developed a methodology for single-blow heat and mass transfer test. Point matching techniques for evaluating performance of exchangers involves the determination of the Ntu of the matrix based on a single experimental point. This point may be the effectiveness at breakthrough, the maximum slope of the breakthrough curve, or another characteristic of the breakthrough curve. Another technique is curve matching, which involves determination of the Ntu that minimizes the root-mean-square error between the experimental breakthrough and the theoretical breakthrough distribution.

Van Den Bulck [1990] concluded that neither of these methods is reliable for single-blow adiabatic sorption experiments because of the non-linearity of the governing equations and equilibrium properties [Van Den Bulck, 1990]. Curve matching provided satisfactory results, but similar results could be obtained with several different parameter sets; therefore, curve matching was deemed of limited use as a method for determination of performance characteristics of heat and mass exchangers.

Van Den Bulck showed numerically [1983] and experimentally [1987] that for the regeneration period of operation the waves become constant-pattern waves. Constant-pattern waves retain their shape as they pass through the matrix and are less dependent on repeatable inlet step conditions. The properties of constant-pattern waves allow a dimensionless flow length to be defined that shifts the time dependent curves of outlet temperature and humidity ratio to obtain a single curve for temperature and humidity ratio distributions in the desiccant matrix. The data that make up these curves and the numerical simulation of the governing differential equations for heat and mass transfer allow the determination of the overall Lewis number (i.e. the ratio of Ntu for heat transfer to the Ntu for mass transfer as given in Equation 2.11). The

effect of the overall Lewis number was to skew the distribution of the outlet curves [Van Den Bulck, 1990]; however, the effect was small and a single overall Lewis could not be determined. The acceptable overall Lewis numbers ranged from 3 to 7 [1990]. The results were only for the regeneration period of desiccant dehumidification because the process period results were too dependent on the inlet step conditions since the waves expand as they pass through the matrix.

Van Den Bulck [1987, 1990] proposed a procedure for single-blow adiabatic heat and mass transfer experiments. First, pressure drop experiments should be done to determine the hydraulic diameter, flow area, transfer area and porosity of the matrix. Secondly, experiments with different inlet and initial matrix conditions should be done to determine the active mass of desiccant on the matrix. The isotherm should be determined from static sorption experiments. And lastly, dynamic experiments with varying air mass flow rates should be done in order to get an accurate determination of the wave shapes in the desiccant matrix.

Chuah et. al. [1989] experimented with isothermal transient mass transfer on parallel plates covered with a thin layer of silica gel. The method used for determination of the heat transfer coefficient was a point matching method based on the slope of the outlet humidity ratio curve. The experimental results were compared with numerical simulation using a two-film model: the solid side resistance was determined by modeling the desiccant as a slab of uniform thickness and a linear moisture distribution, the gas side resistance was assumed constant and was based on analytically calculated results for a constant flux boundary condition. The results show that the difference between the experiment and simulation is sensitive to the uncertainty in the equilibrium isotherm.

1.2.6 Summary of Basic Concepts

A overview of the literature on desiccant dehumidification has been presented. The role of desiccant equilibrium properties, solution methods for the governing differential equations, parametric studies of desiccant dehumidifier performance and experimental studies were discussed.

The methods for solution of the governing partial differential equations that were investigated were the analogy method and the finite-difference method. The finite-difference method was more general than the analogy method because fewer assumptions are needed.

The parametric studies on the desiccant equilibrium properties concluded that there are a wide range of acceptable isotherm shapes, but that the moderate Type I is preferred. The maximum water content of the desiccant was less important than the isotherm shape and the major difference in a reduction of maximum water content is an increase in the rotation speed of a rotary desiccant dehumidifier. Additional matrix thermal capacitance reduced the capacity of the dehumidifier but increased the COP.

Experimental studies confirm that desiccant dehumidification is viable and the COP's can exceed unity. In addition, several methodologies for adiabatic single-blow heat and mass transfer were investigated. Bullock and Threlkeld [1966] offered a methodology for experimentation of the adsorption of water on an initially dry silica gel matrix with good agreement with theory. Van Den Bulck's [1987] methodology was only applied to the desorption (regeneration) of a silica gel matrix. Adsorption was not applicable to the methodology because the results obtained were sensitive to the inlet step condition and were not repeatable. Most of the experimental studies found dealt with isothermal or cooled-bed boundary conditions. In addition, many experiments only determined the system performance and determination of the heat

and mass transfer coefficients was not done.

1.3 Thesis Objective

The objective of this thesis is the experimental determination of desiccant heat and mass transfer for a commercially available core geometry coated with a relatively unresearched polymer desiccant. The experiments done in this thesis will have adiabatic boundary conditions. The experiments will be done on both adsorption and desorption and will loosely follow the methodology set forth by Bullock and Threlkeld [1966]. The experiments use the humidity of the inlet air stream as the driving force for the adsorption and desorption of water from the desiccant matrix. The matrix is regenerated with very dry compressed air and processed with humid air. These conditions result in the outlet response of the dehumidifier to be easily measured with outlet temperature profiles rather than humidity ratios. Comparison of the experimental results with numerical simulation will be done.

The experiment will have two major parts: 1) the validation/determination of the heat transfer coefficient of the matrix geometry without desiccant; and 2) the determination of the mass transfer coefficient of the matrix geometry with desiccant with the determined heat transfer coefficient. The equilibrium isotherm for the polymer coating on the commercial matrix was determined by Stiesch [1994].

The numerical simulation involves three parts: 1) determination of the equilibrium performance (infinite heat and mass transfer coefficients) with the method of characteristics and the combined potentials for heat and mass transfer developed by Close and Banks [1972]; 2) determination of performance with finite heat and mass transfer coefficients using the finite difference method developed by Zheng and Worek [1993]; and 3) simulation of the experimental conditions. The combination of numerical simulation and experimentation will provide insight into the parameters that affect the

desiccant dehumidifier.

1.4 Thesis Outline

1.4.1 Equilibrium Performance

The equilibrium (infinite transfer coefficients) will be investigated. Chapters 2 and 3 will discuss desiccant properties and equilibrium performance. Equilibrium performance is the upper limit for the desiccant dehumidifier and was solved with the combined potentials derived by Maclaine-cross, Close and Banks [1972], Jurinak [1982] and Van Den Bulck [1983].

1.4.2 Non-equilibrium Performance

Once the upper limit to desiccant dehumidification performance is known the non-equilibrium performance will be determined and discussed in Chapter 4. A computer code that utilizes the finite-difference method developed by Zheng and Worek [1993] will be developed that can be an analysis tool for the experiment with time-varying inlet conditions. The code will also be used to perform a parametric study on the effect desiccant properties and regeneration temperature have on optimal performance and resulting size of a counterflow dehumidifier.

1.4.3 Experimental Description and Methodology

The non-equilibrium theory requires the knowledge or assumption of the heat and mass transfer coefficients. A single-blow experiment will be developed to investigate the heat and mass transfer for a commercially available core geometry subject to step changes in inlet humidity ratio and described in Chapter 5.

Single-blow heat transfer experiments will be performed on the experimental setup

without desiccant to determine the heat transfer coefficient without mass transfer. A discussion of the heat and mass transfer for the adsorption and desorption periods will be done in Chapter 6, highlighting the trends and the effect on the heat and mass transfer coefficients and isotherm shape.

The finite-difference program will be used to predict the outlet humidity ratio and temperature for the experimental inlet humidity ratio and temperature and differences between the simulation and the experiment will be discussed in Chapter 6.

Chapter 2

Desiccant Properties

The driving force of mass transfer in desiccant dehumidification is chemical potential *or* concentration gradient [Ruthven, 1984]. Assuming that the air-water mixture is an ideal gas and the air in contact with the surface is in local equilibrium with the desiccant material, the driving force for mass transfer is the humidity ratio difference between the moist air and the humidity ratio in equilibrium with the surface of the desiccant desiccant. The equilibrium humidity ratio is a property of a desiccant material and is defined by the isotherm. The isotherm is a measure of the equilibrium amount of water that the desiccant can adsorb at a given temperature and humidity ratio of the moist air in contact with the desiccant.

2.1 Definition of adsorption

Adsorption is the attraction and "capture" of a gas molecules on the surface of a solid. There are two types of adsorption: chemical and physical. Chemical adsorption, or "chemisorption," behaves more like a chemical reaction and is usually considered irreversible due to the high temperatures required to desorb the adsorbed molecules, or adsorbate.

Physical adsorption occurs when molecules in the fluid above the desiccant become

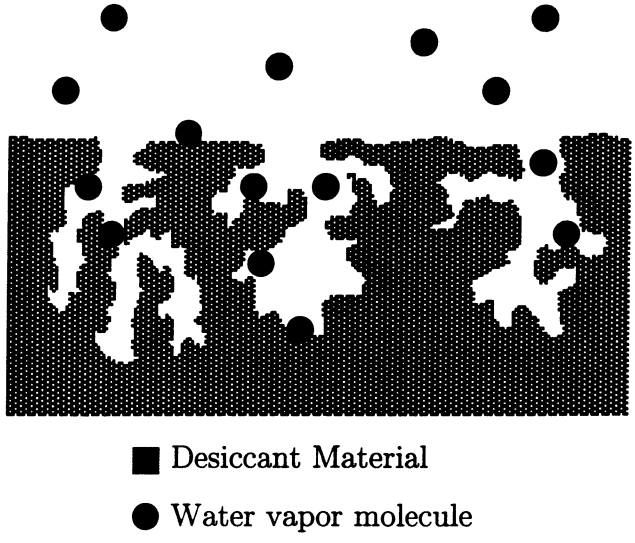

Figure 2.1: Physical adsorption.

trapped on the surface of a desiccant material, or "adsorbent." Figure 2.1 shows a simple schematic of physical adsorption. The driving force for physical adsorption is van der Waal's forces between the vapor molecules and the surface of the desiccant material. Since these forces are relatively weak, physical adsorption can be reversed, i.e. the adsorbed molecules can be desorbed by the adsorbent. Desorption is usually accomplished by increasing the temperature of the adsorbent.

2.2 Desiccant Isotherm

An important desiccant property is the isotherm. The isotherm is the equilibrium amount of water adsorbed on the desiccant as a function of the relative humidity of the air in contact with the desiccant at a constant temperature. The isotherm is determined by plotting the locus of equilibrium water adsorbed in the desiccant for different amounts of water vapor in the air in contact with the desiccant at the same temperature. The different isotherm shapes are classified by Brunauer and are shown

in Figure 2.2. Ruthven, in his book *Principles of Adsorption & Adsorption Processes* describes the Brunauer classifications:

> "The isotherms for true microporous adsorbents, in which the pore size is not very much greater than the molecular diameter of the sorbate molecule, are normally of Type I. This is because with such adsorbents there is a definite saturation limit corresponding to complete filling of the micropores. Occasionally if intermolecular attraction effects are large an isotherm of Type V is observed, as for example in the sorption of phosphorous vapor on NaX. An isotherm of Type IV suggests the formation of two surface layers either on a plane surface or on the wall of a pore very much wider than the molecular diameter of the sorbate. Isotherms of Types II and III are generally observed only in adsobents in which there is a wide range of pore sizes. In such systems there is a continuous progression with increasing loading from monolayer to multilayer adsorption and then to capillary condensation."

A collection of isotherms at differing temperatures is needed to determine the desiccant's performance. Figure 2.3 shows an isotherm for silica gel [Van Den Bulck, 1987].

The difference between the air humidity ratio and the humidity ratio in equilibrium with the desiccant with a given amount of water adsorbed in the desiccant is the driving force for mass transfer.

2.2.1 Dubinin-Polanyi Theory

In order to evaluate the equilibrium performance over a range of temperature, humidity ratio, and equilibrium behavior, a model for the isotherms is needed. The model chosen for this analysis is the Dubinin isotherm formulation. Dubinin [1975]

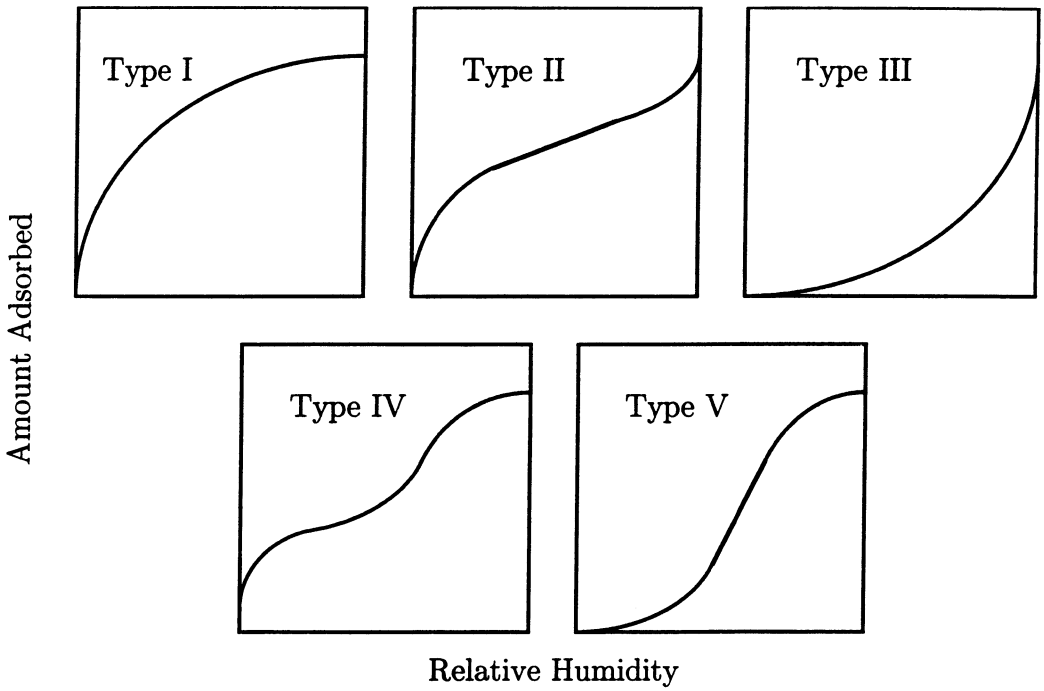

Figure 2.2: Brunauer classification of isotherms.

theorized that the temperature dependence of the isotherms can be predicted by the introduction of the adsorption potential, AP,

$$AP = -RT \ln \phi \tag{2.1}$$

where R is the ideal gas constant, T is the absolute temperature and ϕ is the relative humidity of the air in contact with the desiccant.

The form of the isotherm equation given by Dubinin [1975] for microporous desiccants (i.e. pore diameters $\leq$ 20 Å) is as follows:

$$W = W_1 \exp\left(-\left(AP/E_1\right)^{n_1}\right) + W_2 \exp\left(-\left(AP/E_2\right)^{n_2}\right) \tag{2.2}$$

where $W_{tot} = W_1 + W_2$, E_i's are the characteristic energies of adsorption, and n_i are small integers. W_{tot} is the total amount of water that the desiccant can hold at any temperature and is determined by the amount of water in the desiccant

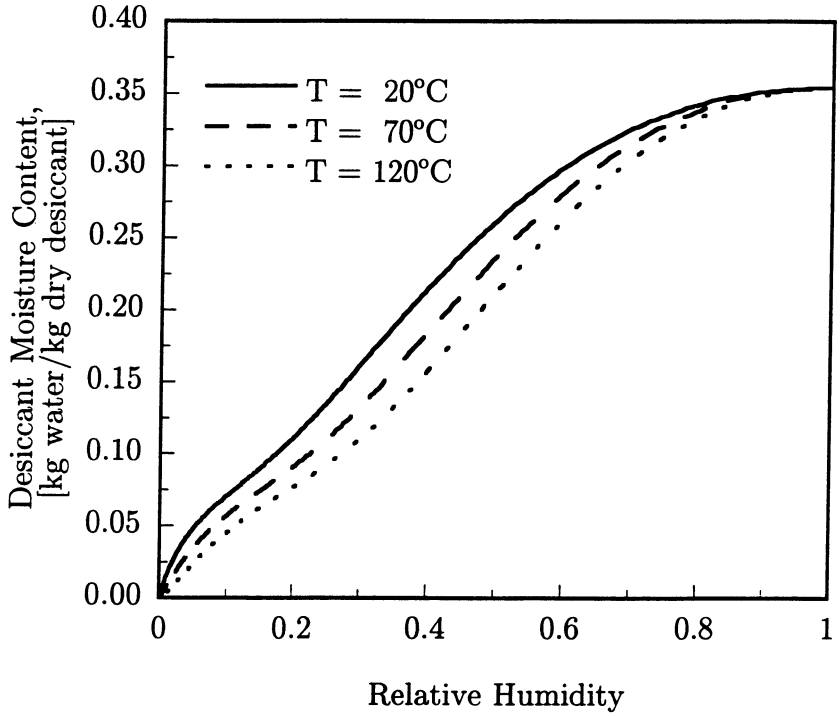

Figure 2.3: Desiccant moisture content for silica gel plotted versus relative humidity [Van Den Bulck, 1987].

when in equilibrium with a saturated air-water mixture. The isotherms for silica gel shown in Figure 2.3 are plotted on desiccant water content versus adsorption potential coordinates in Figure 2.4. The adsorption potential theory collapses the family of equilibrium isotherms into a single curve plotted on adsorption potential coordinates. Dubinin states that the adsorption potential theory holds for activated carbon, molecular sieves, and silica gel. Van Den Bulck [1987] verified the validity of the adsorption potential theory for silica gel and determined the parameters for the Dubinin isotherm form in Equation 2.2 to be the following:

$$W = 0.106 \exp\left(-(AP/8590)^2\right) + 0.237 \exp\left(-(AP/3140)^2\right) \tag{2.3}$$

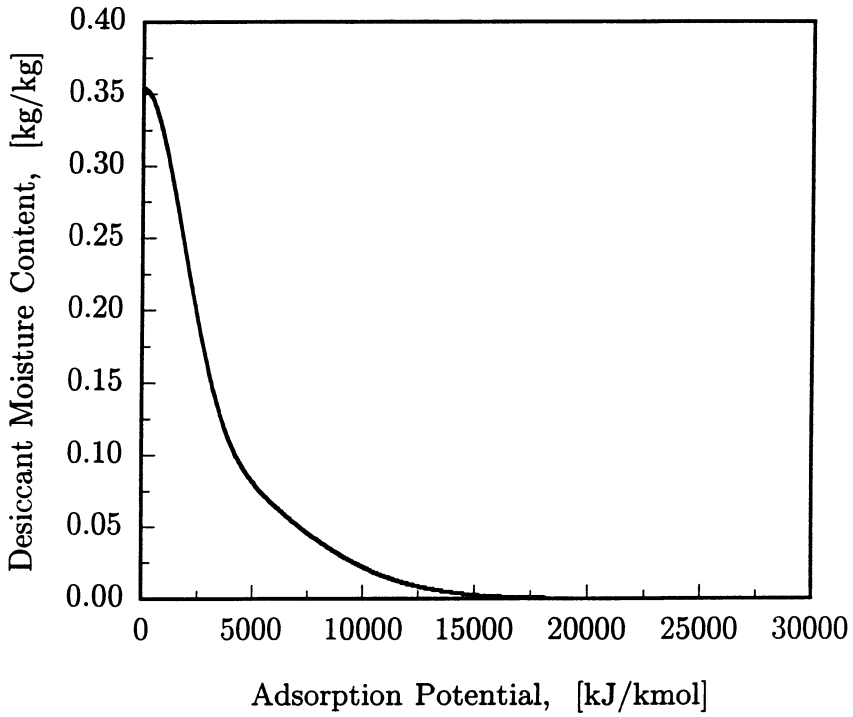

Figure 2.4: Desiccant moisture content versus adsorption potential.

In addition to the driving force for mass transfer, the equilibrium behavior of the desiccant determines the amount of thermal energy liberated in the adsorption process. Determination of the heat of adsorption is done using several isotherms and the Clausius-Clapeyron equation. The Clausius-Clapeyron equations states:

$$\Delta H_s = -R \left. \frac{\partial \ln p}{\partial (1/T)} \right|_W \tag{2.4}$$

The Clausius-Clapeyron equation assumes that the specific volume of the vapor phase is much larger than the liquid phase and can be represented by the ideal gas law.

Using the Clausius-Clapeyron equation and the assumption that the amount of moisture adsorbed by the desiccant is only a function of the adsorption potential the heat of adsorption is determined as follows [Dubinin, 1975; Van Den Bulck, 1987]:

$$\Delta H_s = \Delta H_{fg} + AP \tag{2.5}$$

where ΔH_{fg} is the heat of vaporization of water at the same temperature.

The advantages of using the adsorption potential to characterize the isotherm are the simplification of the determination of the heat of adsorption and the applicability to a large number of desiccants.

The Dubinin-Polanyi theory simplifies the equilibrium properties by accounting for the temperature effect of the isotherm with the introduction of the adsorption potential. The heat of adsorption is related to the heat of vaporization and the adsorption potential.

2.2.2 Variation on Dubinin-Polanyi Theory

Chuah [1989] incorporated the advantage of the Dubinin-Polanyi adsorption potential theory to represent the temperature dependence of the isotherm and the heat of adsorption with the flexibility of a polynominal fit of the isotherm. Stiesch [1994] used the Dubinin-Polanyi form but allowed non-integer exponents, n_i. The adsorption potential theory is used to account for the temperature dependence of the isotherm, but the form of the equation is expanded.

2.3 Desiccant Enthalpy

In order to solve the conservation of energy in the desiccant dehumidifier, the enthalpy of the moist desiccant must be determined. The enthalpy depends not only on the dry desiccant properties, and the adsorbed water properties, but also on the heat liberated by the phase change during adsorption. From the Clausius-Clapeyron equation, it can be proven that the adsorption potential is equal to the differential heat of adsorption (Equation 2.5). The differential heat of adsorption is the added heat that is liberated in addition to the heat of condensation.

The enthalpy of the desiccant is the sum of the sensible change of the matrix

material, dry desiccant and the adsorbed water and the phase change associated with adsorption.

$$I = (1 - f)\, c_m + f\, (c_d + c_w W)\, T + \int_0^W (\Delta H_{fg} - \Delta H_s)\ dW \tag{2.6}$$

where c_m, c_d and c_d are the specific heats of the matrix, dry desiccant and water respectively and f is the fraction of the matrix mass that is desiccant material. Substituting Equation 2.5 into the integral simplifies the equation to:

$$I = (1 - f)\, c_m + f \left[(c_d + c_w W)\, T - \int_0^W AP\ dW \right] \tag{2.7}$$

where the integral is determined from the desiccant isotherm. However, the adsorption potential, AP, cannot be rearranged into an explicit function of W in either the Dubinin-Polanyi theory or the variation used in this work. Therefore, the integral is rewritten as follows:

$$\int_0^W AP\ dW = AP\, W + \int_{AP}^{\infty} W dAP \tag{2.8}$$

Integer values of unity for n allow for analytic solution of this integral, but in general the integral will require numerical determination.

2.4 Conclusion

The isotherm is the most important property of a desiccant. From it, both the driving force for mass transfer and the heat of adsorption can be determined. The Dubinin adsorption potential theory is used to account for the temperature dependence of the isotherm. The adsorption potential is equal to the difference between the heat of adsorption and the heat of vaporization at the same temperature.

Chapter 3

Equilibrium Performance

In order to understand the performance of a desiccant dehumidifier, one must understand its limiting performance; that is, the equilibrium performance. Equilibrium performance is defined as the performance such that at every point in the desiccant matrix the air is in equilibrium with the desiccant matrix. In other words, the performance is as if the system has infinite heat and mass transfer coefficients.

3.1 Dehumidification Analysis

The nomenclature and coordinate system for a rotary desiccant dehumidifier are shown in Figure 3.1. The axial coordinate x is defined as positive in the direction of flow. The total length of desiccant in the direction of flow is L. Since the rotation speed is assumed to be constant, the angular coordinate θ is equivalent to time. The assumptions used in the analysis follow [Van Den Bulck, 1983]:

1. Parallel passage matrix with constant characteristics and porosity.
2. Constant air velocity with negligible pressure drop.
3. Spatially uniform inlet properties for each period.
4. Matrix initial condition constant in equilibrium with previous period air temperature and humidity ratio.

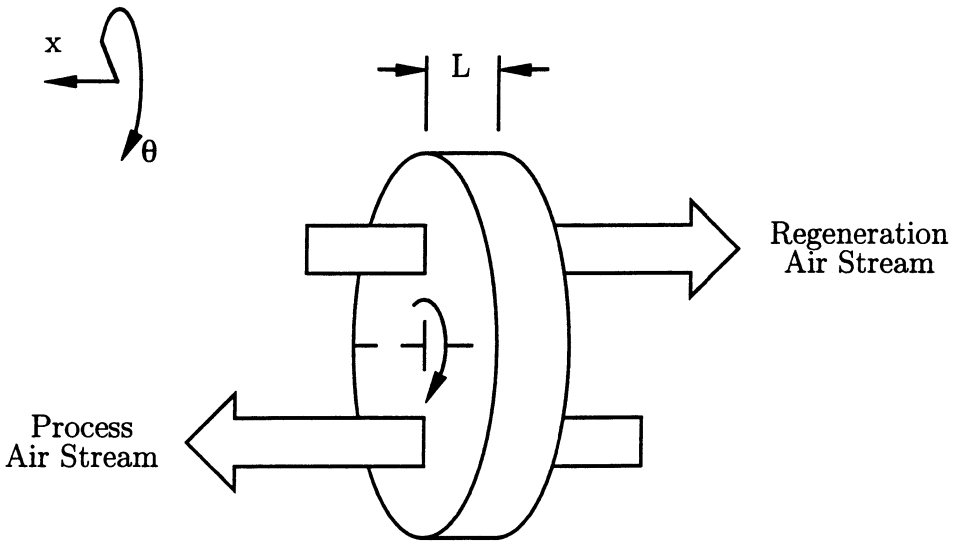

Figure 3.1: Nomenclature and coordinate system.

5. One-dimensional fluid flow in the axial direction.
6. Axial heat conduction and water vapor diffusion are negligible in both the matrix and the air streams.
7. Thermal and moisture capacities of the air are negligible compared to the matrix capacities.
8. No flux coupling of heat and mass transport by thermal diffusion or Dufour effects.
9. The air is locally in thermal and moisture equilibrium with the desiccant at every point in the dehumidifier, i.e. infinite transfer coefficients for heat and mass.

3.2 Governing Equations

The mass and energy conservation equations for the modeling of an equilibrium rotary heat and mass exchanger with the assumptions listed above simplify to a set

of hyperbolic partial differential equations that are given as follows [Van Den Bulck, 1983]:

$$\dot{m}\frac{\partial w}{\partial x} + \frac{M}{L}\frac{\partial W}{\partial \theta} = 0 \tag{3.1}$$

$$\dot{m}\frac{\partial i}{\partial x} + \frac{M}{L}\frac{\partial I}{\partial \theta} = 0 \tag{3.2}$$

The lower- and upper-case letters refer to the dry air, moist air and desiccant matrix respectively. M is the mass of dry desiccant and $\dot{m}$ is the mass flow rate of air through the dehumidifier. The moist air humidity ratio, w, is in equilibrium with the desiccant water content, W, at every point in the dehumidifier. That is, the desiccant and air humidity ratio are coupled using the equilibrium isotherm.

The introduction of the following dimensionless variables allows the conservation equations to be simplified.

$$z = \frac{x}{L} \qquad\qquad \tau = \frac{\dot{m}\theta}{M} \tag{3.3}$$

With these dimensionless variables, the conservation equations can be written in the following form:

$$\frac{\partial w}{\partial z} + \frac{\partial W}{\partial \tau} = 0 \tag{3.4}$$

$$\frac{\partial i}{\partial z} + \frac{\partial I}{\partial \tau} = 0 \tag{3.5}$$

The boundary conditions for the processing period are uniform over the inlet.

$$t(0,\tau) = t_P \qquad\qquad w(0,\tau) = w_P$$

The initial conditions of the fully reactivated desiccant matrix for the processing period are equilibrium with the regeneration temperature and humidity ratio.

$$T(x,0) = t_R \qquad\qquad w_{eq}(x,0) = w_R$$

For the reactivation period, the boundary equations are uniform over the inlet and the initial conditions of the fully processed desiccant matrix are equilibrium with the processing temperature and humidity ratio.

$$t(0,\tau) = t_R \qquad w(0,\tau) = w_R$$

$$T(x,0) = t_P \qquad w_{eq}(x,0) = w_P$$

3.3 Combined Potentials

In order to simplify the discussion of the governing equations, combined potentials of temperature and humidity ratio are introduced. The combined potentials were developed by Close and Banks [Banks, 1972; Close, 1971] and further studied by Jurinak [1982] and Van Den Bulck [1983]. The combined potentials are state property functions.

3.3.1 Derivation

The equilibrium desiccant water content can be written in terms of temperature and humidity ratio and substituted into Equations 3.4 and 3.5 to eliminate it from the mass and energy balances.

$$\frac{\partial w}{\partial z} + a_1 \frac{\partial T}{\partial \tau} + a_2 \frac{\partial w}{\partial \tau} = 0 \tag{3.6}$$

$$a_3 \frac{\partial t}{\partial z} + a_4 \frac{\partial w}{\partial z} + a_5 \frac{\partial t}{\partial \tau} = 0 \tag{3.7}$$

where the functions a_k are state properties and defined as:

$$a_1 = \left.\frac{\partial W}{\partial t}\right|_w$$

$$a_2 = \left.\frac{\partial W}{\partial w}\right|_t$$

$$a_3 = \left.\frac{\partial i}{\partial t}\right|_w \tag{3.8}$$

$$a_4 = \left.\frac{\partial i}{\partial w}\right|_t - \left.\frac{\partial I}{\partial W}\right|_t$$

$$a_5 = \left.\frac{\partial I}{\partial t}\right|_W$$

Introduction of the total differentials of air temperature and air humidity ratio yields the following conservation equations.

$$-\left(a_1 dz\right)\frac{\partial t}{\partial z} + \left(d\tau - a_2 dz\right)\frac{\partial w}{\partial z} = -a_4 dt - a_2 dw \tag{3.9}$$

$$\left(a_3 d\tau - a_5 dz\right)\frac{\partial t}{\partial z} + \left(a_4 d\tau\right)\frac{\partial w}{\partial z} = -a_4 dt \tag{3.10}$$

This system of partial differential equations is linear in derivates $\partial t/\partial z$ and $\partial w/\partial z$, and can be written in matrix form.

$$\begin{bmatrix} -a_1 dz & d\tau - a_2 dz \\ a_3 d\tau - a_5 dz & a_4 d\tau \end{bmatrix} \begin{bmatrix} \partial t/\partial z \\ \partial w/\partial z \end{bmatrix} = \begin{bmatrix} -a_4 dt - a_2 dw \\ -a_4 dt \end{bmatrix} \tag{3.11}$$

Define a variable λ, which is a velocity.

$$\lambda = \frac{dz}{d\tau}$$

Substitution of this variable into the previous set of equations and setting the determinant of the coefficient matrix to zero determines λ as a function of the state property functions a_k. The result is a quadratic equation in λ.

$$a_2 a_5 \lambda^2 + \left(a_1 a_4 - a_2 a_3 - a_5\right)\lambda + a_3 = 0 \tag{3.12}$$

The two roots to this equation are the state property functions λ_1 and λ_2. The quadratic formula gives the following relation for the roots.

$$\lambda = \frac{-\left(a_1 a_4 - a_2 a_3 - a_5\right) \pm \sqrt{\left(a_1 a_4 - a_2 a_3 - a_5\right)^2 - 4 a_2 a_3 a_5}}{2 a_2 a_5} \tag{3.13}$$

Substituting the solution vector from Equation 3.11 into column 2 of the coefficient matrix and setting the determinant to zero gives the differential expressions for the characteristic lines of the system of partial differential equations. The characteristic lines are lines of constant combined potential, called F_i. The combined potentials are the Riemann invariants [Van Den Bulck, 1983].

$$a_1 a_3 dt + (a_2 a_3 - a_2 a_5 \lambda_i)\, dw = 0 \qquad i = 1, 2 \tag{3.14}$$

where

$$\lambda_i = \lambda_i\,(t, w) = \frac{dz}{d\tau} \tag{3.15}$$

Klein [1988] has shown that the Equation 3.14 is not an exact differential. Equation 3.14 can be transformed into an exact differential by the introduction of an integrating factor, G_i.

$$dF_i = G_i a_1 a_3 dt + G_i\,(a_2 a_3 - a_2 a_5 \lambda_i)\, dw \qquad i = 1, 2 \tag{3.16}$$

In order for $G_i(t, w)$ to be the integrating factor, the following must be true.

$$\frac{\partial^2 F_i}{\partial t \partial w} = \frac{\partial^2 F_i}{\partial w \partial t} \tag{3.17}$$

or

$$\frac{\partial}{\partial w}\,(G_i a_1 a_3) = \frac{\partial}{\partial t}\,(G_i\,(a_2 a_3 - a_2 a_5 \lambda_i)) \tag{3.18}$$

Expanding this expression gives the following partial differential equation for the integrating factor:

$$(a_2 a_3 - a_2 a_5 \lambda_i)\frac{\partial G_i}{\partial t} - a_1 a_3 \frac{\partial G_i}{\partial w} + \left(\frac{\partial\,(a_2 a_3 - a_2 a_5 \lambda_i)}{\partial t} - \frac{\partial a_1 a_3}{\partial w}\right) G_i = 0 \tag{3.19}$$

This partial differential equation is linear because a_k and λ_i are not functions of G_i [John, 1971]. The integrating factor can be determined by solving two ordinary differential equations for each combined potential.

$$\frac{dw}{dt} = \frac{-a_2 a_3}{(a_2 a_3 - a_2 a_5 \lambda_i)} \tag{3.20}$$

$$\frac{dG_i}{dw} = \left(\frac{\partial (a_2 a_3 - a_2 a_5 \lambda_i)}{\partial t} - \frac{\partial a_1 a_3}{\partial w} \right) \frac{G_i}{a_1 a_3} \tag{3.21}$$

where the second ordinary differential equation is integrated along the first ordinary differential equation. The first ordinary differential equation is the equation for constant combined potentials (Equation 3.14). The initial condition for G_i can be chosen arbitrarily so that the initial condition is nowhere parallel to the curves defined by the first ordinary differential equation. The integrating factor allows the combined potentials to be used like any other state property function because they can be determined by integrating Equations 3.20 and 3.21 in order to assign them numerical values.

The conservation of mass and energy equations can be written in terms of the combined potentials to give the following:

$$\frac{\partial F_i}{\partial \tau} + \lambda_i \frac{\partial F_i}{\partial z} = 0 \qquad\qquad i = 1, 2 \tag{3.22}$$

where λ_i is the speed of propagation of the F_i potential. Since the λ_i's are positive, Equation 3.22 is a system of hyperbolic partial differential equations.

The F_i potentials simplify not only the appearance of the conservation equations, but also the determination of equilibrium performance. In order to completely describe the performance of the desiccant, both lines of constant F_i and wave speeds, λ_i are required. Lines of constant F_i are plotted on psychrometric coordinates in Figure 3.2 for silica gel. Figure 3.2 is generated using a simplified representation of silica

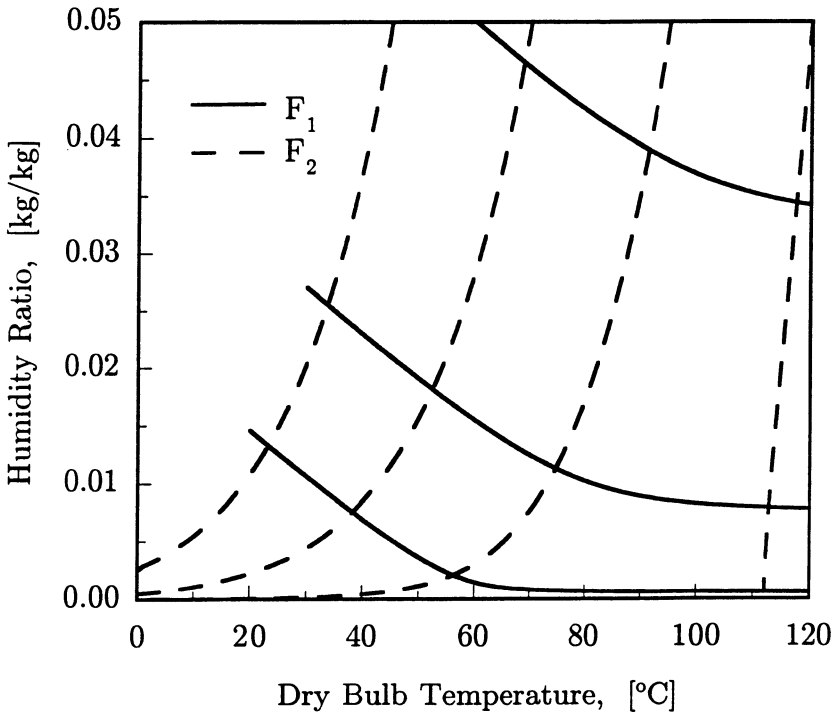

Figure 3.2: Lines of constant F_1 and F_2 for silica gel.

gel used by Jurinak [1984] and Van Den Bulck [1983] and is the nominal design parametric study later in this chapter. Each curve is generated by solving Equation 3.14 from an starting state point of temperature and humidity ratio.

3.3.2 Wave types

The outlet of the processing period is transient (or spatial in the case of a rotary device operating in periodic steady state); therefore, the wave speeds are an important aspect of the determination of desiccant performance. When air having a state different than that which is in equilibrium with the desiccant is passed through a desiccant matrix, two waves occur [Close, 1971]: 1) a fast wave in which both the temperature and humidity ratio decrease, and 2) a slow wave in which the temperature continues to decrease and the humidity ratio increases. The speeds of these waves are given by λ_i.

There are three types of waves: 1) expansion waves, 2) shock waves, and 3) waves with contact discontinuities. The air state changes as it passes through the desiccant matrix. If the wave speed decreases as a result of this change in air state, the wave spreads out and is called an expansion wave. Alternatively, if the wave speed increases the wave becomes a sharp discontinuity and is called a shock wave. Waves can also exhibit properties of both of these wave types if the wave speed is not strictly increasing or decreasing. These waves are said to have contact discontinuities [Pan, 1971; Knight, 1992].

The wave behavior of the adsorption or desorption process can be categorized in four possible ways: 1) both the fast and slow waves are expansion waves; 2) both the fast and slow waves are shock waves; 3) one of the waves is an expansion wave and the other is a shock wave; and 4) one or both of the waves have contact discontinuities.

3.3.3 Air Flow through a Regenerated Desiccant

During the dehumidification period of desiccant dehumidification operation, both waves are usually expansion waves. The first wave is significantly faster than the second wave; therefore, between the trailing edge of the fast wave and the leading edge of the slow wave is a region of constant temperature and humidity ratio, called the "intersection" state (temperature and humidity ratio). Within the waves the humidity ratio and temperature of the air change simultaneously; however, the combined potentials (i.e. F_1 and F_2) change independently. Figure 3.3 shows the waves of temperature and humidity ratio at specific time in the processing period, and the waves of F_1 and F_2 at the same dimensionless time. Figure 3.3 also shows that the intermediate state I has the same F_1 as the processing state (P), and the same F_2 as the reactivating state (R); therefore, state I is referred to as the intersection point. A chart of F_1 and F_2 makes determination of equilibrium performance as easy as

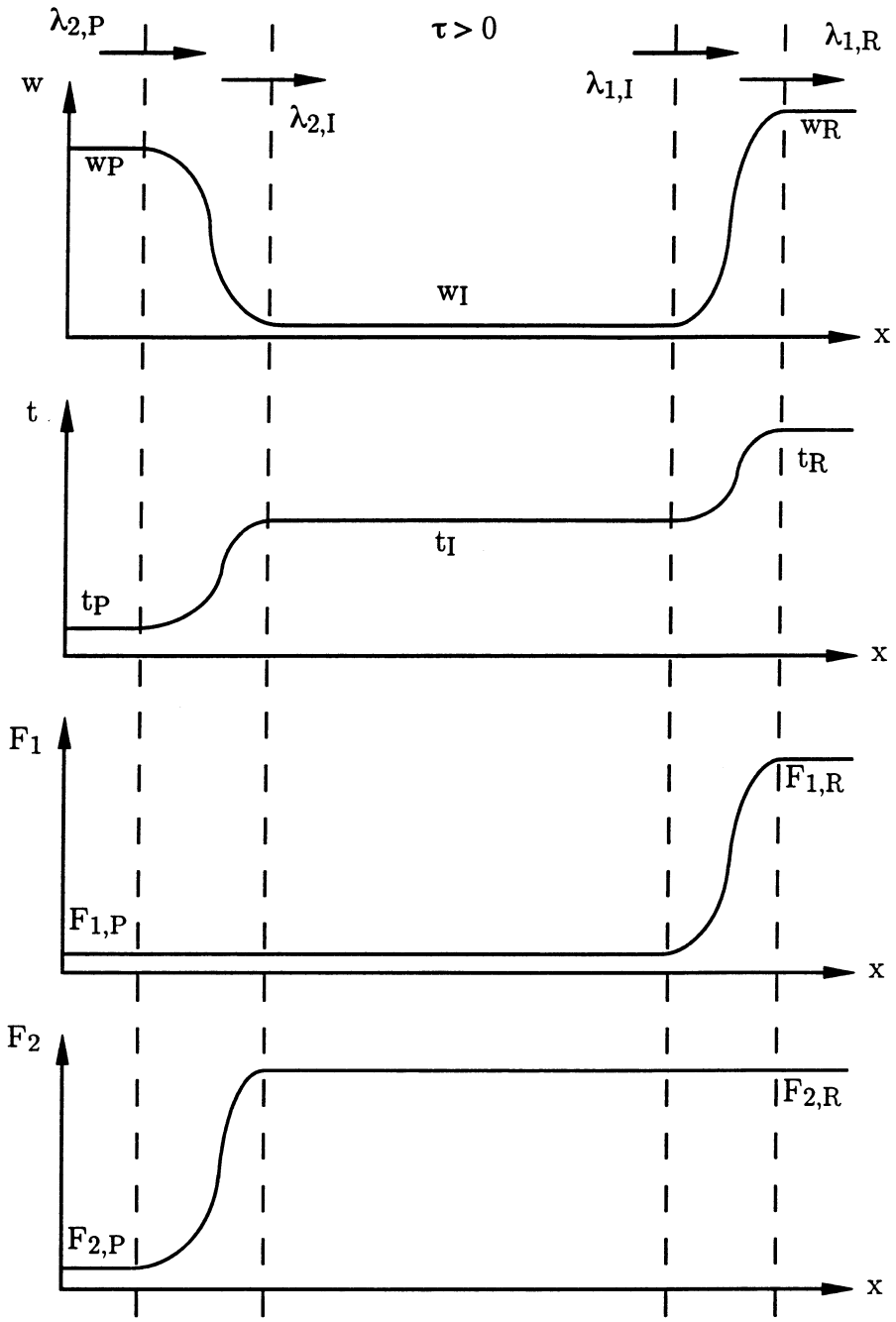

Figure 3.3: Waves of temperature, humidity ratios and combined potentials in space during the processing period.

finding the intersection of two lines (Figure 3.4). The waves shown in Figure 3.3 are both expansion waves, that is, the leading edge is moving at a speed greater than the trailing edge; therefore, the waves widen or "smear" as they pass through the desiccant matrix. The solution technique for this case is to solve Equation 3.14 to determine the outlet temperature and humidity ratio. The temperature and humidity profile for the fast wave is determined by solving along the line of constant F_2 equal to the F_2 of the fully reactivated desiccant matrix. The inverse of λ_1 determines the dimensionless time (Equation 3.3) at which that temperature and humidity ratio exits the desiccant. Similarly for the slow wave, the temperature and humidity ratio are determined by solving along the line of constant F_1 equal to the F_1 of the fully processed desiccant matrix and the inverse of λ_2 determines the dimensionless time at which that temperature and humidity ratio exits the desiccant. Figure 3.5 shows the outlet humidity ratio and temperature as a function of dimensionless time for this case.

3.4 Shock Wave Analysis

If the trailing edge speed of a wave is faster than the leading edge, a shock wave occurs [Lax, 1973; Van Den Bulck, 1983]. The method of characteristics (i.e. the F_1-F_2 charts) cannot be used to solve this case. Lax [1973] presents a method for solving this case. Similarly to the behavior to the expansion waves, a fast shock and a slow shock occur separated by a region of constant temperature and humidity ratio. Similar to the expansion wave speeds, λ_i, described in Section 3.3.1, the shock wave speeds are dimensionless. The speeds of the shocks are S_1 and S_2 for the fast and slow shock respectively. Van Den Bulck [1983] derived the following equations from integral conservation laws for mass and energy.

$$(w_s - w_a) = S_1 (W_s - W_a) \qquad (i_s - i_a) = S_1 (I_s - I_a) \tag{3.23}$$

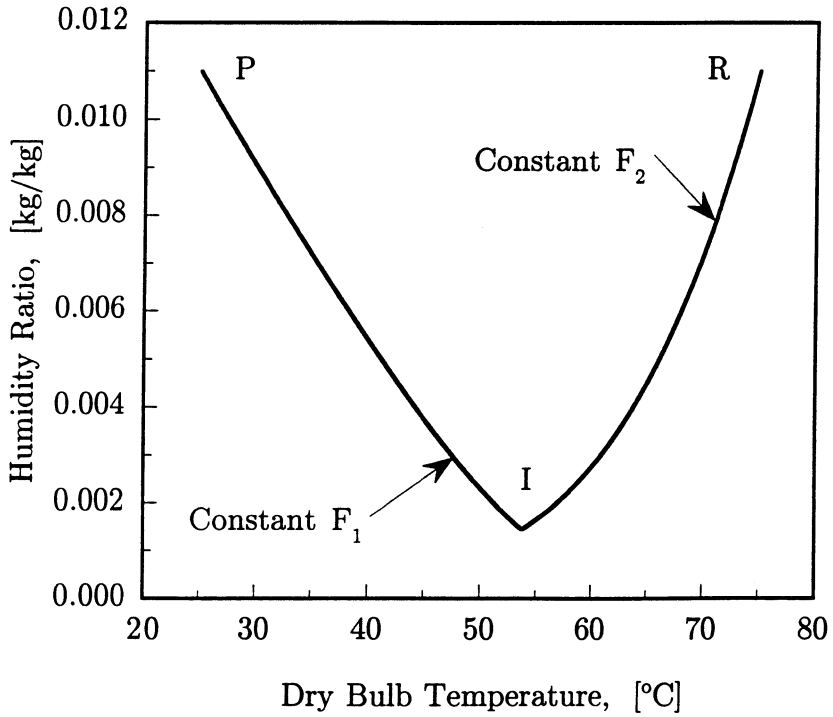

Figure 3.4: Determination of intersection point with F_i potentials.

$$(w_b - w_s) = S_2 (W_b - W_s) \qquad (i_b - i_s) = S_2 (I_b - I_s) \tag{3.24}$$

State a is before the first shock, state b is after the second shock, and state s is between the first and second shock (see Figure 3.6). Equations 3.23 and 3.24 are called the Rankine-Hugoniot jump conditions [Lax, 1973]. Elimination of the shock speeds from the equations allows the temperature and humidity ratio of the shock state, s, to be determined. Equations 3.23 and 3.24 provide two solutions of which one is physically possible. The shock wave speeds must satisfy the following constraints in order for the solution to be possible [Lax, 1973; Van Den Bulck, 1983].

$$\lambda_{1,a} < S_1 < \lambda_{1,s}$$

$$\lambda_{2,s} < S_2 < \lambda_{2,b}$$

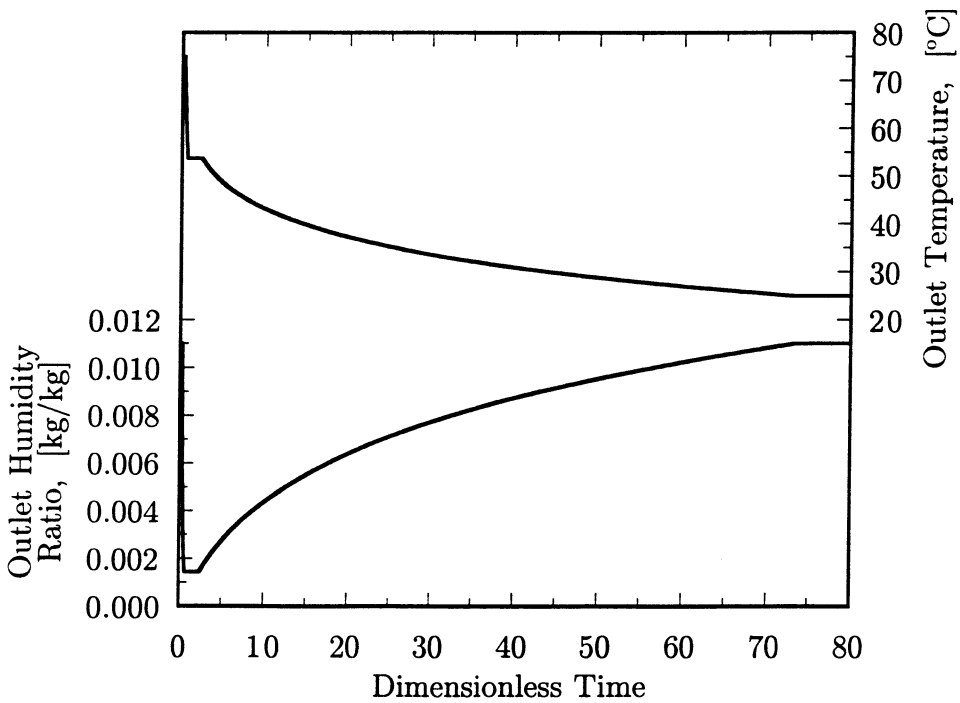

Figure 3.5: Outlet humidity ratio and temperature for two expansion wave case.

where the λ's are the wave speeds determined in the method of characteristics derivation. These conditions are called entropy conditions because in compressible flow problems they require that the entropy across a shock increases. Figure 3.6 shows the outlet temperature and humidity ratio as a function of dimensionless time is for the regeneration of silica gel.

Unlike the case of expansion waves, the shock wave speeds cannot be determined at a given temperature and humidity ratio. The shock wave speeds are dependent on both the initial condition of the matrix (temperature and humidity ratio in equilibrium with the process stream) and the regeneration temperature and humidity ratio.

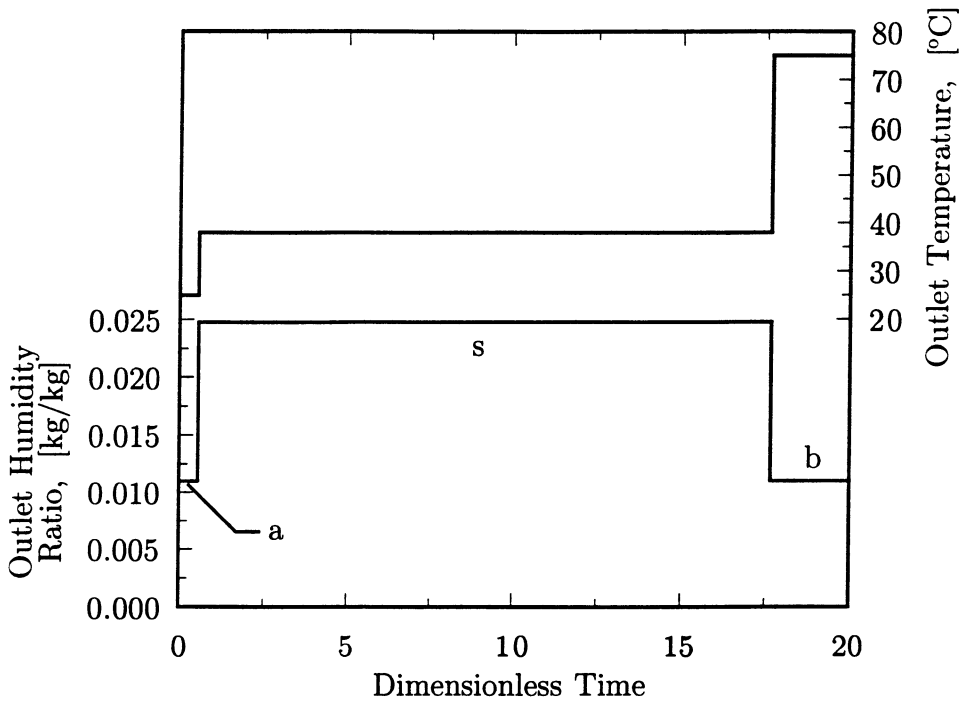

Figure 3.6: Outlet temperature and humidity ratio for two shock wave case.

3.5 Combination Wave Set

As stated earlier, it is also possible for one of the waves to be an expansion wave, and the other a shock wave [Pan, 1971]. In this case, the solution technique contains parts of both of the previous techniques. Equation 3.14 is used to solve for the expansion wave profile, and Equation 3.23 or 3.24 is used to solve for the shock wave. The intersection point is determined by solving these equations simultaneously. For example, if the fast wave is an expansion wave and the slow wave is a shock wave, the solution is determined by the following system of equations.

$$F_2\left(t_s, w_s\right) = F_{2,R}$$

$$\left(w_P - w_s\right)\left(I_P - I_s\right) = \left(W_P - W_s\right)\left(i_P - i_s\right)$$

where s is the state between the first and second wave. The shock wave speed, S_2, can be determined by substituting the states into either of the equations in 3.24.

3.6 Contact Discontinuities

The previous cases outline only waves that are of a single type; however, it is also possible for waves to exhibit behavior of both expansion and shock waves. For example, the wave starts as an expansion wave and at some point become a shock wave because the speeds are not strictly decreasing along the characteristic. This phenomenon is called a contact discontinuity [Pan, 1971; Knight, 1992]. The state at which the shock occurs is determined by the requirement that the expansion wave speed is equal to the shock wave speed. The solution to this case is complicated, but does not require any equations additional to those discussed earlier for both the expansion and shock waves.

The complexity arises from the determination of the ranges of application of each equation. For example, consider the process period for a desiccant whose first wave is an expansion wave and the second wave starts as an expansion wave but has a contact discontinuity at the trailing edge. The first wave (constant F_2 equal to the regeneration state, R) and beginning of the second wave (constant F_1 equal to the process state, P) are solved using the method of characteristics; however, at some point in the second wave the speed, λ_2, increases and the method of characteristics is no longer able to solve the problem. The point at which the speed increases is not the point at which the contact discontinuity occurs. It occurs such that the following equations hold:

$$(w_P - w_{CD})(I_P - I_{CD}) = (W_P - W_{CD})(i_P - i_{CD})$$

$$(w_P - w_{CD}) = S_2 (W_P - W_{CD})$$

$$\lambda_{2,CD} < S_2 < \lambda_{2,P}$$

where CD is the point at which the contact discontinuity occurs and lies on the same F_1 characteristic as the process state.

The previous example is relatively simple because contact discontinuity occurs at the end of the wave and between points on the same F_1 characteristic. A more complicated case has the contact discontinuity occur at the trailing edge of the first wave or the leading edge of the second wave, requiring solution of the shock equation between points on the $F_{1,P}$ and $F_{2,R}$ characteristics. Note that the state between the first and second wave in this case is *not* at the intersection of $F_{1,P}$ and $F_{2,R}$.

3.7 Effect of Desiccant Properties on Performance

The Dubinin isotherm form (Equation 2.2) with only a single term and an exponent of unity is used to investigate the effects of desiccant properties on the performance of a desiccant dehumidifier. This isotherm was chosen because it represents Type I to Type III isotherms well and the wave speeds do not result in contact discontinuities for a large range of isotherm types and total water contents. The isotherm form used is as follows:

$$W = W_{tot} \exp\left(-AP/E\right)$$

where W_{tot} is the total water content and E is the characteristic energy of adsorption and dictates the shape of the isotherm. The effect of E on the isotherm shape on both relative humidity and adsorption potential coordinates is shown in the Figure 3.7.

3.7.1 Adsorption

For the following parametric study, the definition of performance for the equilibrium adsorption process is the difference between the inlet and the intersection humidity

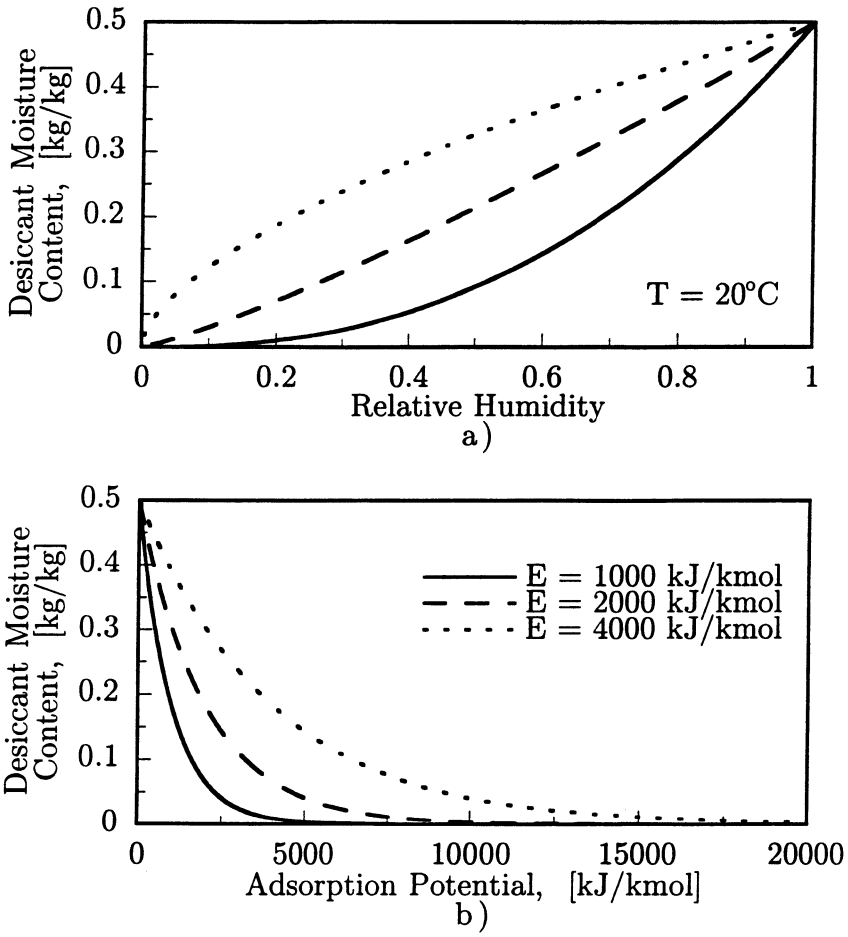

Figure 3.7: Effect of characteristic energy of adsorption, E, on the isotherm plotted versus: a) relative humidity, and b) adsorption potential.

ratios. This definition simplifies the analysis. In addition, the non-dimensional time difference at the intersection point (i.e. the time between the trailing edge of the first wave and the leading edge of the second wave) will also be considered because of its important in system sizing and operation strategy. Nominal values of the isotherm approximate properties of silica gel (E = 2000 kJ/kmol, W_{tot} = 0.50 kg water/kg dry desiccant and c_d = 1 kJ/kg-K) [Jurinak, 1984; Van Den Bulck, 1983].

Effect of Isotherm Shape on Performance

Figure 3.8 is a plot of the F_i potentials on psychrometric coordinates for a range of isotherm shapes. Figure 3.8 shows that as the isotherm becomes more similar to Type III (Figure 2.2), the F_1 characteristics become horizontal at higher temperature and lower humidity ratio (high adsorption potential) when plotted on psychrometric coordinates. The F_2 characteristic becomes vertical in the same area. These effects correspond to the lack of water adsorbing capacity in this region (high adsorption potential) for Type III desiccants. Figure 3.7 shows that at high adsorption potential a more Type III desiccants cannot adsorb any water. Therefore, a more Type I desiccant will have a higher potential for dehumidification for the same regeneration and process states.

In addition to the change in the shape of the characteristics, the speeds at which the waves propagate change. As the isotherm becomes more similar to Type III, Table 3.1, which summarizes wave speeds and intersection states for a range of isotherm shapes, shows that the first wave speeds up and becomes a shock wave and the leading edge of the second wave "breaks through" faster but the trailing edge is much slower. Therefore, the speed difference between the trailing edge of the first wave and the leading edge of the second wave decreases. This decreases the duration of the intersection state in Figure 3.3.

In addition to the decreased potential dehumidification capacity of Type III desiccants, the shorter duration at the intersection point means either that more mass of desiccant or a faster rotational speed is required for the same process air flow rate (Equation 3.3).

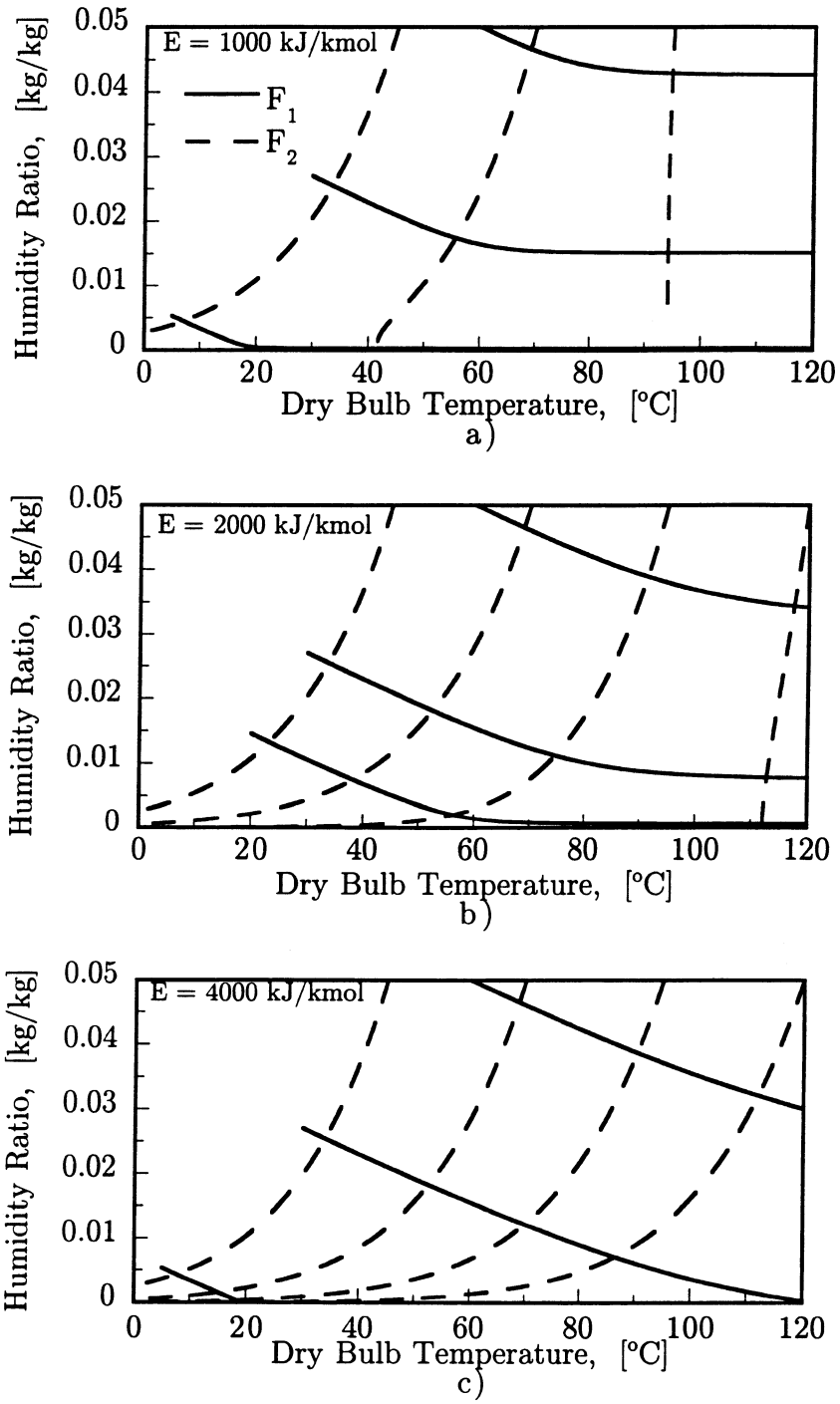

Figure 3.8: Characteristic charts for several isotherm shapes: a) a Type III desiccant, b) approximately silica gel, and c) a Type I desiccant. All other values nominal.

Table 3.1: Wave speeds and intersection state as a function of isotherm shape.

	$E = 1000$ kJ/kmol Type III	$E = 2000$ kJ/kmol Silica Gel	$E = 4000$ kJ/kmol Type I
	Regeneration State: 75°C, 11.0 g/kg		
λ_1	$S_1 = 108.6$	3.526	2.321
	Intersection State:		
t, °C	74.83	53.75	49.30
w, g/kg	4.391	1.440	2.258
λ_1	$S_1 = 108.6$	1.446	1.190
λ_2	1.003	0.413	0.049
	Process State: 25°C, 11.0 g/kg		
λ_2	0.0142	0.0136	0.0187

Effect of Total Water Content on Performance

As the total water content of the desiccant decreases, the change in the characteristics has the same effect as that of the Type III isotherm. This is shown in Figure 3.9 which is a plot of the F_i potentials plotted on psychrometric coordinates. Table 3.2 outlines the wave speeds and intersection states for a range of total water contents and illustrates that the intersection state is at both a higher temperature and humidity ratio. Therefore, desiccants with low total water content have decreased potential for dehumidification.

Table 3.2 also shows that desiccants with lower total water content display increased wave speeds for all states during the adsorption process. Note in the table that for the chosen isotherm form, the first wave has a contact discontinuity when the desiccant has a low total water content.

Decreasing the total water content increases both the speed at which the dehumidifier is rotated and the outlet temperature and humidity ratio. Therefore, desiccants with lower total water content have decreased potential for dehumidification and require more desiccant mass or increased rotation speed to process the same air flow

Table 3.2: Wave speeds and intersection state as a function of total water content.

	$W_{tot} = 0.125$ kg/kg	$W_{tot} = 0.500$ kg/kg
	Regeneration State: 75°C, 11.0 g/kg	
λ_1	7.244	3.526
	Intersection State:	
t, °C	70.86	53.75
w, g/kg	2.267	1.440
λ_1	$S_1 = 7.11$	1.446
λ_2	0.952	0.413
	Process State: 25°C, 11.0 g/kg	
λ_2	0.05315	0.01363

rate.

3.7.2 Desorption

While the dehumidification period is the desired effect of a system, regeneration plays a necessary and equally important role. Properties of the desiccant will effect the regeneration period of operation; therefore, neglecting their effect would lead to an incomplete assessment of the effect that the desiccant properties have on performance. Using the second (slow) shock wave speed as an assessment of the speed of regeneration, it can be concluded that desiccants that exhibit more Type III behavior and desiccants that have low total moisture contents will be the fastest to regenerate. This is concluded because the shock wave speeds are bounded by the expansion wave speeds on either side of the shock and both of these changes increase the wave speed λ_2.

3.8 Assessment of Adsorption Potential Theory

The advantages of the Dubinin adsorption potential theory are: 1) the temperature dependence of the isotherm and the heat of adsorption are accommodated; 2) rela-

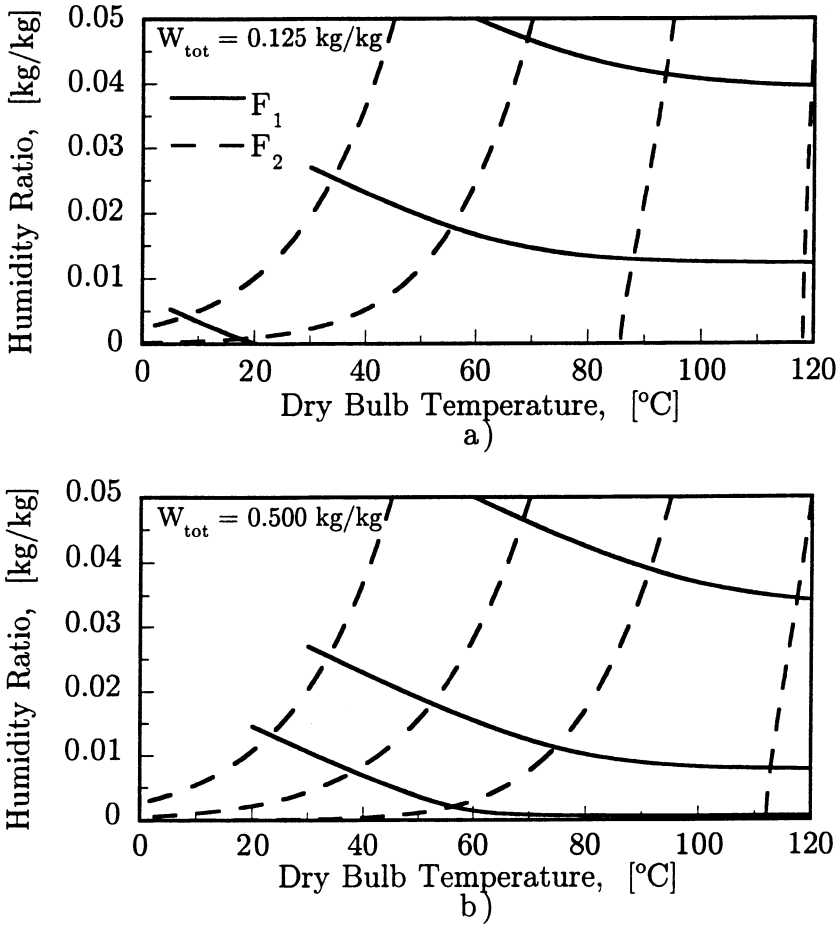

Figure 3.9: Characteristic charts for total desiccant water contents: a) W_{tot} = 0.125 kg/kg, and b) W_{tot} = 0.500 kg/kg. All other values nominal.

tively few parameters are needed to define the isotherm; 3) the theory is applicable to a wide range of desiccant types [Dubinin, 1975]; and 4) data for silica gel are replicated [Van Den Bulck, 1987]. The disadvantages are: 1) the heat of adsorption cannot be varied independently of isotherm shape; and 2) the wave behavior of isotherms with $n = 2$ and with isotherms with $n = 1$ and low characteristic energies of adsorption, E, and/or low total water content, W_{tot}, predicts combination and/or contact discon-

tinuity wave behavior which may or may not occur in reality. The advantages of the adsorption potential theory outweigh the disadvantages because the for applicable desiccants the heat of adsorption is correctly accounted for and non-infinite transfer coefficients diffuses the exact equilibrium wave behavior.

3.9 Conclusions

Although equilibrium behavior is impossible in real desiccant applications, the study of the equilibrium behavior of adsorption and desorption processes provides insight into the effect of desiccant parameters on dehumidifier performance. This will prove invaluable when evaluating non-equilibrium behavior.

The effects of desiccant isotherm shape and total water content were investigated and "linear" to Type I desiccants with relatively large total water contents were found to have advantages both in dehumidification capacity and parameters that effect sizing and operation.

A more detailed parametric study and assessment of the effects of the isotherm is left for the next chapter in order to include the effects of finite transfer coefficients and time-averaged values.

Chapter 4

Non-equilibrium Performance

Non-equilibrium performance is heat and mass transfer with finite transfer coefficients. Unlike equilibrium performance, which was solved using the Method of Characteristics, non-equilibrium performance evaluation must be solved with a numerical solution method like finite difference or finite element. The non-equilibrium cannot be solved with the Method of Characteristics because the assumptions required for transformation of the governing equations are not met, i.e. the combined potentials, F_i, are not linear functions of the moist air enthalpy and relative humidity and the heat and mass transfer coefficients are not infinite. A finite difference method was used to solve the non-equilibrium problem that allows more flexibility in simulation and a more completeness in parametric study.

4.1 Assumptions

The assumptions for non-equilibrium performance are identical to the equilibrium case discussed in Chapter 3 except that the requirement of desiccant matrix equilibrium with the contacting moist air is eliminated. The difference between the matrix and moist air state is defined with finite heat and mass transfer coefficients that are assumed to be uniform around the perimeter of the flow passage and constant over

the length of the dehumidifier. The resistance to both heat and mass transfer is assumed to be controlled by the air-side resistance.

4.2 Governing Equations

The governing equations for the solution of the non-equilibrium performance of a desiccant dehumidifier are the conservation of mass and energy along with the rate equations that define the transfer of heat and mass between the air stream and the desiccant matrix [Van Den Bulck, 1983, 1987; Jurinak, 1982; Zheng, 1993; Maclaine-Cross, 1974].

$$\dot{m}\frac{\partial w}{\partial x} + \frac{M}{L}\frac{\partial W}{\partial \theta} = 0 \tag{4.1}$$

$$\dot{m}\frac{\partial i}{\partial x} + \frac{M}{L}\frac{\partial I}{\partial \theta} = 0 \tag{4.2}$$

$$\dot{m}\frac{\partial w}{\partial x} = \frac{h_m A}{L}\left(w_{eq}\left(T, W\right) - w\right) \tag{4.3}$$

$$\dot{m}\frac{\partial i}{\partial x} = \frac{h_t A}{L}\left(T - t\right) + i_{wv}\frac{h_m A}{L}\left(w_{eq}\left(T, W\right) - w\right) \tag{4.4}$$

where i_{wv} is the enthalpy of water vapor. The desiccant isotherm is represented as $w_{eq}\left(T, W\right)$ in the mass transfer rate equation above. Non-dimensionalizing the system of governing equations results in the following:

$$\frac{\partial w}{\partial z} + \frac{\partial W}{\partial \tau} = 0 \tag{4.5}$$

$$\frac{\partial i}{\partial z} + \frac{\partial I}{\partial \tau} = 0 \tag{4.6}$$

$$\frac{\partial w}{\partial z} = Ntu_m\left(w_{eq}\left(T, W\right) - w\right) \tag{4.7}$$

$$\frac{\partial i}{\partial z} = \frac{h_t A}{\dot{m}}\left(T - t\right) + i_{wv} Ntu_m\left(w_{eq}\left(T, W\right) - w\right) \tag{4.8}$$

where the non-dimensional time, τ, and space, z, are defined as follows:

$$\tau = \frac{\theta \dot{m}}{M} \qquad z = \frac{x}{L} \tag{4.9}$$

The number of transfer units for mass transfer, Ntu_m, is defined as:

$$Ntu_m = \frac{h_m A}{\dot{m}} \tag{4.10}$$

Representing the enthalpy of the matrix with a first-order Taylor series expansion in temperature and water content, the conservation of energy equation (Equation 4.6) becomes:

$$\left.\frac{\partial i}{\partial t}\right|_w \frac{\partial t}{\partial z} + \left.\frac{\partial i}{\partial w}\right|_t \frac{\partial w}{\partial z} + \left.\frac{\partial I}{\partial T}\right|_W \frac{\partial T}{\partial \tau} + \left.\frac{\partial I}{\partial W}\right|_T \frac{\partial W}{\partial \tau} = 0 \tag{4.11}$$

Substitution of the conservation of mass (Equation 4.5) into the previous yields:

$$\left.\frac{\partial i}{\partial t}\right|_w \frac{\partial t}{\partial z} + \left.\frac{\partial I}{\partial T}\right|_W \frac{\partial T}{\partial \tau} + \left(\left.\frac{\partial I}{\partial W}\right|_T - \left.\frac{\partial i}{\partial w}\right|_t \right) \frac{\partial W}{\partial \tau} = 0 \tag{4.12}$$

Performing a similar operation with the moist air enthalpy on the energy rate equation (Equation 4.8) results in the following:

$$\left.\frac{\partial i}{\partial t}\right|_w \frac{\partial t}{\partial z} + \left.\frac{\partial i}{\partial w}\right|_t \frac{\partial w}{\partial z} = \frac{h_t A}{\dot{m}} (T - t) + i_{wv} Ntu_m \left(w_{eq}(T, W) - w\right) \tag{4.13}$$

Substitution of the mass transfer rate equation (Equation 4.7) and utilizing that $\partial i / \partial w|_t$ is equal to i_{wv} results in the following for the energy rate equation:

$$\frac{\partial t}{\partial z} = Ntu_t (T - t) \tag{4.14}$$

where Ntu_t is the number of heat transfer units and is defined as:

$$Ntu_t = \frac{h_t A}{\dot{m}\, \partial i / \partial t|_w} \tag{4.15}$$

4.3 Methodology

The finite difference method used to solve the governing equations follows Zheng and Worek [1993] and represents both time and space derivatives with central differences. The finite difference scheme is unconditionally stable and second order accurate in both time and space coordinates.

The governing equations are rearranged as follows:

$$\frac{\partial w}{\partial z} = Ntu_m \left(w_{eq} - w\right) \tag{4.16}$$

$$\frac{\partial W}{\partial \tau} = Ntu_m \left(w - w_{eq}\right) \tag{4.17}$$

$$\frac{\partial t}{\partial z} = Ntu_t \left(T - t\right) \tag{4.18}$$

$$\left.\frac{\partial I}{\partial T}\right|_W \frac{\partial T}{\partial \tau} = Ntu_m \left(\left.\frac{\partial i}{\partial w}\right|_t - \left.\frac{\partial I}{\partial W}\right|_T \right) \left(w - w_{eq}\right) + Ntu_t \left.\frac{\partial i}{\partial t}\right|_w \left(t - T\right) \tag{4.19}$$

The time and space derivatives are evaluated using a central difference scheme at the points $(n + 1/2, i + 1)$ and $(n + 1, i + 1/2)$ respectively. An example of this method is shown for Equations 4.16 and 4.17 respectively:

$$\frac{w_{i+1}^{n+1} - w_i^{n+1}}{\Delta z} = Ntu_m \left(w_{eq}{}_{i+1/2}^{n+1} - w_{i+1/2}^{n+1}\right) \tag{4.20}$$

$$\frac{W_{i+1}^{n+1} - W_{i+1}^{n}}{\Delta \tau} = Ntu_m \left(w_{i+1}^{n+1/2} - w_{eqi+1}^{n+1/2}\right) \tag{4.21}$$

where quantities at the center of time or space increments are evaluated as follows:

$$w_{i+1}^{n+1/2} = \frac{w_{i+1}^{n+1} + w_{i+1}^{n}}{2}$$

A first-order Taylor series expansion of the isotherm is used to linearize the governing equations [Zheng, 1993].

$$dw_{eq} = \left.\frac{\partial w_{eq}}{\partial T}\right|_W dT + \left.\frac{\partial w_{eq}}{\partial W}\right|_T dW \tag{4.22}$$

The full equation set is shown in Appendix C.

The solution method is to solve the system of equations (Equations 4.16-4.19) at each space node for the new time and then step in time. A backward space scheme is used to "start" the simulation and solve the first space node at each time.

4.4 Effect of Desiccant Properties on Performance

The effect of the desiccant equilibrium behavior on the non-equilibrium performance of a desiccant dehumidifier was determined for ranges of isotherm shapes, total desiccant water content and matrix specific heat. Desiccant performance is quantified by the minimum time-averaged outlet humidity ratio because it represents the maximum dehumidification capacity of a rotary heat and mass exchanger. Figure 4.1 shows the instantaneous and time-averaged outlet humidity ratio. A desirable criterion for choice of desiccant is a low minimum time-averaged minimum outlet humidity ratio.

The non-dimensional time at which the minimum time-averaged humidity ratio occurs and its fraction of the total non-dimensionless time are other important parameters because they relate to the total mass, M, of the dehumidifier required and/or the rotational speed, θ, of dehumidifier for a given mass flow rate. Considering both the processing and the regeneration periods, the total non-dimensional time is defined as:

$$\tau_{tot} = \tau_P + \tau_R \tag{4.23}$$

where

$$\tau_P = \frac{\theta \dot{m}_P}{M_P} \qquad \tau_R = \frac{\theta \dot{m}_R}{M_R} \tag{4.24}$$

If both the process and regeneration mass flow rates are equal and the desiccant mass is uniformly distributed throughout the matrix, then the matrix mass in a given

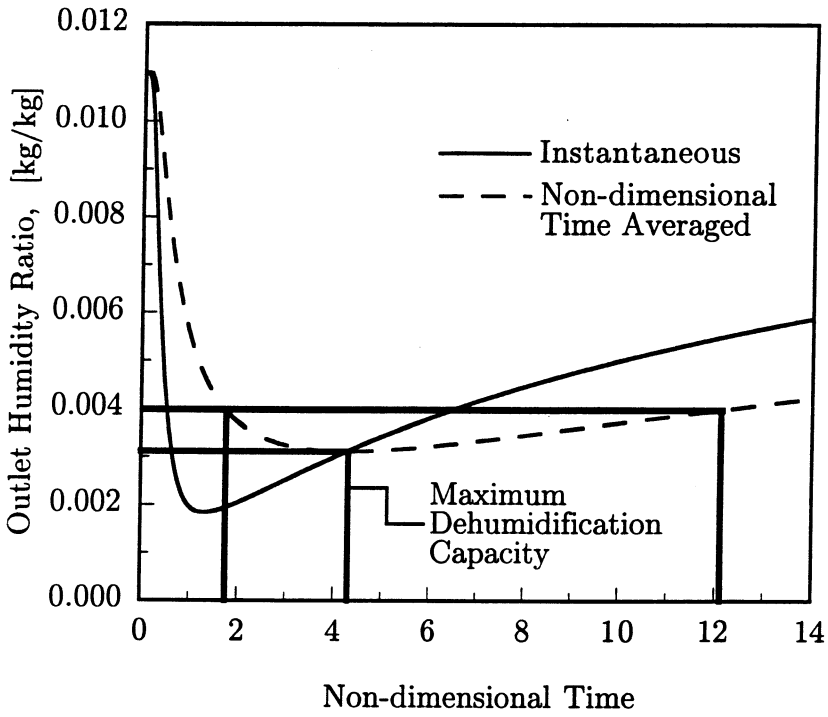

Figure 4.1: Minimum time-averaged outlet humidity ratio.

period can be written as the total matrix mass times the fraction of the total face area, $\mathcal{F}$, for that period. The non-dimensional time for the process period can be written as follows:

$$\tau_P = \frac{\theta \dot{m}_P}{\mathcal{F}_P M} \tag{4.25}$$

The dehumidification capacity is the most important aspect in sizing and operating a desiccant dehumidifier; therefore, both the non-dimensional processing time and the fraction of total face area for the process period are important in determining the total desiccant dehumidifier mass and rotation speed. The fraction of total face area for the process period was determined by taking the ratio of the process and total non-dimensional time after simulating both the optimum process period and regeneration period resulting in total regeneration. For a unit process period desiccant mass, an increased non-dimensional time means a larger mass flow rate of air can be processed,

or a higher time, θ. For a rotary dehumidifier, a higher time is equivalent to a slower rotation speed. An increased fraction, $\mathcal{F}_P$, results in smaller total dehumidifier mass because the fraction of the dehumidifier used to regenerate the desiccant is smaller. A desirable desiccant will have process period with a large non-dimensional time and fraction of total face area. The inverse of $\mathcal{F}_p$ is the total desiccant dehumidifier mass per unit mass of desiccant in the process period.

The initial desiccant matrix temperature and water content are assumed to be uniform and in equilibrium with the regeneration air state. The inlet processing air state was assumed to be constant. The regeneration state temperature is 75°, 125°, or 175°C and humidity ratio is 11 g/kg. The process state temperature is 25°C and humidity ratio is 11 g/kg. The dehumidifier was assumed to be counterflow (Figure 3.1) and the matrix was considered fully regenerated when the difference between the regeneration temperature and the outlet air temperature was less than 0.5% of the regeneration temperature. The number of transfer units for both heat and mass were assumed to be the same for both the process and regeneration periods.

A range of isotherm shapes, total water content and dry desiccant specific heat was investigated to determine the best desiccant properties for the processing period. The nominal value and the ranges are shown in Table 4.1. The nominal design approximates the silica gel properties used by Jurinak [1982] and Van Den Bulck [1983]. The total water content and specific heat are per mass of desiccant and supporting matrix (i.e. $f = 1$ in Equation 2.7).

The single sited Dubinin isotherm representation with an exponent of one was used and is defined as follows:

$$W = W_{tot} \exp\left(-A/E\right)$$

A high E value is more Brunauer Type I and a low E value is more Brunauer Type III (Figure 3.7).

4.4.1 Isotherm shape

The shape of the desiccant isotherm has been given much attention in attempts to improve desiccant dehumidification air-conditioning. According to Collier [1990] and Jurinak [1982] a Brunauer Type I isotherm shape is superior for adsorption. Figure 4.2 is a plot of the minimum time-averaged humidity ratio and the time-averaged temperature at the outlet of the dehumidifier over the range of isotherm shapes. Figure 4.2 shows that the most desirable performance (i.e. minimum time-averaged outlet humidity ratio) occurs at a moderate Type I ($E > 3000$ kJ/kmol) isotherm regardless of regeneration temperature; however, based solely on dehumidification capacity there are a wide range of acceptable isotherm shapes. Figure 4.2 also shows:

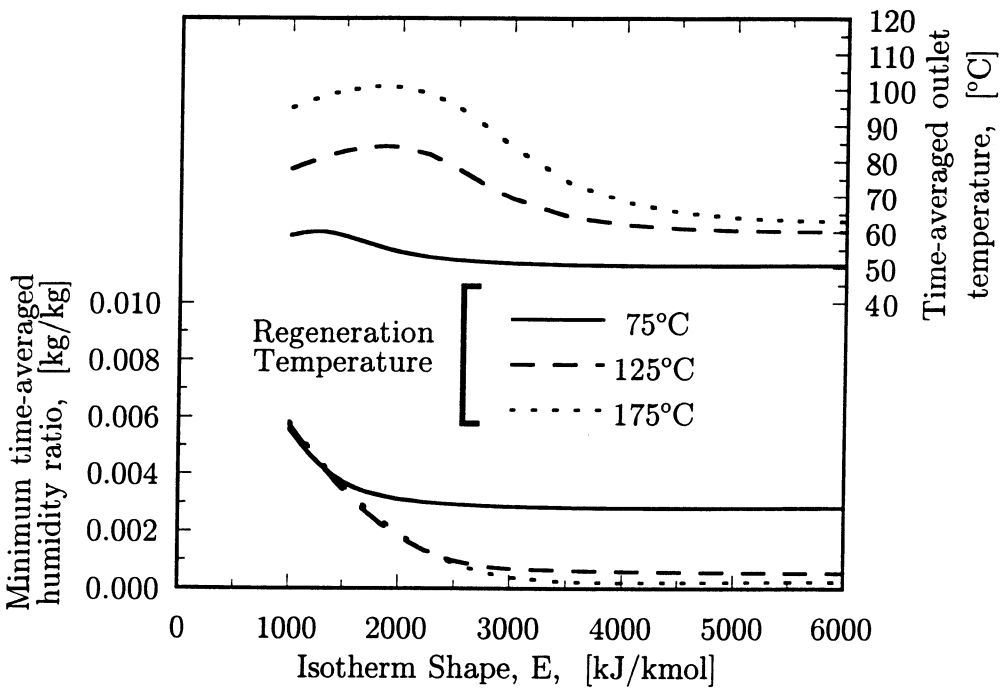

Figure 4.2: Minimum time-averaged outlet humidity ratio and temperature for range of isotherm shapes and regeneration temperatures. All other values nominal.

1) that the dehumidification capacity of desiccants with $E < 1500$ kJ/kmol (similar to Type III) is uneffected by increasing the regeneration temperature; 2) that for desiccants with $E > 1500$ kJ/kmol that an increase in the regeneration temperature from 75°C to 125°C increases the capacity of the dehumidifier; and 3) in order to be beneficial to increase the regeneration temperature to 175°C, the isotherm must be more Type I with an $E > 2500$ kJ/kmol.

Figure 4.3 is a plot of the process dimensionless time that gives optimum performance and the total mass of the dehumidifier per mass of the process section over the range of isotherm shapes. Figure 4.3 shows that the as the isotherm shape varies from more Type III to more Type I the non-dimensional time at which the minimum

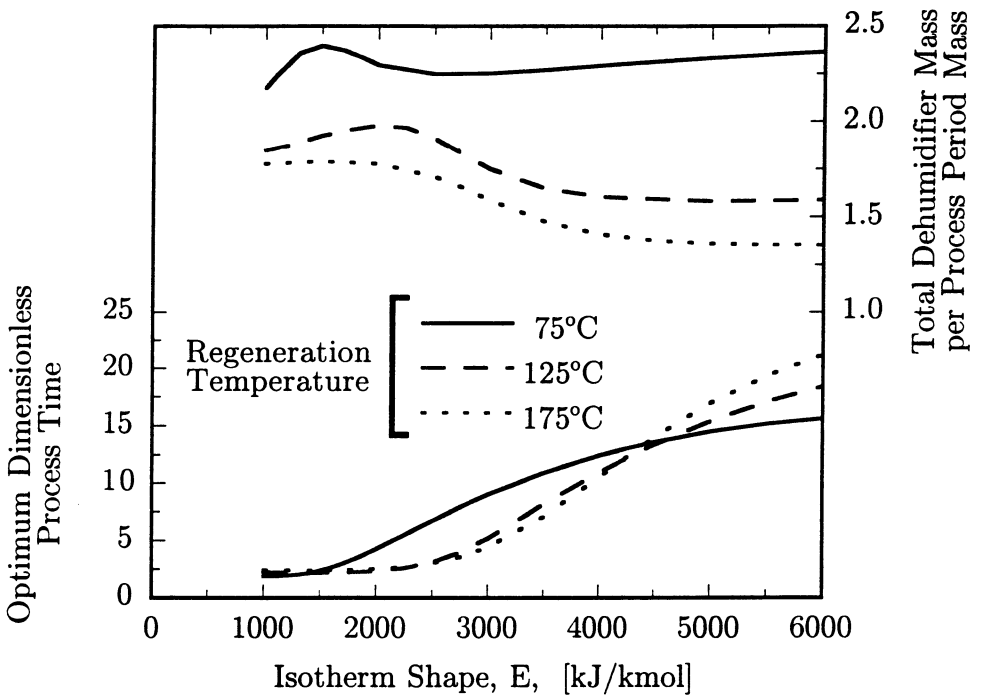

Figure 4.3: Optimum dimensionless time and total dehumidifier mass per unit process period mass for range of isotherm shapes and regeneration temperatures.

outlet humidity ratio occurs increases thus leading to a slower dehumidifier rotation speed or smaller desiccant wheel for all regeneration temperatures. Figure 4.3 also shows that the effect of isotherm shape and regeneration temperature on the total dehumidifier mass per unit process mass. For the regeneration temperature of 75°C, the isotherm shape does not have a large effect the total dehumidifier mass per process period mass; however, for the higher regeneration temperatures, a more Type I isotherm decreases the total dehumidifier mass per process period mass resulting in a smaller total dehumidifier mass.

A more Type I isotherm increases the dehumidification capacity for the entire range of regeneration temperatures considered and can result in a decreased rotation speed or increased process air flow rate and decreased total dehumidifier mass depending on combination of isotherm shape and regeneration temperature. These results are consistent with the findings of Jurinak [1984], Collier [1990] and Zheng and Worek [1993].

4.4.2 Total Water Capacity

The total water capacity, W_{tot}, is the amount of water that is adsorbed when the desiccant is in equilibrium with saturated air at any temperature. Figure 4.4, which is a plot of the minimum time-averaged humidity ratio and time-averaged temperature at the outlet of the dehumidifier for a range of desiccant total water capacities, shows that as the total water capacity of the desiccant increases, the dehumidification performance increases. Figure 4.4 also shows that the effect of increased regeneration temperature is more pronounced with desiccants with higher total water capacities. There is no dehumidification performance advantage to increasing the regeneration temperature from 125° to 175°C for the nominal isotherm shape. Figure 4.5 is a plot of the dimensionless time that results in optimum dehumidification performance and

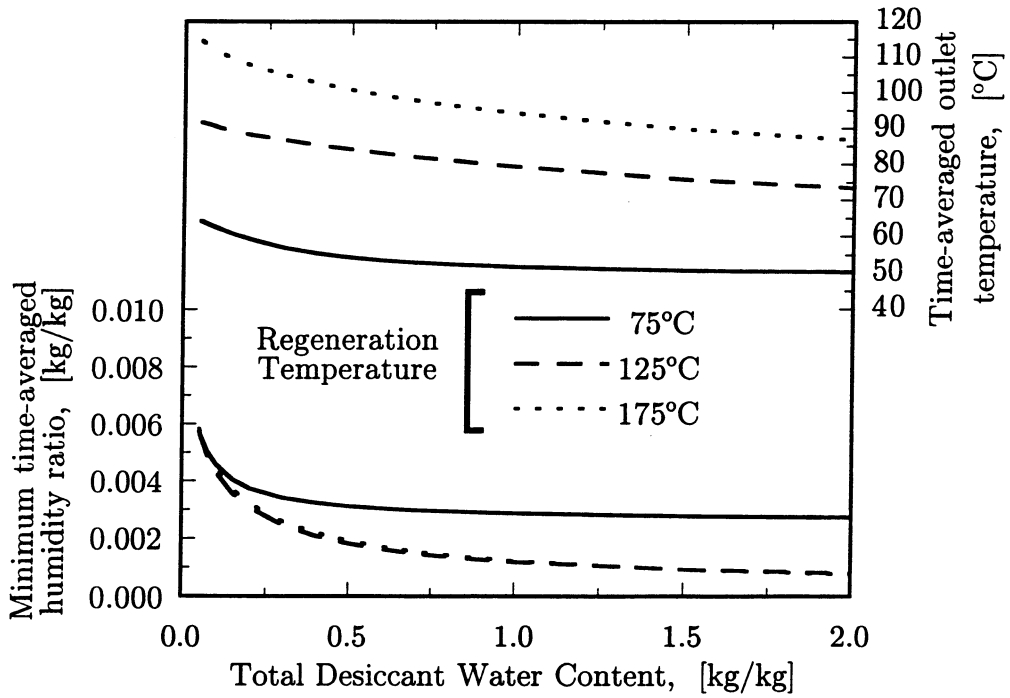

Figure 4.4: Minimum Time-averaged outlet humidity ratio and temperature for range of desiccant water capacities and regeneration temperatures. All other values nominal.

the total mass of the dehumidifier per mass process section for a range of desiccant total water contents. Figure 4.5 shows that the increased water capacity increases the optimal non-dimensional process time which increases the amount air mass flow rate per mass of process period mass or decreases the rotation speed of the rotary dehumidifier. These results are consistent with those of Jurinak [1984], Collier [1990], and Zheng and Worek [1993]. The total dehumidifier mass is reduced both as the total water capacity and regeneration temperature are increased. Although there was no capacity or non-dimensional process time increase when the regeneration temperature was increased from 125° to 175°C the total mass of the dehumidifier decreases.

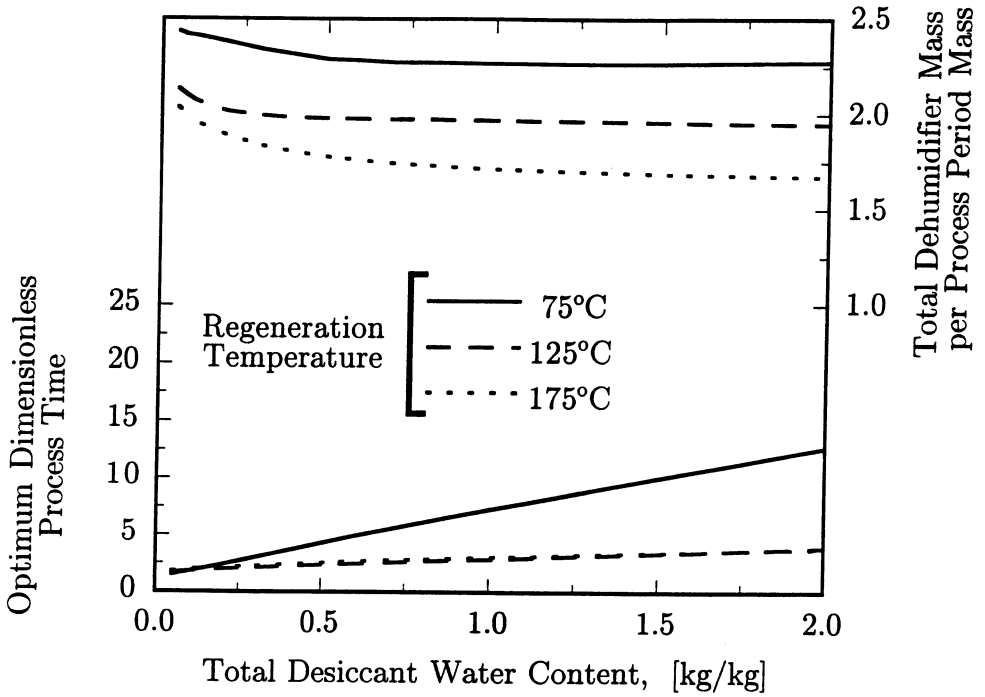

Figure 4.5: Optimum dimensionless time for the process period and total dehumidifier mass per unit process period mass for range of desiccant water capacities and regeneration temperatures.

4.4.3 Matrix Specific Heat

The specific heat of the matrix effects the enthalpy of the matrix (Equation 2.7) and the derivatives in the conservation of energy (Equation 4.19), which effects the temperature of the matrix and thus, the equilibrium water capacity of the desiccant. The matrix specific heat is defined as the total specific heat of the the desiccant specific heat and the non-adsorbing matrix. Figure 4.6, which is a plot of the minimum time-averaged humidity ratio and time-averaged temperature at the outlet of the dehumidifier over a range of matrix specific heats, shows that increased matrix specific heat reduces the dehumidification capacity of the desiccant and decreases the

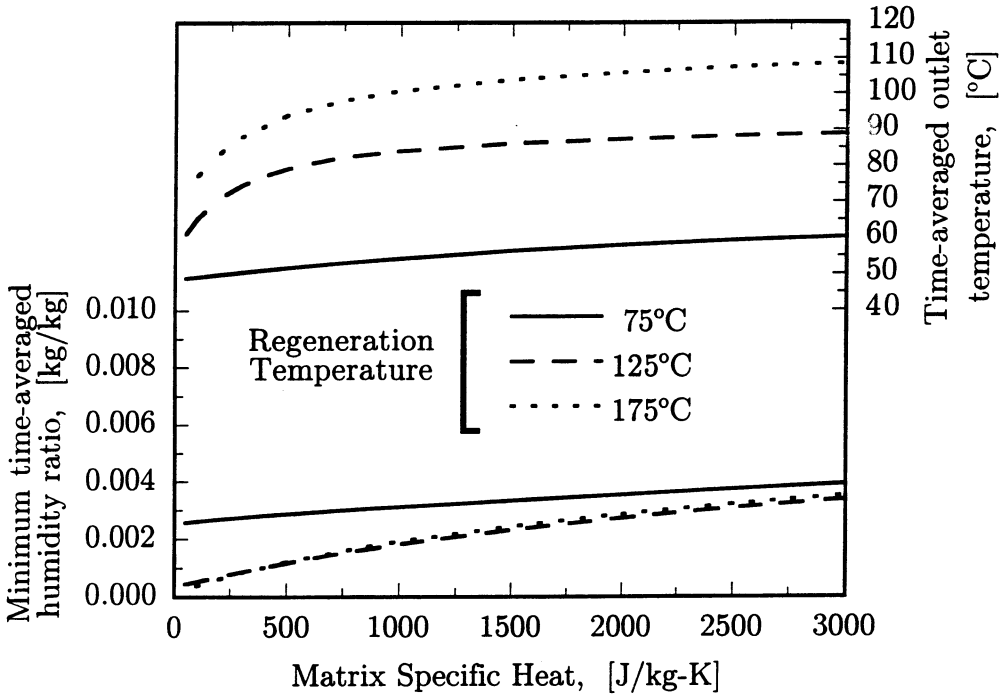

Figure 4.6: Minimum time-averaged outlet humidity ratio and temperature for a range of desiccant matrix specific heats and regeneration temperatures. All other values nominal.

advantage of increased regeneration temperature.

Figure 4.7 is a plot of the dimensionless time that results in optimum dehumidification performance and the total mass of the dehumidifier per process section mass. Figure 4.7 shows that although the dehumidification capacity is reduced as shown in Figure 4.6, the additional matrix thermal capacity increases the optimal non-dimensional time thus increasing the amount of process air mass flow rate or decreasing the rotation speed of the rotary dehumidifier. Increased thermal capacitance increases the total dehumidifier mass per unit process period mass. These results are consistent with those of Jurinak [1982, 1984] and Collier and Cohen [1991].

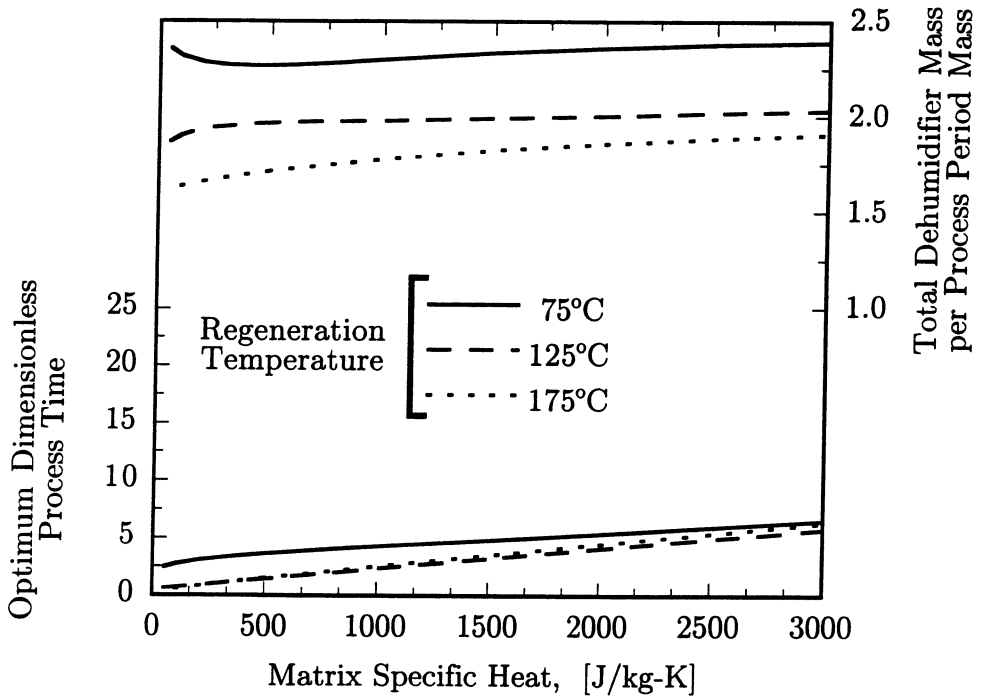

Figure 4.7: Optimum dimensionless process time and total dehumidifier mass per unit process period mass for a range of desiccant matrix specific heats and regeneration temperatures.

4.5 Effect of Transport Properties on Performance

In the previous section, the importance of desiccant properties was addressed; however, the transport properties, i.e. heat and mass transfer coefficients, are equally important. The number of transfer units for heat and mass transfer will be varied and their importance will be addressed.

4.5.1 Number of Heat Transfer Units

The number of heat transfer units affects both the temperature and humidity ratio of the outlet state since both temperature and humidity ratio effect the amount of

water that the desiccant can adsorb. As expected, the dehumidification capacity increases with increasing number of heat transfer units and an overall Lewis number held constant (so the number of mass transfer units increases as well).

Figure 4.8 is a plot of the minimum time-averaged humidity ratio and time-averaged temperature at the outlet for a range of number of heat transfer units. As expected, Figure 4.8 shows that as the number of transfer units are increased the dehumidification capacity is increased. A high regeneration temperature requires a high number of transfer units in order to realize the benefit of increased dehumidification capacity.

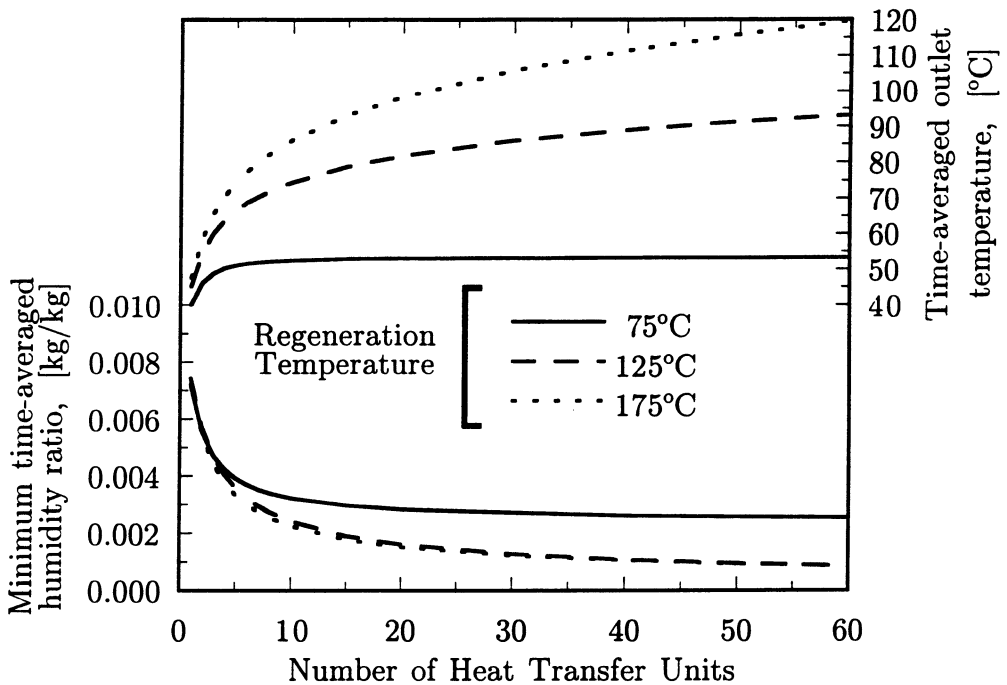

Figure 4.8: Minimum time-averaged humidity ratio for a range of number of heat transfer units and regeneration temperatures.

4.5.2 Overall Lewis Number

The overall Lewis number, Le_o, is the ratio of the number of transfer units for heat and mass transfer. Therefore, for a constant number of heat transfer units a change in the overall Lewis number is a change in the number of mass transfer units. Figure 4.9 is a plot of the minimum time-averaged humidity ratio and time-averaged temperature at the outlet of the dehumidifier over a range of overall Lewis numbers. As expected, the dehumidification capacity decreases as the overall Lewis number increases. The trends are independent of regeneration temperature. Similarly to the requirement that the number of heat transfer units must be high in order to realize the increased dehumidification capacity that results from increased regeneration temperature, the

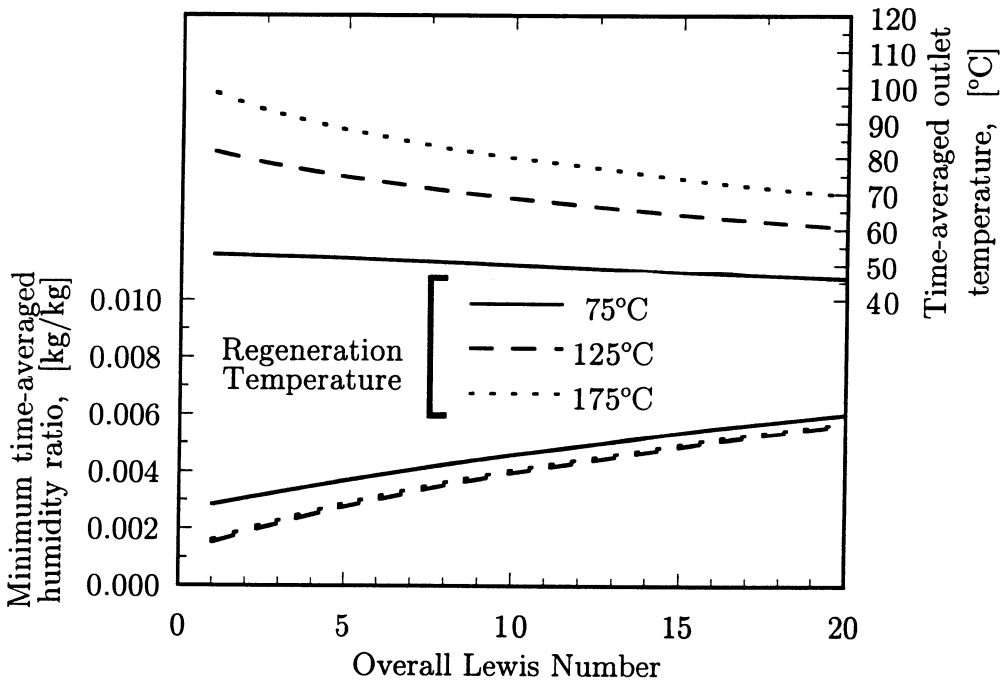

Figure 4.9: Minimum time-averaged humidity ratio for a range of overall Lewis numbers and regeneration temperatures.

overall Lewis number must be low (i.e. high number of mass transfer units).

4.6 Conclusions

The equations to solve for the non-equilibrium performance of a desiccant dehumidifier were developed and solved numerically. A parametric study on the effects of desiccant properties, transport properties and regeneration temperature on the performance of an optimally controlled counterflow rotary dehumidifier was performed.

The desiccant properties included in the study were the isotherm shape, total water capacity and matrix specific heat. It was found that a more Type I isotherm has several benefits: 1) increased dehumidification capacity, 2) smaller total dehumidifier mass per process period mass, and 3) lower rotation speed or increased process air flow rate.

Desirable desiccants have larger total water contents. The advantages were that the dehumidification capacity was increased slightly and the rotational speed was lower or the process air flow rate was higher.

Matrix thermal capacitance decreases the performance of the dehumidifier and increases the total dehumidifier mass per unit process period mass. However, added capacitance allows lower rotational speeds or increased process air flow rate.

Increased heat and mass transfer coefficients (higher number of transfer units and an overall Lewis number of unity) increase the performance of the dehumidifier.

Increased regeneration temperatures are advantageous because not only is the the dehumidification capacity increased, but the overall size of the dehumidifier is reduced. The effect of increased regeneration temperature is more pronounced for more Type I desiccants and high number of transfer units for both heat and mass transfer.

Table 4.1: Nominal design and ranges for parametric study.

	Ntu_t	Le_o	E kJ/kmol	W_{tot} kg/kg	c_d J/kg
Nominal	20	1	2000	0.50	1000
Low	0	1	1000	0.05	50.0
High	60	20	6000	2.00	3000

Chapter 5

Experimental Description

The purpose of the experiment is determine parameters needed to simulate the adiabatic operation of a rotary desiccant dehumidifier. The experiment is single blow and uses a commercially available desiccant matrix. In the single blow experiment, the outlet temperature and humidity ratio of the test section is measured as a function of time.

5.1 Matrix Specifications and Properties

The commercially available matrix consists of a myriad of triangular channels. The matrix was fashioned by winding a flat sheet (2.5 mil) of 1145 H19 aluminum and a corrugated sheet of the same aluminum stock around a spool approximately 15 cm (6 in) in diameter. The sheets had been previously coated on both sides by immersion in a liquid polymeric desiccant bath. The polymer coating was measured to be approximately 0.7 mil thick.

5.1.1 Experimental Test Section

To ensure adiabatic boundary conditions, a circular section of the larger matrix was extracted using a sharpened stainless steel pipe approximately 3.49 cm (1-3/8 in) in

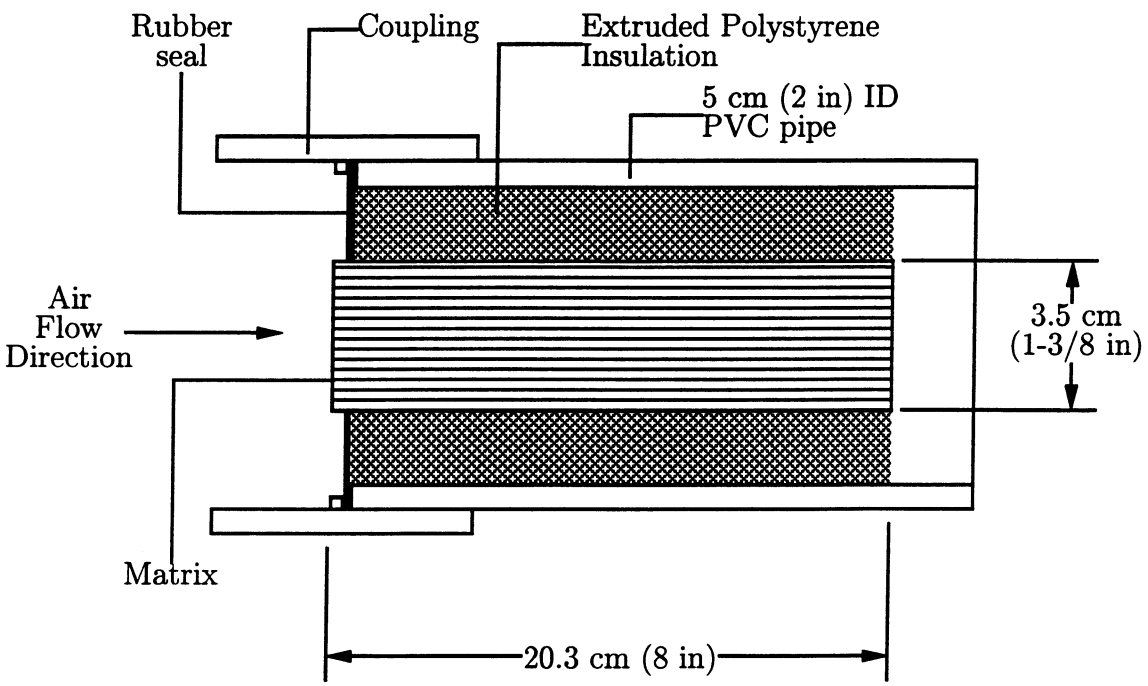

Figure 5.1: Matrix test section schematic.

diameter. The extracted piece is insulated by extruded polystyrene and fitted into a 5 cm (2 in) diameter PVC pipe. The assembled test section is shown in Figure 5.1. A rubber seal keeps the air from bypassing the matrix. The passages along the edge of the extracted section are fractional and could allow air to possibly bypass the matrix and flow through the space between the matrix and the insulation; therefore, these passages are filled with silicone sealant to keep air from flowing through them.

The number of passages and total mass of the 3.49 cm (1-3/8 in) diameter by 20.32 cm (8 in) deep extracted test section was measured to verify the measured passage dimensions. The test section has 290 active (full) passages and weighs 50.18 g (0.111 lb). The measured dimensions of a representative passage are shown in Figure 5.2. The thickness of the aluminum sheet and desiccant coating is 3.95 mil. The polymer desiccant coating has negligible mass compared to the aluminum matrix.

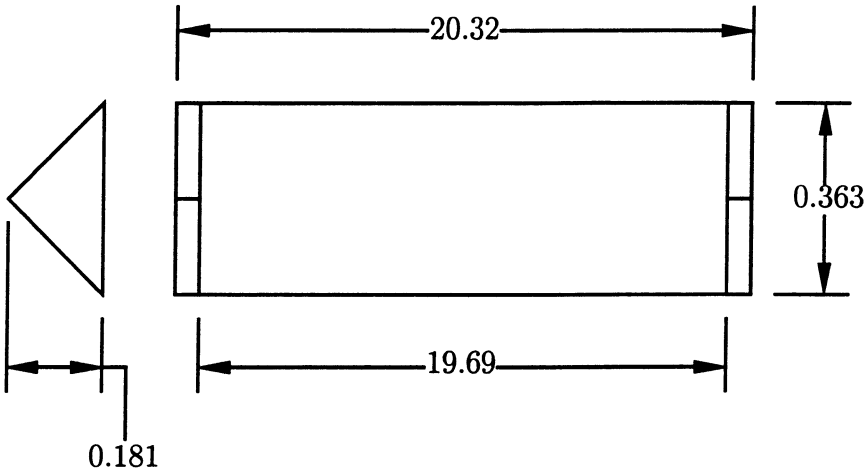

Figure 5.2: Measured passage dimensions. All values are in cm.

The thickness is assumed to be 2.5 mil and the density and specific heat of the matrix are thus assumed to be that of the pure aluminum sheet ($\rho = 2700$ kg/m^3 and $c = 900$ J/kg-K).

Comparison of the measured mass and the calculated mass from the geometric measurements and property assumptions yielded significantly different results. The calculated test section mass from the measured geometry, measured number of passages and assumed density and sheet thickness was 43.86 g (0.097 lb), compared to the measured value of 50.18 g. The density was checked on both coated and uncoated sheet samples to try to explain the discrepancy. A section of sheet was cut, weighed and dimensions were measured (thickness as assumed to be 2.5 mil). The samples ranged from 1 to 3 g total. The resulting densities were from 2% lower to 10% higher than the tabulated value for pure aluminum. Density measurements on a polymer desiccant coated sample resulted in similar densities to the uncoated aluminum. This confirms that the polymer contributed negligible mass.

Erroneous passage dimensions could also explain the discrepancy between the measured and calculated mass of the test section. Therefore, the total frontal area

was estimated from the passage dimensions shown in Figure 5.2. The tool used to extract the test section has an inside diameter of 3.49 cm (1-3/8 in). The calculated frontal area was 9.546 cm^2 (1.480 in^2) which compares well to the 9.580 cm^2 (1.485 in^2) area of the tool inside area.

The difference between the measured and calculated mass of the test section is due to neglecting fractional passages on the perimeter of the extracted matrix when the mass was calculated.

5.1.2 Calculated Matrix Properties

The quantities of interest to the thermal performance are the hydraulic diameter, the ratio of passage length to hydraulic diameter, the Reynolds number and the heat transfer coefficient.

The hydraulic diameter is 0.150 cm (0.0592 in). The typical face velocity for the experiment is 2.0 m/s (394 ft/min) resulting in a Reynolds number of approximately 200. The flow is considered fully developed when the L/D ratio is greater than approximately $0.05Re_D$ [Incropera, 1996], which is 10.0 for the Reynolds number approximation for the experiment. Since the L/D ratio for the matrix passage is approximately 540, the flow can be considered to be hydrodynamically fully developed.

Since the heat transfer coefficient is not known *a priori*, it is assumed that the Nusselt number based on the hydraulic diameter is provided by the fully developed laminar Nusselt number of a isosceles right triangular channel for a constant heat flux boundary condition [Van Den Bulck, 1987] of 3.05 [Abdel-Wahed, 1984]. For the geometry shown in Figure 5.2, the resulting heat transfer coefficient is 52.3 W/m^2-K and independent of air flow rate. For a air velocity of 2.3 m/s, the Ntu_t is 10.5. The temperature can be assumed to be uniform in the matrix perpendicular to the flow direction because the Biot number is less than 1.0×10^{-5}.

In order to check the assumption of constant Nu an uncoated matrix with the same passage geometry was subjected to a temperature pulse in time. The pulse was created with a brief step change of power to the electric resistance heater. Due to the capacitance effects in the heater and experimental flow passages, etc. the result is a pulse as opposed to a step change in temperature. The measured input to the matrix was used as the input to a finite difference program that models the transient response of a heat exchanger with adiabatic boundary conditions, negligible axial conduction and constant heat transfer coefficient subject to an arbitrary inlet temperature profile. Figure 5.3 is a plot of the experimental inlet and outlet temperature and the simulated outlet with the calculated number of heat transfer units of 10.5, aluminum matrix mass, and assumed physical properties of aluminum. Comparison of the experimental and simulated output is very good, especially at the beginning of the experiment. The maximum temperature difference between the experimental and simulated outlet is less than 0.5°C.

While the theoretical number of transfer units reasonably describes the experiment, the experiment is not very sensitive to the number of heat transfer units. If the number of heat transfer units is determined that best represents the experimental output data near the maximum outlet temperature, it is significantly lower than theory. The value that best represents the maximum temperature is an Ntu_t value of approximately 3, nearly 3.5 times smaller than the theoretical value of 10.5.

Three conclusions are drawn from Figure 5.3: 1) the experiment is not sensitive to heat transfer coefficient, 2) the fully developed heat transfer coefficient is a reasonable estimate for this matrix, and 3) the calculated matrix mass and measured mass flow rate accurately defines the time scale of the experiment.

Cai et. al. [1984] claims that for a step change in temperature input to test section the effect of axial conduction must be considered when the number of heat transfer

units, Ntu_t, is greater than 3 or heat conduction parameter of the solid material, $Ntu_t\lambda_l$, is greater than 0.06, where

$$\lambda_l = \frac{kA_m}{\dot{m}c_aL} \tag{5.1}$$

In the previous equation, k is the thermal conductivity of the matrix, A_m is the cross sectional area of the matrix available for heat conduction in the flow direction, $\dot{m}$ and c are the mass flow rate and specific heat of the air passing through the matrix, and L is the flow length of the test section. Since the number of heat transfer units and the aluminum matrix properties and air flow conditions of the experiment correspond to value of Ntu_t and $Ntu_t\lambda_l k$ of 10.55 and 0.39, axial conduction must be investigated. Figure 5.3 also shows the output with the effect of axial conduction. The effect of

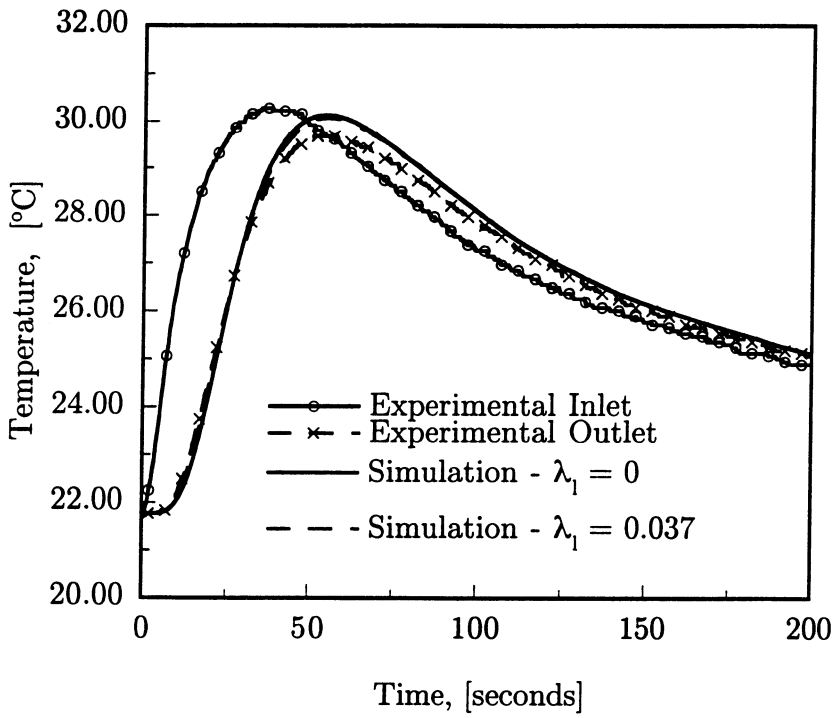

Figure 5.3: Comparison of experimental and simulated outlet response to an inlet temperature pulse test on a test section with no desiccant coating.

axial conduction is less that 0.1°C at all times. The effect of axial conduction in this case is insignificant because the inlet temperature rise is very spread out. Closer inspection of Cai et. al. [1984] showed that as the step inlet became more spread out the effect of axial conduction was reduced.

5.1.3 Polymeric Desiccant Isotherm

The desiccant coating on the aluminum sheet is a water based polymer. The desiccant isotherm was determined by Stiesch [1994] for temperatures of 5°, 22° and 40°C and is shown in Figure 5.4 as a plot of desiccant water capacity as a function of adsorption potential. Stiesch used the Dubinin [1975] adsorption potential theory, but relaxed the recommended form to include non-integer exponents. The resulting isotherm representation is

$$W = 0.03878 \exp\left(-\left(AP/618.9\right)^{0.4857}\right) + 0.04668 \exp\left(-\left(AP/193.5\right)^{1.546}\right) \quad (5.2)$$

where W has units of kg of water per kg of total (aluminum and desiccant) dry matrix and AP has units of kJ/kmol. Stiesch states that the accuracy of the measured isotherm data was approximately ±6%. The isotherm was verified by a series of single static sorption measurements at ambient temperature by the author from a portion cut from the experimental matrix. Figure 5.4 also shows the isotherm data from the extracted matrix plotted with Equation 5.2. The isotherm is Brunauer Type III and has a relatively low total moisture content of approximately 0.085 kg/kg.

5.2 Experimental Setup

The experimental setup schematic is shown in Figure 5.5. An equipment list for the experiment is found in Appendix D. Compressed air from the University of Wisconsin Physical Plant is used as the input to the experiment. The pressure of the compressed

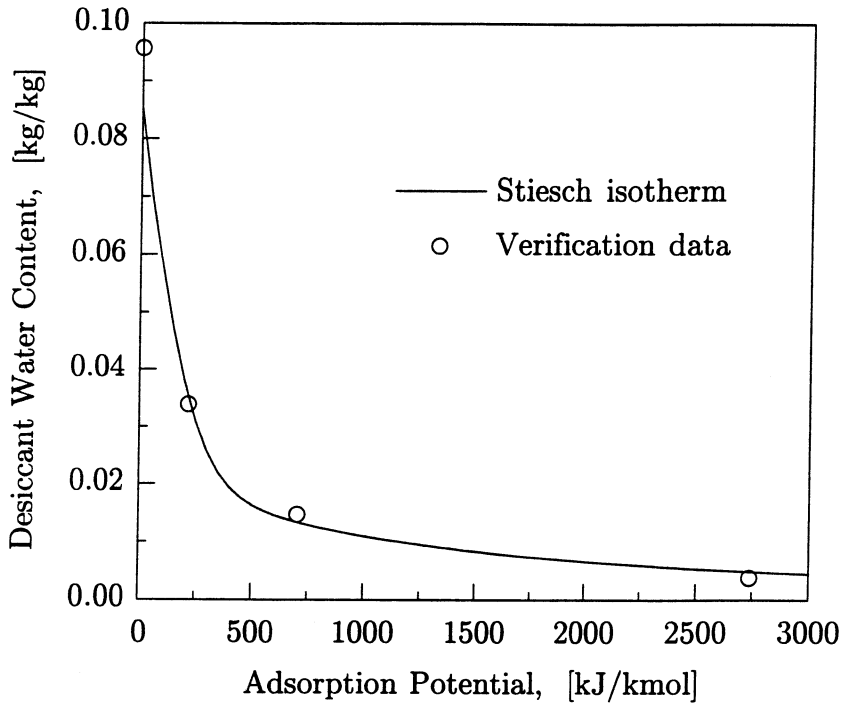

Figure 5.4: Polymer coated aluminum isotherm.

air line is approximately 690 kPa gauge pressure (100 psig). The air stream travels through either thick wall PVC pipe or Tygon tubing to the test section.

Depending on the whether experimentation of adsorption or desorption was being done, the dry air is either passed directly to the matrix test section or humidified before being passed to the matrix test section. The humidification is accomplished by bubbling the dry air stream through a temperature controlled column of water. Direction of the dry air stream is done with three valves. The valve at the outlet of the humidifier ensures that the pressure difference between the humid air above the water column and the dry air stream results in no flow and subsequent mixing of the two air states.

An electric resistance heater attached to a voltage regulator is used to manually increase the temperature of the air stream. This heater is used to keep the humid

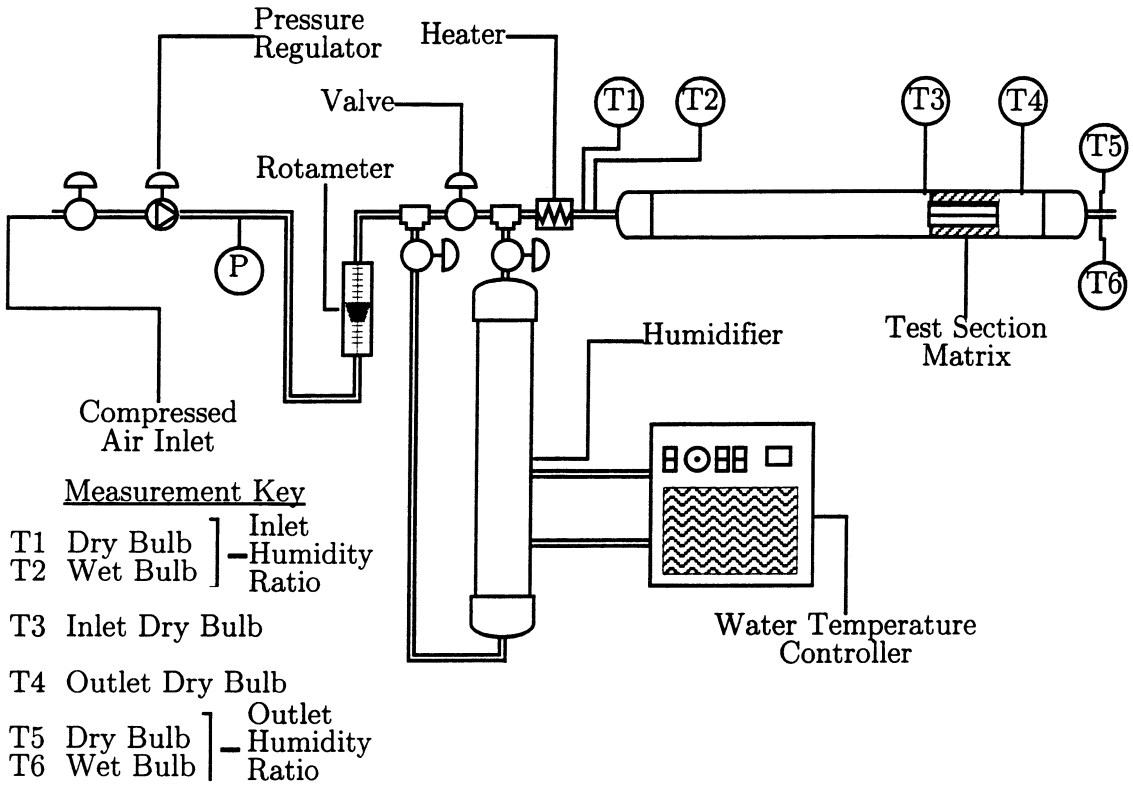

Figure 5.5: Schematic of the experimental setup.

air from being saturated and possibly condensing in the PVC pipe upstream of the matrix test section.

The air stream passes through several flow straightening devices before entrance to the matrix test section. Care was taken to choose materials that do not adsorb considerable water vapor.

5.2.1 Humidification Water Column

The dry air stream is humidified by bubbling it through a water column at a constant temperature. A schematic of the humidifier is shown in Figure 5.6. A 10 cm (4 in) diameter PVC pipe is sealed at both ends and filled approximately half full with water. The water is conditioned by temperature controlled heat transfer equipment

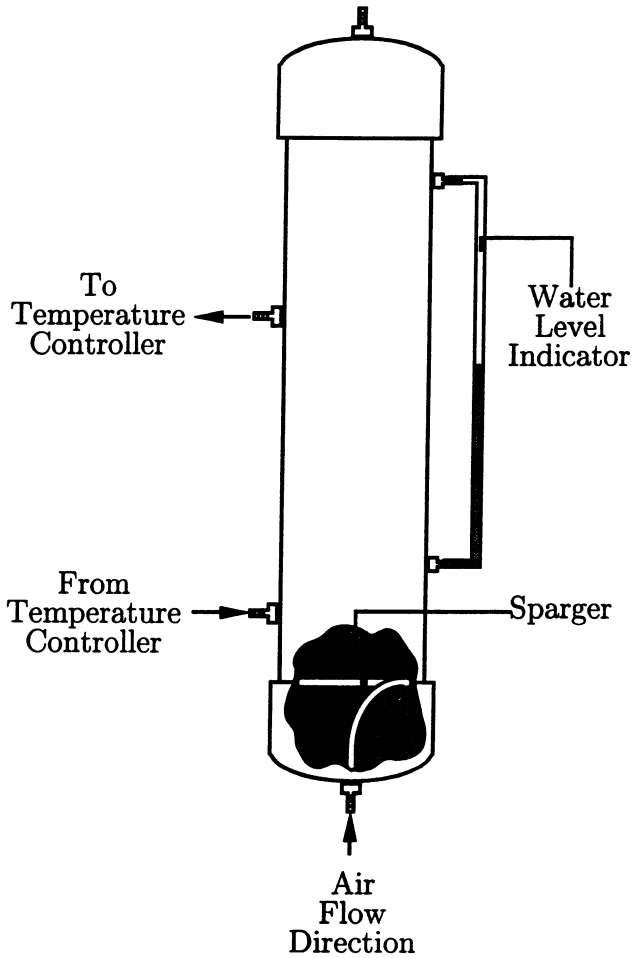

Figure 5.6: Humidifier schematic.

that can both add or remove energy. The air is passed through a "sparger" to ensure that the bubbles are small enough to effectively humidify the air. The pressure in the space above the water column is measured in order to verify the state of the exiting humid air stream.

5.2.2 Temperature Measurement

The experimental temperatures are measured with 0.02 in-diameter T-type (Copper-Constantan) thermocouples. The thermocouples are connected to a Keithley A/D

Board and the voltage difference between the thermocouple and reference junction is logged with LabTech Notebook. The voltage difference was measured rather than the absolute temperature to improve the incremental temperature measurement. Since LabTech Notebook uses a voltage range large enough to measure the entire temperature range of Type-T thermocouple measurement, the smallest increment in temperature was $\pm 0.6°C$. Measurement of voltage differences allowed measurement with a smaller voltage range resulting in an incremental temperature difference of $\pm 0.13°C$. These voltage differences are converted to temperatures by taking a temperature measurement with a Solomat MPM 500e to determine the reference voltage and then using the equation that converts the thermocouple voltage to temperature.

The thermocouples were positioned at the center of the flow area and subjected to a common air stream and the temperature was measured to determine any comparative bias between the thermocouples. Measurements were taken at 0.5 s intervals for 1000 s. The average of the six thermocouples at each measurement was assumed to be the *true* temperature. The air stream temperature varied less the 1°C during the measurements. The average difference between the true temperature and measured temperature for each thermocouple for the duration of the experiment is shown in Table 5.1. This is considered the bias error. The table also shows the standard deviation of the measurements after the bias is eliminated. Since the Keithley A/D board claims that the uncertainty of the reference temperature is $\pm 0.25°C$ and the average bias errors between the individual thermocouples are much smaller than this, the uncertainty of the dry-bulb temperature measurements is assumed to be $\pm 0.25°C$.

The location of the six temperature measurements on the schematic of the experiment are shown in Figure 5.5. The inlet and outlet humidity ratios are determined from dry and wet-bulb temperature measurements. The inlet and outlet dry-bulb temperatures are measured very close to the matrix. The humidity ratio is assumed

Table 5.1: Bias and random errors in thermocouple temperature measurement.

Location	Average Bias Error °C	Standard Deviation °C
Inlet Dry-Bulb	-0.005	0.039
Inlet Wet-Bulb	-0.051	0.051
Matrix Inlet	0.021	0.035
Matrix Outlet	0.022	0.033
Outlet Dry-Bulb	-0.076	0.042
Outlet Wet-Bulb	0.089	0.060

to be unchanged between the humidity ratio determination locations and the matrix.

The wet-bulb temperature measurement is done in the high velocity areas of the experiment to ensure accurate measurement. According to Tuve and Domholdt [1966], velocities of greater than 5 m/s (1000 ft/min) are required for the wet-bulb temperature to approach the adiabatic saturation temperature. Figure 5.7 shows a schematic of the dry and wet-bulb temperature measurement at the outlet of the test section. The inlet dry- and wet-bulb temperature measurements are done similarly. For a typical mass flow rate for the experiment, the velocity in the tygon tubing where the wet-bulb temperatures are measured is 15 m/s (3000 ft/min). The uncertainty of the wet-bulb temperature measurement is estimated to be ± 0.5°C. The uncertainty is greater than the dry-bulb temperature uncertainty because of the sensitivity to the placement of the thermocouple in the cotton wet-bulb sock.

The dry- and wet-bulb temperature of the dry air are approximately 22.5°C and 9.5°C respectively. The resulting calculated humidity ratio is 2.09 ± 0.46 g of water per kg of dry air. The humid air state was dependent on the experimental air flow rate. The higher the flow rate the higher the pressure above the water column in the humidifier and the lower the wet-bulb temperature relative to the dry-bulb temperature. For a wet-bulb temperature of 20°C, the humidity ratio is 13.65 ± 0.68 g/kg (dry-bulb temperature is equal to that of the dry air).

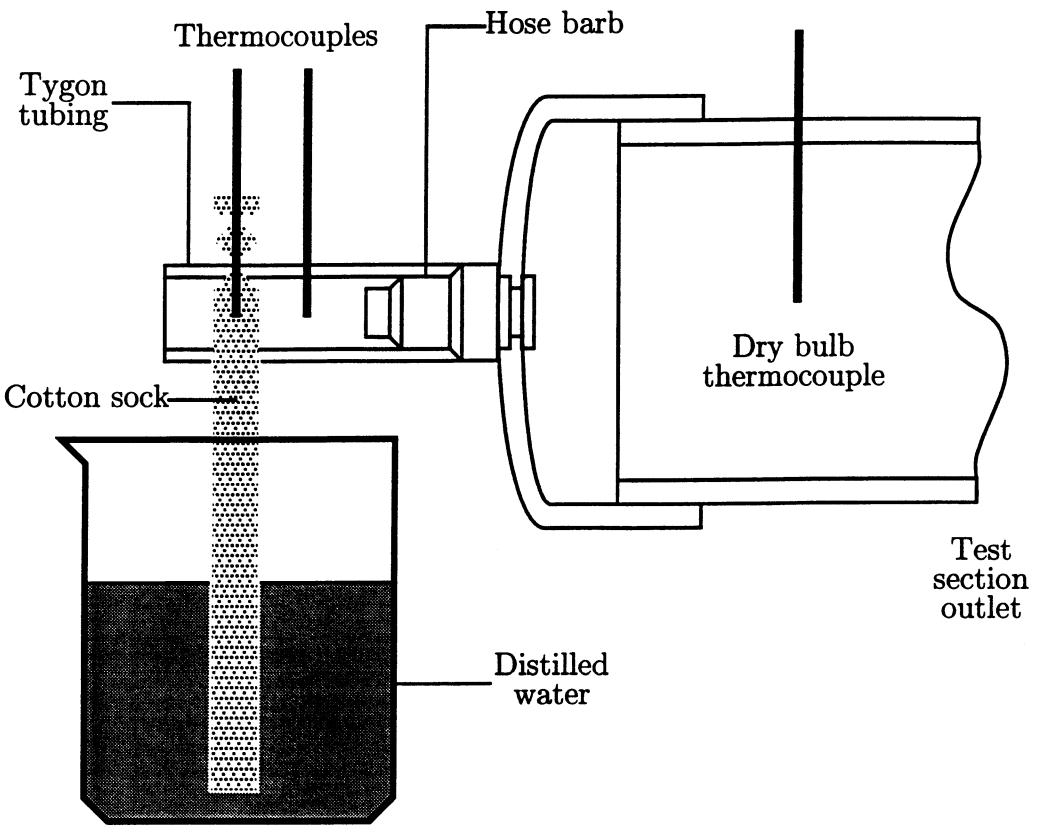

Figure 5.7: wet-bulb temperature measurement.

The humidity ratio was determined at the inlet and outlet of the experiment. The two measurements agreed for high wet-bulb temperature (high humidity ratio), but did not agree for low wet-bulb temperature. The wet-bulb temperature measurement was always higher than the outlet wet-bulb temperature during both the steady state portions of the experimental measurements. While the means of measurement of the wet-bulb temperature are nearly identical, the inlet wet-bulb measurement has a tighter seal to avoid air leakage than the outlet. The seal limits the water available to maintain the saturation of the wet-bulb sock and results in an artificially high wet-bulb measurement. Therefore, the inlet calculated humidity ratio is adjusted to agree with the outlet calculated humidity ratio at both the humid and dry steady state

values. Values between these values are adjusted by linearly interpolating between the two steady state adjustments.

5.2.3 Mass Flow Rate Measurement

The air mass flow rate is determined from measurements of the volume flow rate with a rotameter and the inlet pressure. The uncertainty is ±2% of the full scale reading of 20.5 scfm. The mass flow rate of the air is determined with the following relation which accounts for inlet pressure different from standard conditions of 21.1°C (70°F) and 101.3 kPa (14.7 psia):

$$\dot{m} = \rho \dot{V} \sqrt{\frac{\rho_{std}}{\rho}} \tag{5.3}$$

where $\dot{V}$ is the volume flow rate displayed on the rotameter and ρ_{std} and ρ are the air densities at standard and actual conditions respectively. The typical volume flow rate is 4 ± 0.41 cfm.

5.3 Conclusions

In conclusion, an experimental setup was built to measure the time dependent performance of a commercially available desiccant matrix. The isotherm measured by Stiesch was verified with single static sorption measurements at ambient temperature.

The dimensions of the triangular passages and the properties were determined for the matrix. The hydrodynamic conditions of the experiment are fully developed laminar flow. The heat transfer coefficient can be determined from the fully developed laminar flow Nusselt number for a triangular passage with a constant heat flux boundary condition and used to predict the transient heat transfer process; however, the experiment to verify the heat transfer coefficient was reasonably simulated with a wide range of heat transfer coefficients.

The uncertainty of the temperature measurements is ±0.25° and ±0.5°C for dry- and wet-bulb temperature measurement respectively. The uncertainty in the volume flow rate is approximately ±0.4 cfm.

Chapter 6

Experimental Procedure and Discussion of Results

In desiccant air-conditioning systems, desiccant dehumidifiers are regenerated with relatively hot, dry air and processed with cool, humid air. For the regeneration period, the desiccant is initially cool and relatively saturated with water and the inlet air temperature is high. For the process period, the desiccant is initially hot and dry and the inlet air is cool and humid. These conditions exhibit a maximum or minimum in outlet humidity ratio for the regeneration and process periods respectively. An experiment using these boundary and initial conditions would require a fast, accurate measurement of humidity ratio of the outlet of the test section. Fast, accurate measurement of humidity ratio is more difficult and expensive than the measurement of dry-bulb temperature; therefore, an alternative methodology was implemented for the experiment such that the outlet dry bulb temperature was the more important measurement. A description of the procedure, simulated outlet profiles and a discussion of the experimental results is presented. Two sub-experiments are described: 1) an inlet humidity step up with a constant temperature, and 2) an inlet humidity step down with a constant temperature.

6.1 Experimental Results

The procedure and results are presented for both the humidity step up (adsorption) and the humidity step down (desorption) experiments.

6.1.1 Experimental Procedure

The desiccant matrix is initially regenerated with a dry air stream from the compressed air line provided by the University of Wisconsin Physical Plant. The air temperature and humidity ratio werr approximately 22°C and 1 g water per kilogram of dry air respectively. Once regenerated fully, the temperature measurements are started and the air stream is directed through the humidifier. After the test section is fully processed, the air stream bypasses the humidifier and the test section is regenerated with the dry air. Each experiment contains a humidity step increase and a humidity step decrease. The electric resistance heater is used to ensure that the dew point of the humid air is higher than any of the experimental surfaces so that condensation does not occur.

6.1.2 Humidity Step Increase: Adsorption Experiment

Table 6.1 shows the experimental conditions for the experiment and the calculated number of transfer units for heat transfer as outlined in Section 5.1.2. Figure 6.1a shows the inlet and outlet temperature profiles as a function of time for an inlet humidity step experiment.

The maximum temperature rise across the matrix occurs 30 s after the beginning of the humidity step increase and is approximately 5°C. The test section is fully processed approximately 500 s after the humidity step increase occurs. Figure 6.1b is a plot of the outlet temperature and humidity on psychrometric coordinates. Immediately (less than 5 s) after the humidity step is implemented, the outlet humidity

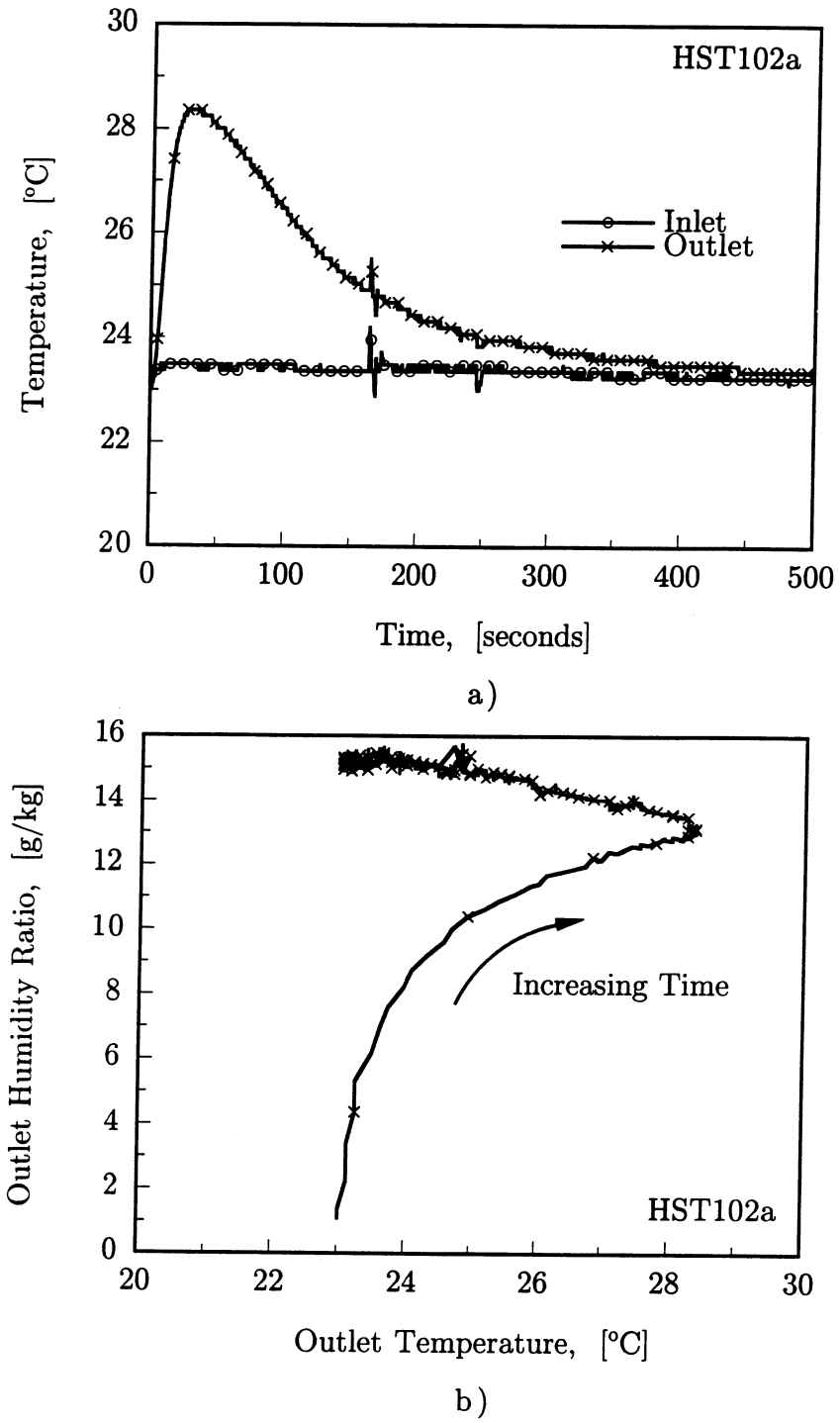

Figure 6.1: Adsorption experimental inlet and outlet results.

Table 6.1: Experimental conditions for an adsorption experiment (HST102a).

Quantity	Value	Units
Measured Values		
Initial Temperature	23.0	°C
Initial Humidity Ratio	1.1	g/kg
Passage Mass Flow Rate	7.5 x 10^{-7}	kg/s
Final Temperature	23.0	°C
Final Humidity Ratio	15.1	g/kg
Calculated Values		
Ntu_t	12.4	

Table 6.2: Experimental conditions for a desorption experiment (HST102d).

Quantity	Value	Units
Measured Values		
Initial Temperature	23.0	°C
Initial Humidity Ratio	15.1	g/kg
Passage Mass Flow Rate	7.8 x 10^{-7}	kg/s
Final Temperature	23.0	°C
Final Humidity Ratio	1.1	g/kg
Calculated Values		
Ntu_t	11.6	

ratio increases and the outlet temperature is unchanged. Since the temperature rise is caused by the liberation of the heat of adsorption, the lack of temperature rise indicates that very little mass is transferred during the very early stages of the experiment.

6.1.3 Humidity Step Decrease: Desorption Experiment

Table 6.2 shows the experimental conditions for the desorption experiment and the calculated number of heat transfer units. Figure 6.2a shows the inlet and outlet temperature profiles as a function of time for an inlet humidity step experiment.

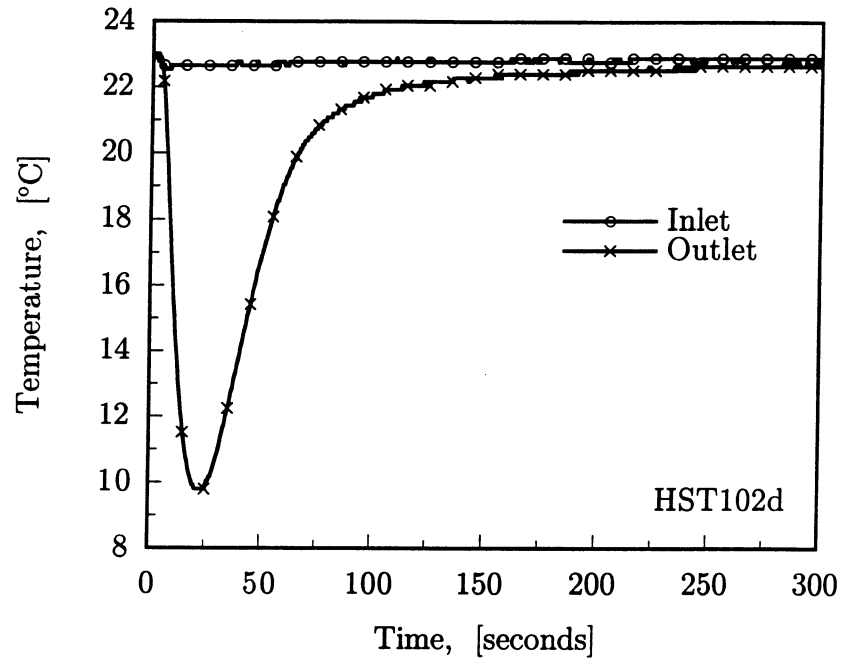

a)

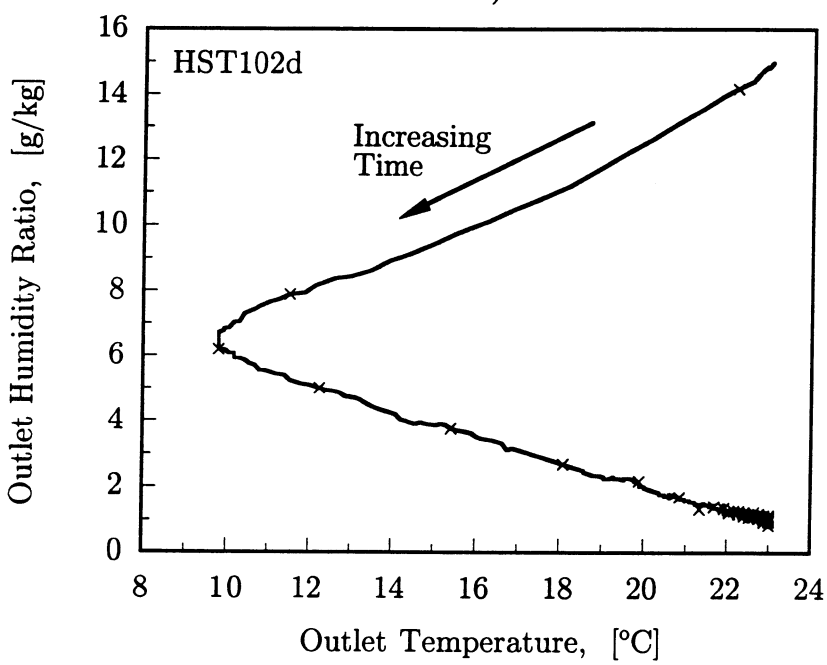

b)

Figure 6.2: Desorption experimental inlet and outlet results.

The maximum temperature drop across the matrix occurs 22 s after the beginning of the humidity step decrease and is approximately 13°C. The test section is fully regenerated in approximately 150 s. Figure 6.2b is a plot of the outlet temperature and humidity on psychrometric coordinates. Unlike the adsorption experiment, immediately after the humidity step decrease is implemented, the outlet humidity ratio is equal to that of the air stream that processed the test section and the outlet temperature drops. The large humidity difference between the inlet and outlet and the associated temperature drop indicates that mass is transferred during the very early stages (less than 5 s) of the experiment.

6.1.4 Experimental Repeatability

Since neither the temperature or humidity ratio is precisely controlled, the repeatability is as good as the agreement of the initial test section temperature and humidity ratio and the steady state temperature and humidity ratio between experiments. Figure 6.3 is a plot of experimental outlet temperature as a function of time and the experimental outlet temperature and humidity ratio on psychrometric coordinates for two adsorption and desorption experiments. The repeatability is within the uncertainty outlined in Chapter 5.

6.2 Comparison of Numerical and Experimental Results

Calculation of the equilibrium wave speeds discussed in Section 3.3.1 for the isotherm provide by Stiesch [1994] and shown in Figure 5.4 predicts that the outlet temperature profile from an inlet step change in humidity from dry to humid air at the same temperature is a fast shock wave temperature increase followed by an slower expansion wave temperature decrease.

Using the isotherm provided by Stiesch, the number of transfer units for heat

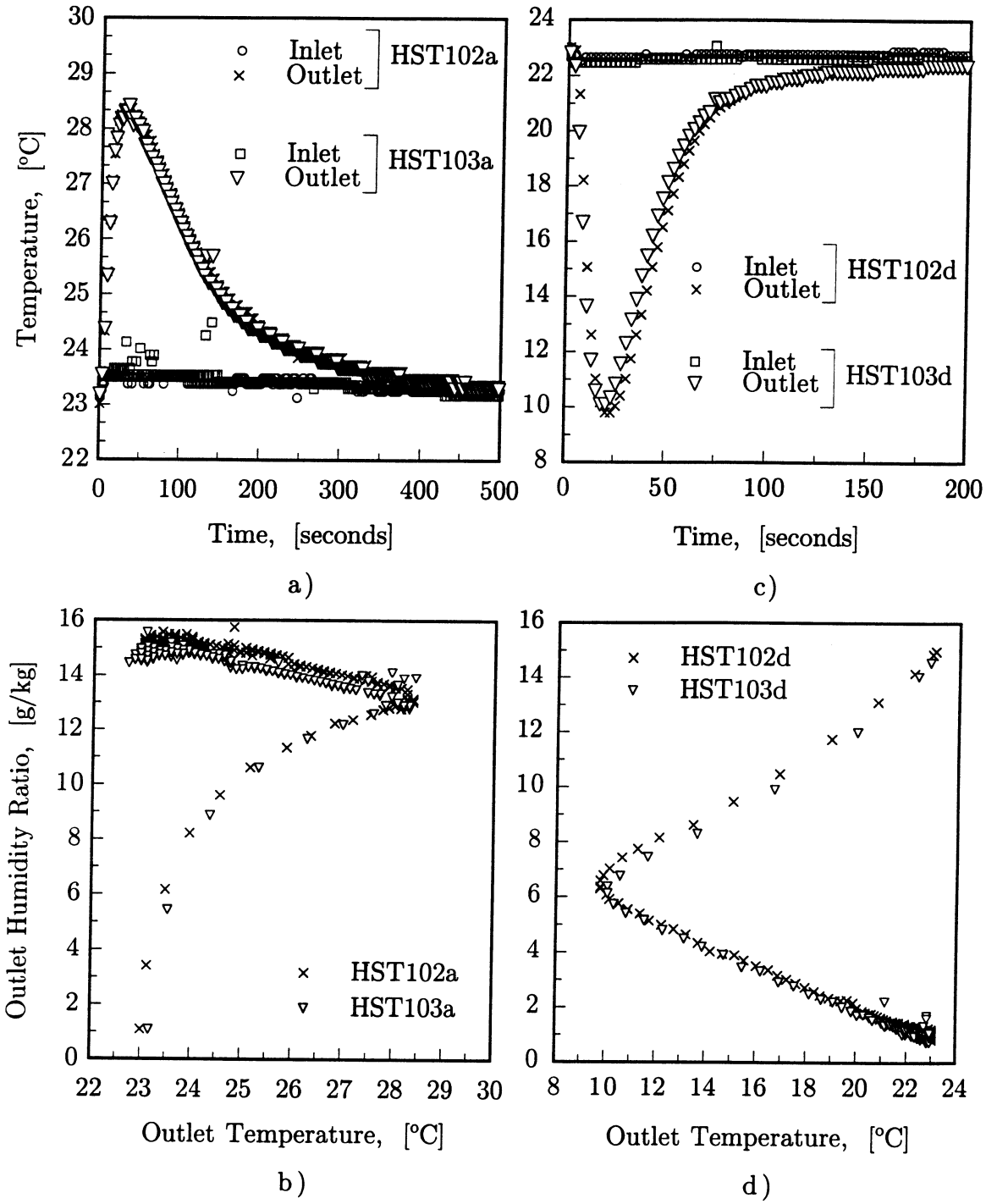

Figure 6.3: Repeatability of adsorption and desorption experiments.

transfer in Table 6.1 and the historically used value of unity for the overall Lewis number, the outlet temperature profile for the experiment was numerically determined with the finite-difference scheme outlined in Section 4.3 and is shown in Figure 6.4 versus time and on psychrometric coordinates.

The difference between the adsorption experimental and simulated outlet temperature is significant and beyond the uncertainty limits of the experimental measurements outlined in Chapter 5. The maximum temperature is 35.5°C and 28.4°C for the simulation and experiment respectively. A comparison of the wave behavior of the simulation and experiment is difficult to do because of the difference in the maximum temperature rise. Figure 6.4b indicates that the simulation predicts too much mass transfer at the beginning of the adsorption experiment.

The equilibrium expected outlet temperature profile from the step change in humidity from humid to dry air at the same temperature is a fast expansion wave followed by a slower shock wave.

Once again, using the number of transfer units for heat transfer given in Table 6.2 and an overall Lewis number of unity, the outlet temperature profile for the experiment was numerically determined and is shown as a function of time and on psychrometric coordinates in Figure 6.5.

The agreement between the desorption experiment and simulated outlet is better than the adsorption test. The difference between the simulated first wave and minimum temperature of the experiment agree well. The experimental second wave starts faster and is more spread out than the simulation suggests.

The agreement between simulation and experiment for both the adsorption and desorption processes is reasonable during the high humidity areas and poor for the low humidity areas.

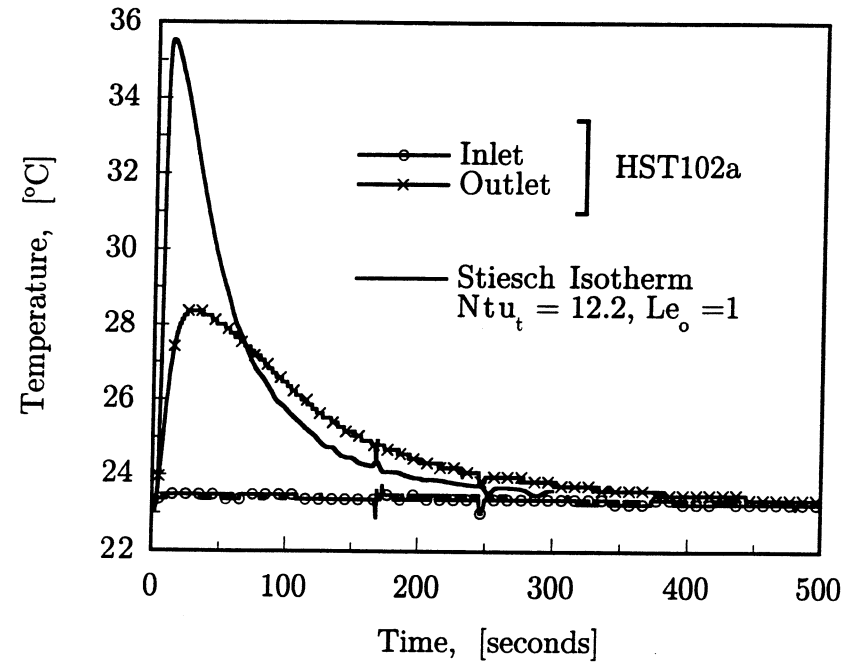

a)

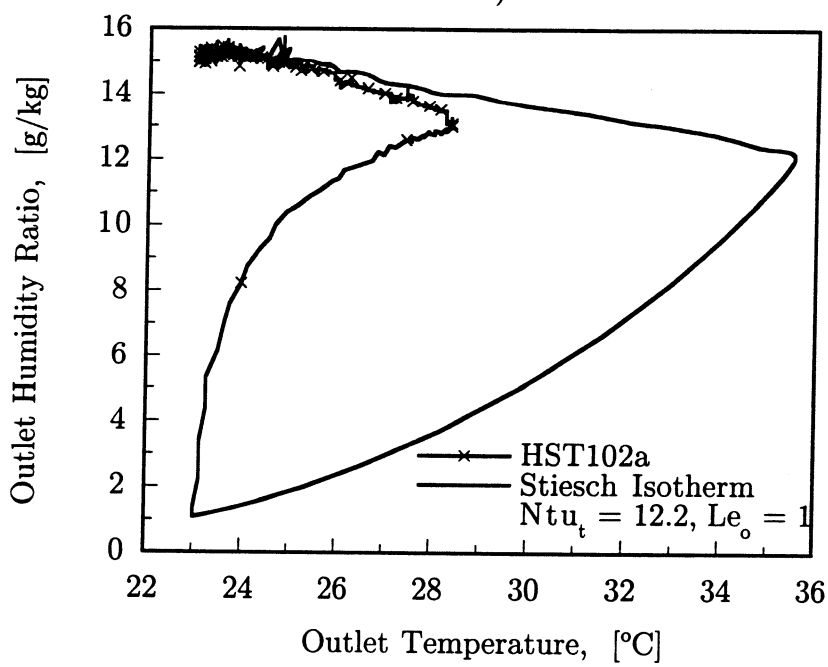

b)

Figure 6.4: Comparison of experimental and simulated adsorption outlet results.

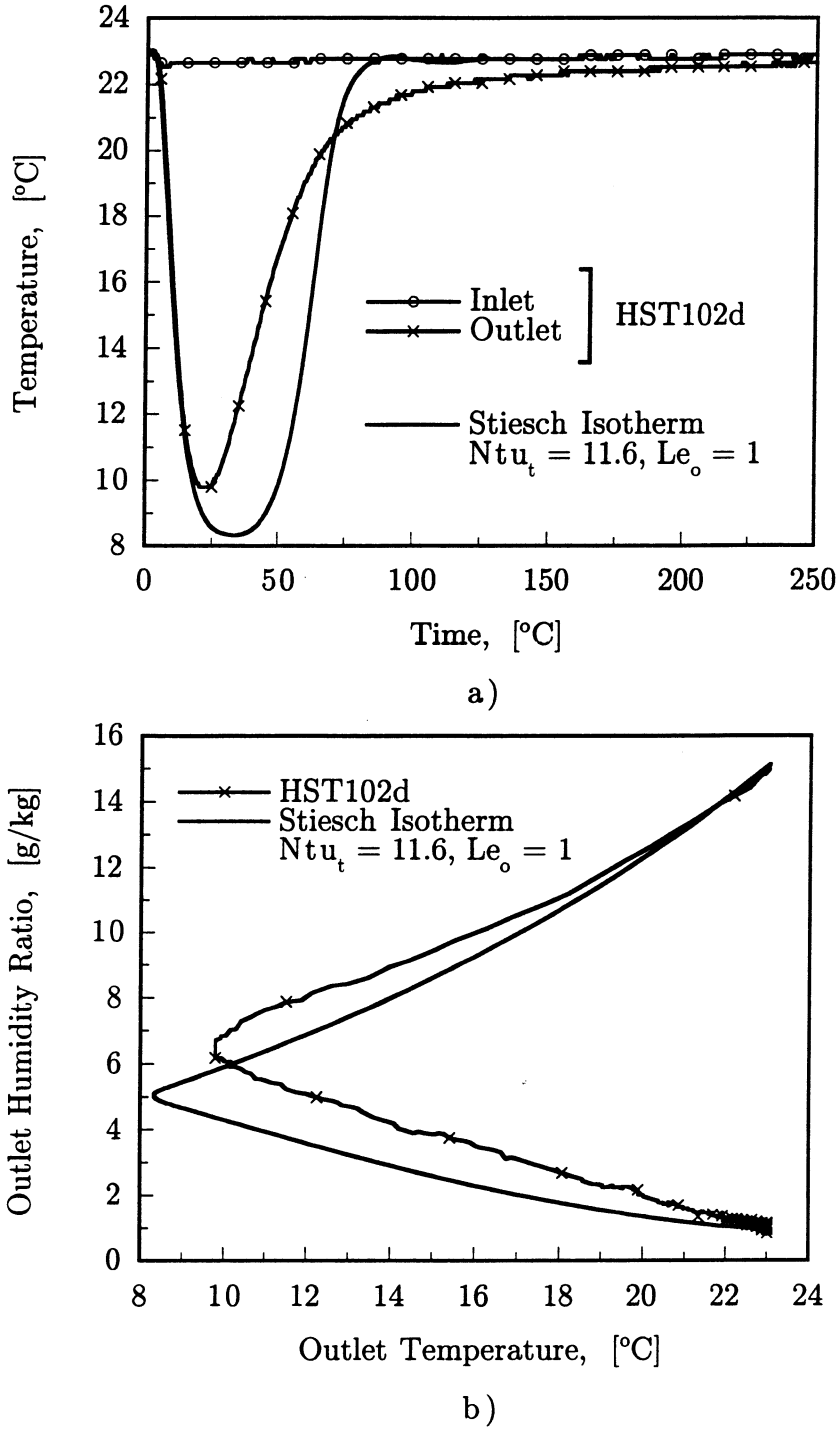

Figure 6.5: Comparison of experimental and simulated desorption outlet results.

6.3 Reasons for Differences

The differences between the experimental and simulated results is significant and it suggests there is something more fundamentally wrong than the assumption of the constant heat and mass transfer coefficients. Some possible reasons for the differences are that the resistance to mass transfer with this polymer desiccant is much larger than expected, the number of heat transfer units is overestimated by theory, or the driving force for mass transfer (desiccant isotherm) is in error.

6.3.1 Effect of Overall Lewis Number

A large overall Lewis number would explain the low temperature rise in the adsorption experiment and the expansion of the second wave in the desorption experiment. The effect of overall Lewis number on the simulated outlet is shown in Figure 6.6 for adsorption and desorption. Figure 6.6 is a plot of the outlet temperature in time and outlet temperature and humidity ratio on psychrometric coordinates for a range of overall Lewis numbers. The adsorption simulation is less sensitive to overall Lewis number than the desorption simulation. A high overall Lewis number does not allow the numerical simulation to replicate the first wave of the desorption test.

The overall Lewis number that best represents the experimental data is found by minimizing the sum of square error between the experimental outlet temperature and the simulated outlet temperature. The best fit overall Lewis number for the adsorption experiment is approximately 50. This means that the number of transfer units for mass transfer is 50 times smaller than for heat transfer. The best fit overall Lewis number for the desorption experiment is approximately 7. Since the overall Lewis numbers for adsorption and desorption that best represent the experimental data are very different, the overall resistance to mass transfer alone is not the cause of the discrepancy between the experiment and simulation.

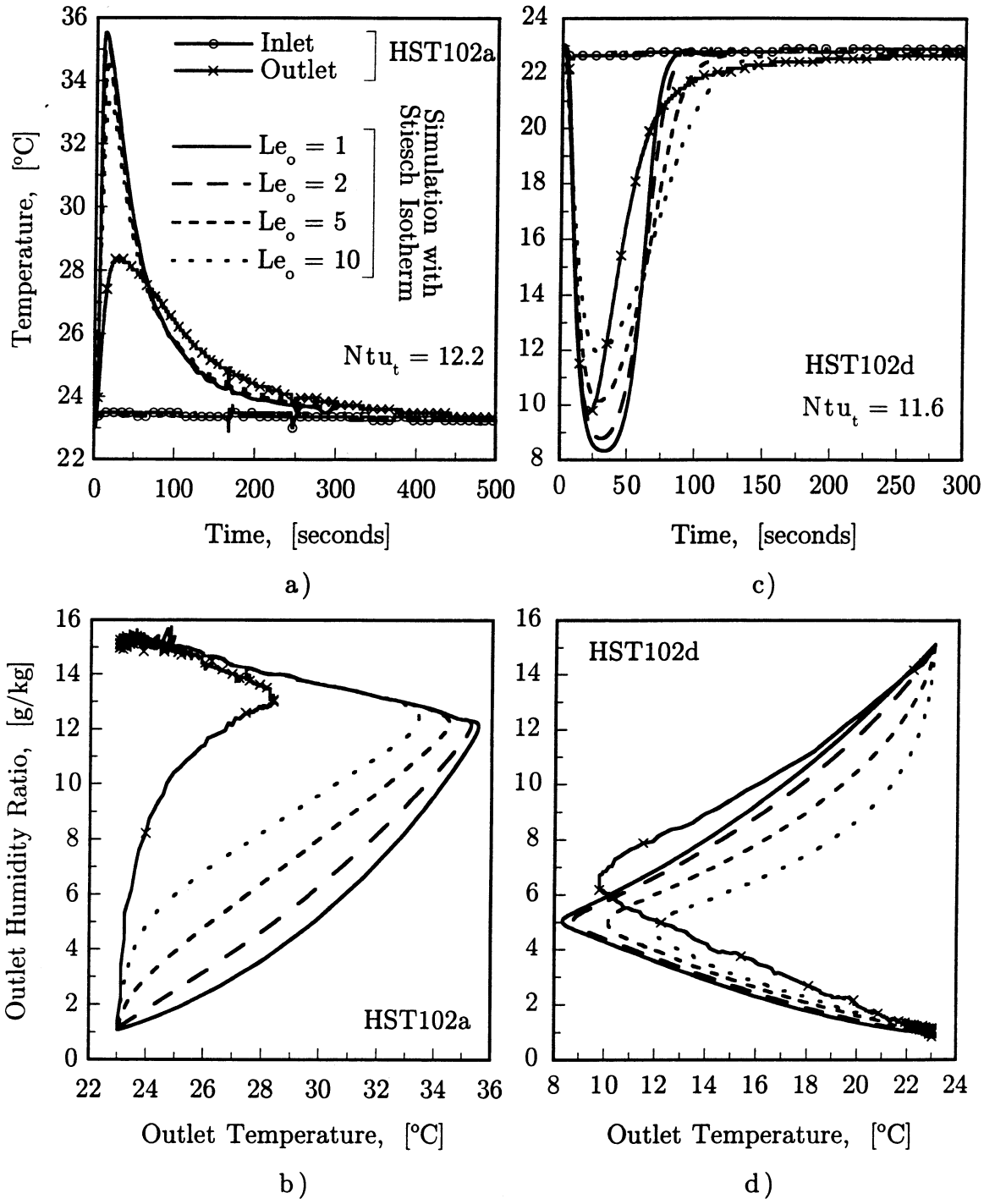

Figure 6.6: Effect of overall Lewis number on simulation of adsorption and desorption experiments.

6.3.2 Effect of Number of Heat Transfer Units

The number of heat transfer units is calculated from theory for fully developed laminar flow in triangular passages with an adiabatic boundary condition. The experimental temperature rise in adsorption and drop in desorption are both larger than simulation suggests. If the number of heat transfer units is overpredicted by theory, the magnitudes of the maximum temperature changes will be increased.

Figure 6.7 is a plot of the experimental and simulated outlet temperature with both the theoretical and reduced number of heat transfer units calculated in Section 5.1.2 as a function of time and the outlet state on psychrometric coordinates for both the adsorption and desorption experiments. As expected, the magnitudes of the maximum temperature changes are reduced. The simulated outlet with the lower Ntu_t still overpredicts the maximum temperature rise in the adsorption experiment, but it underpredicts the maximum temperature drop in the desorption experiment.

Comparing Figure 6.7d and Figure 6.6d shows that regardless of the number of transfer units for heat transfer, the first wave of the desorption experiment on psychrometric coordinates is best represented with a number of transfer units for mass transfer that is of the same order of magnitude as that for heat transfer ($Le_o \approx 1$).

6.3.3 Effect of Isotherm Shape

Mass transfer rate is a function of the mass transfer coefficient and the driving force, which is the difference between the air humidity ratio and the humidity ratio that is in equilibrium with the desiccant at the matrix temperature and water content. The equilibrium humidity ratio is determined from the isotherm of the desiccant. The isotherm is very important in this experiment because no heat transfer occurs without mass transfer because the inlet air stream is at the same temperature as the initial matrix temperature. The combination of experimental conditions that include

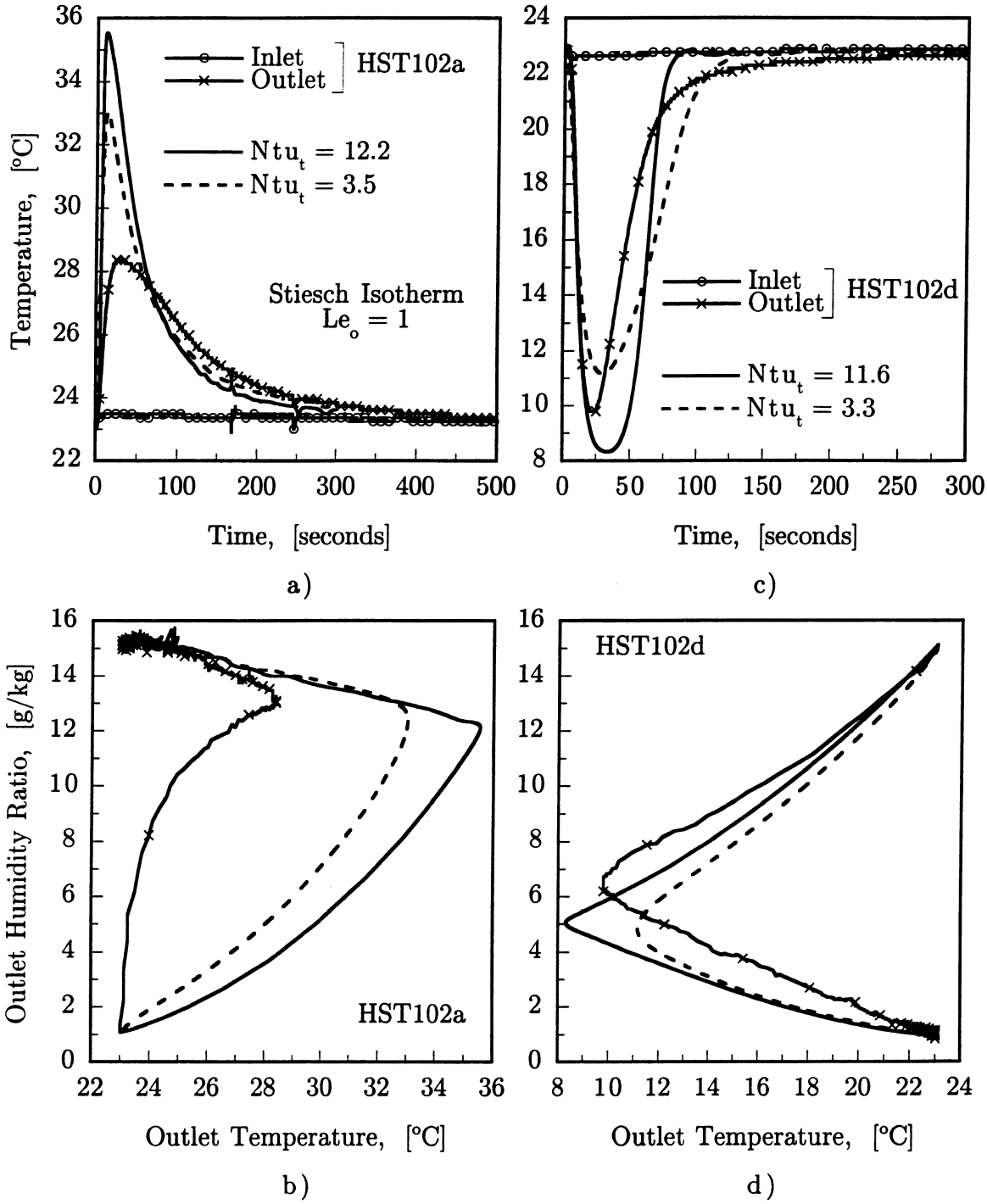

Figure 6.7: Effect of number of heat transfer units on simulation of adsorption and desorption experiments.

very dry air states, low maximum water capacity and a Brunauer Type III isotherm shape makes the simulation very sensitive to the isotherm shape.

Stiesch [1994] measured isotherms at three temperatures (5°, 22° and 40°C) and five relative humidities corresponding to pure water; saturated salt solutions of magnesium chloride, sodium chloride, potassium nitrate and water; and sodium pentoxide. The data are shown in Figure 6.8 versus both relative humidity and adsorption potential. The lines are best fit following the same form as the Stiesch equation:

$$W = W_1 \exp\left(-\left(AP/E_1\right)^{n_1}\right) + W_2 \exp\left(-\left(AP/E_2\right)^{n_2}\right) \tag{6.1}$$

Table 6.3 contains the fitted isotherm parameters for the individual isotherms. Plotted on adsorption potential coordinates (Figure 6.8b), the three isotherms agree well at low adsorption potential, but deviate significantly at higher adsorption potential. As the temperature is increased, the isotherm becomes more Brunauer Type III.

The effect of the difference in isotherm is shown for both adsorption and desorption in Figure 6.9 as plots of outlet temperature versus time and outlet temperature and humidity ratio on psychrometric coordinates.

The isotherm fit provided by Stiesch [1994] overpredicts the temperature rise shown in Figure 6.9a in the adsorption experiment because it has a relatively high equilibrium water content at high adsorption potential (low relative humidity). Figure 6.9a and c shows that the high adsorption potential region of the isotherm controls the maximum temperature rise of the adsorption experiment and the second wave of

Table 6.3: Fitted parameters of individual isotherms from Stiesch [1994].

Temperature °C	W_1 kg/kg	E_1 kJ/kmol	n_1	W_2 kg/kg	E_2 kJ/kmol	n_2
5	0.073	220	0.59	0.014	3070	1.4
22	0.079	220	0.74	0.008	2590	1.3
40	0.071	170	0.81	0.015	1310	1.0

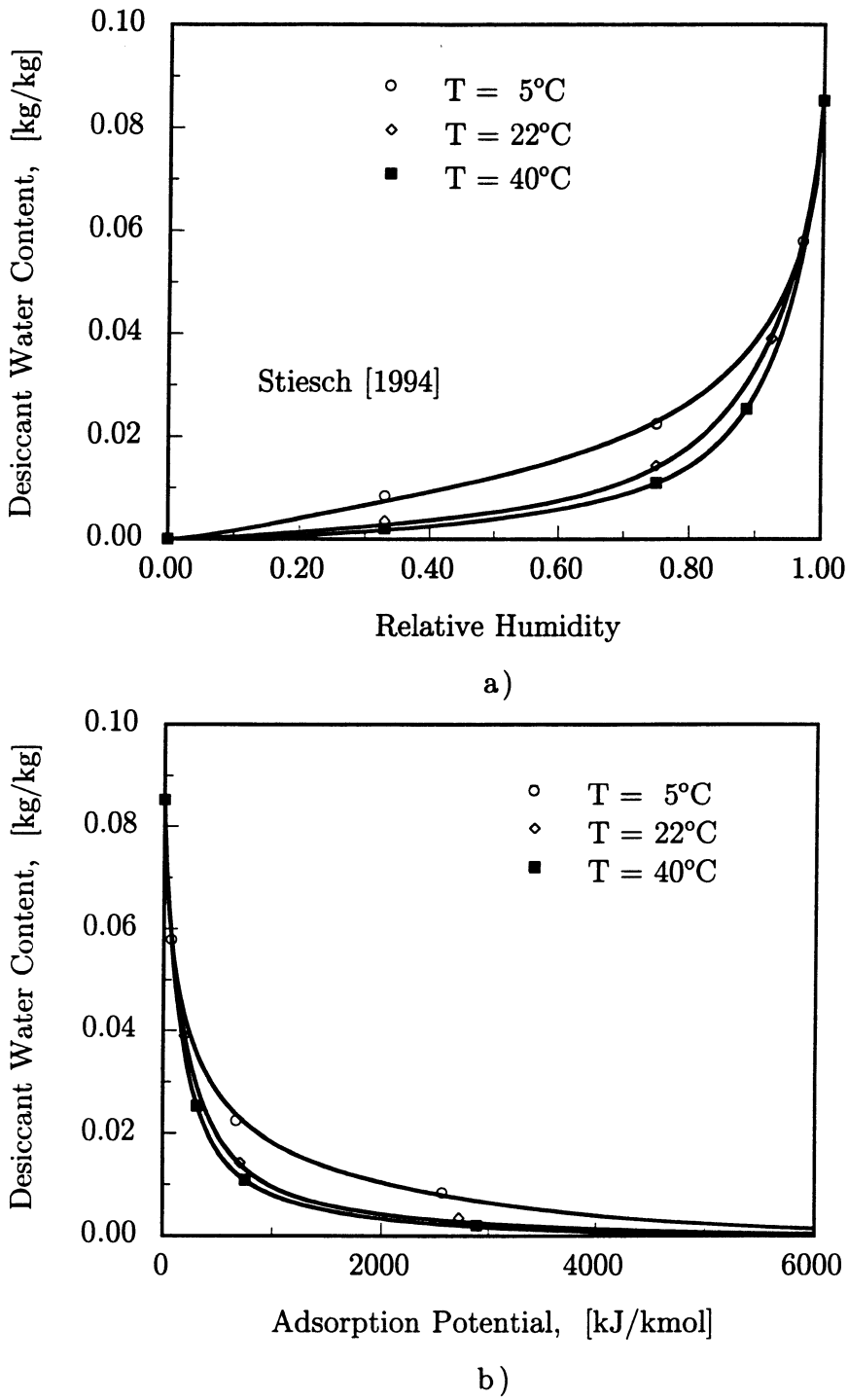

Figure 6.8: Stiesch isotherm data plotted versus relative humidity and adsorption potential.

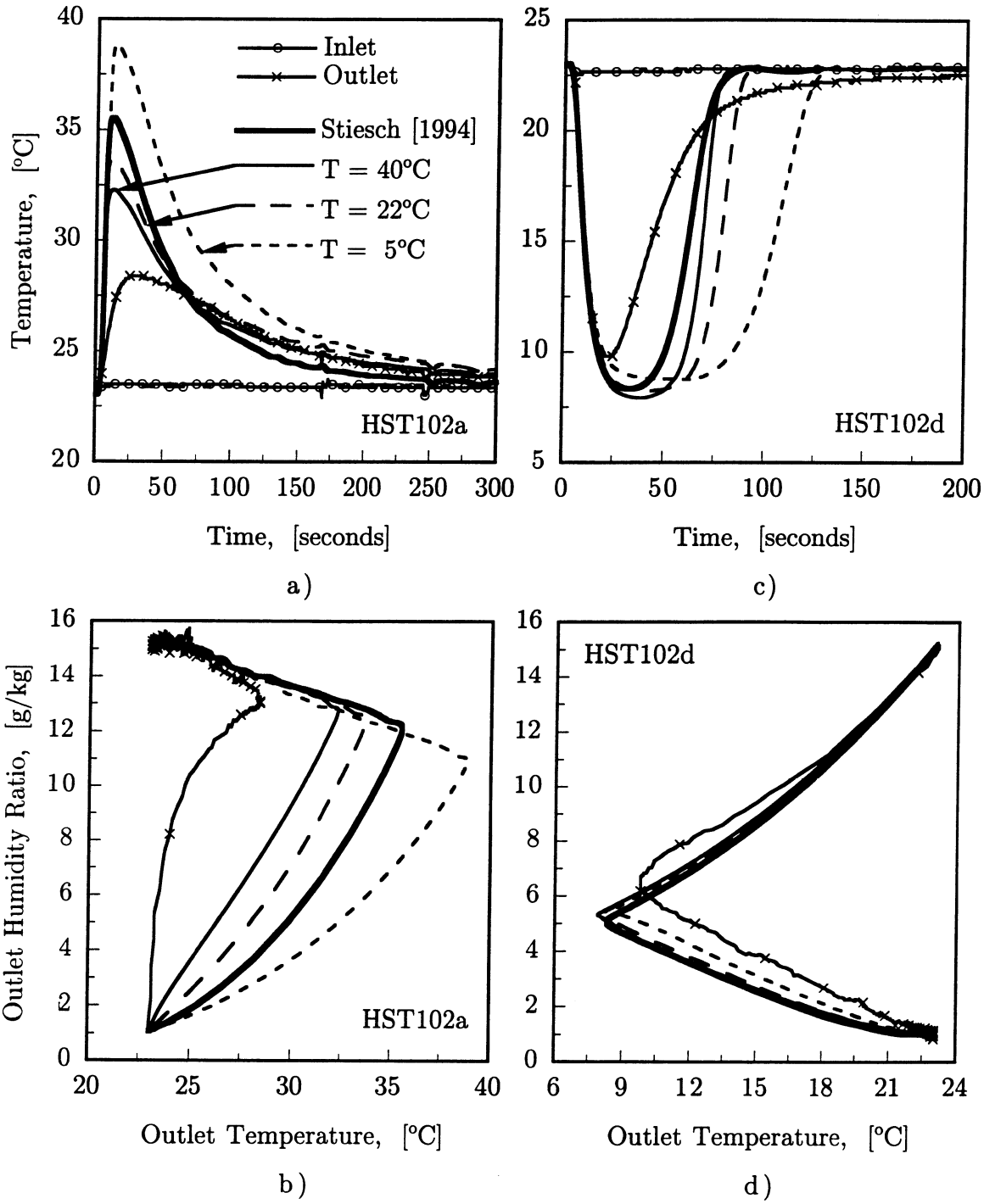

Figure 6.9: Effect of isotherm shape on simulation of adsorption and desorption experiments.

the desorption experiment. As the capacity is decreased in this region, the maximum temperature rise decreases and the speed of the second wave of the desorption period varies. The different isotherm shapes effect the time scale of the desorption experiment more than the adsorption experiment.

Figure 6.9a and c also shows that the low adsorption potential region (high relative humidity) of the isotherm controls the second wave of the adsorption experiment and the first wave and minimum temperature of the desorption experiment.

Figure 6.9b and d show that the isotherm shape has a larger effect on the outlet state on psychrometric coordinates of the adsorption experiment than the desorption experiment.

The effect of the isotherm shape is very significant. However, variation within the experimental uncertainty of Stiesch's data does not adequately explain the difference between the experimental and simulated outlet.

6.3.4 Problem Formulation

To this point, overall resistance to mass transfer has been assumed to be controlled by the air-side resistance, that is, assuming that there is no distribution of water content in the desiccant coating. According to Suzuki [1990] when the non-linearity of the isotherm is large, the difference between the simulation assuming a controlling air-side resistance and a controlling solid-side resistance is significant. The representation of the mass transfer with solid-side resistance is as follows:

$$\frac{\partial W}{\partial \tau} = \frac{KA}{\dot{m}} \left(W_{eqm}\left(w, T\right) - W \right) \tag{6.2}$$

where W_{eqm} is the desiccant water content in equilibrium with the moist air humidity ratio and the desiccant matrix temperature at the surface of the desiccant coating, K is the coefficient that describes the diffusion of mass through the desiccant, and τ is the non-dimensional time.

The trends exhibited for an increase in solid-side mass transfer resistance were identical to an increase in air-side resistance to mass transfer; however, the sensitivity of the experiment to increased solid-side resistance was changed. If the solid-side resistance to mass transfer is increased relative to the resistance to heat transfer, the adsorption experiment became more sensitive to the increase than the desorption experiment. This is contrary to the results for an air-side controlling resistance. The first wave of the adsorption experiment became more spread out and the magnitude of the temperature rise was reduced more than for a similar increase in air-side resistance. The magnitude of the temperature drop during the desorption experiment was less effected by an increase in solid-side resistance.

Despite the improved qualitative description of the experiment, a simulation with controlling solid-side resistance still suffers from the same quantitative problems as the simulation with controlling air-side resistance: the magnitude of the temperature rise is too large for the adsorption experiment and the second wave of the desorption experiment is too sharp and slow.

6.4 Conclusions

The differences between the experimental and simulated outlet states of the test section are significant and cannot be explained as due to the variation of heat transfer coefficient, air-side mass transfer coefficient, or solid-side diffusion coefficient.

The first wave of the adsorption experiment suggests that the desiccant has very little water capacity at very dry conditions or a resistance to mass transfer that is over one magnitude larger than the resistance to heat transfer (high overall Lewis number). The first wave of the desorption experiment suggests that the resistance to mass transfer is on the same order of magnitude as heat transfer. The diffuse character of second wave of the desorption experiment in time suggests that the

resistance to mass transfer is large. The second wave of the desorption experiment on psychrometric coordinates suggests that the desiccant has non-zero capacity at high adsorption potential because the slope is not zero on psychrometric coordinates.

The experiment is very sensitive to isotherm shape. If the isotherm is more Type III (has lower water capacity at low relative humidities) the maximum temperature rise during the adsorption experiment decreases. If the isotherm is steeper in the high relative humidity region of the isotherm the the speed of the second wave of the desorption experiment increases.

The sensitivity to the isotherm shape coupled with the uncertainty of the isotherm shape at low relative humidities and its possible temperature dependence are a major reason for the difference between the experiment and simulation.

Chapter 7

Conclusions and Recommendations

7.1 Conclusions

A single-blow experiment was designed and implemented that measured the heat and mass transfer in a commercially available aluminum core matrix of triangular passages with a polymer desiccant coating. The experimental procedure used a step in inlet humidity ratio to drive the adsorption and desorption processes. The advantage of this method is the outlet temperature response undergoes a maximum or mininum for adsorption and desorption respectively. This allows the performance to be more accurately determined by the measurement of dry-bulb temperatures instead of humidity ratios.

The experiment showed that very little mass is transferred after a step increase in humidity ratio at the same temperature implying that the resistance to mass transfer is large. Since the mass transfer is small, the corresponding temperature rise is also small. For a step decrease in humidity ratio at the same temperature, however, the experiment showed immediate, significant mass transfer. The second wave of the step decrease in humidity ratio is very spread out in time.

The simulated outlet of the experimental conditions was significantly different

than the experimental data. For the step increase in humidity, when using the theoretical value of heat transfer coefficient for laminar flow in triangular passages and an overall Lewis number of unity, the simulated temperature rise is nearly 2.5 times larger than the experiment. Similar analysis on the step decrease in humidity showed that the first wave was in good agreement and temperature drop was only approximately 10% larger, but the second wave was expected to be start sooner and finish later (shock) than the experiment.

Increasing the overall Lewis number did not explain the discrepancies between simulation and experiment. An increased overall Lewis number represented the low mass transfer rate early in the adsorption experiment, but failed to represent the mass transfer rate early in the desorption experiment. The overall Lewis number that best fits the step increase in humidity experimental data was approximately 50. The best fit overall Lewis number for the step decrease was approximately 7. The differences between the overall Lewis numbers that best fit the experimental data for adsorption and desorption suggest that the resistance to mass transfer alone is not the reason for the differences.

An experiment on a test section without desiccant coating to determine the heat transfer coefficient resulted in satisfactory agreement with the theoretical fully developed Nusselt number for an isosceles right triangle with a constant heat flux boundary condition. However, a large range of number of transfer units provided satisfactory results. Therefore, a reduction of the number of transfer units for heat transfer by a factor of 3.5 was investigated. A reduction of the number of transfer units for heat transfer by a factor of 3.5 was investigated. The reduced Ntu_t decreased the maximum temperature rise during the step increase in humidity, but it still *overpredicted* the temperature rise by nearly 2 times. The temperature drop during the humidity step down was *underpredicted* by approximately 10% when the number of transfer

units for heat transfer was decreased.

The simulation of experimental conditions are very sensitive to isotherm shape at low relative humidities (high adsorption potential). Since no isotherm data was collected between 0% and 33% for the polymer desiccant [Stiesch, 1994], the isotherm is not well defined in the that region. Closer inspection of the Stiesch data showed that the isotherm may not be independent of temperature when plotted on adsorption potential coordinates. Therefore, the heat of adsorption could also be in error.

The sensitivity to the isotherm shape coupled with the uncertainty of the isotherm shape at low relative humidities and its possible temperature dependence are a major reason for the difference between the experiment and simulation.

7.2 Recommendations

Previous studies [Schultz, 1987; Van Den Bulck, 1987] confirmed that the use of overall transfer coefficients is valid; however, an accurate assessment of the applicability of overall transfer coefficients could not be made for the experimental conditions and polymer desiccant coating due to the large differences between the simulation and experimental results. Therefore, the experiment method should be tested with a desiccant that has well defined equilibrium behavior and higher water capacity. The higher water capacity increase both the time of the experiment and the temperature increase during the step increase in humidity ratio experiment.

The simulated outlet of the experimental conditions was very sensitive to the isotherm shape. The isotherm for the polymer should be measured at more temperatures and relative humidities and the isotherm should be checked for hysteresis between adsorption and desorption. In addition, the temperature dependence of the isotherm at low relative humidities should be investigated. The significant difference between individual isotherms measured by Stiesch [1994] suggests that the heat

of adsorption may not be adequately predicted by the adsorption potential theory. Therefore, independent measurements of the heats of adsorption should also be done.

Appendix A

Nomenclature

Roman symbols

a_i	state property functions (Equation 3.8)
A	heat transfer area [length^2]
A_m	cross sectional area of the matrix available for heat conduction in the flow direction [length^2]
AP	adsorption potential [energy/mole]
c	specific heat [energy/mass-temperature]
E	characteristic free energy of adsorption [energy/mass]
F_i	ith combined potential [dimensionless]
$\mathcal{F}$	fraction of total dehumidifier mass [dimensionless]
h_m	mass transfer coefficient [mass/time-length^2]
h_t	heat transfer coefficient [energy/time-length^2-temperature]
ΔH_{fg}	heat of vaporization [energy/mass]
ΔH_s	heat of adsorption [energy/mass]
i	moist air enthalpy [energy/dry mass]
I	desiccant enthalpy [energy/dry mass]
k	desiccant matrix thermal conductivity [energy/time-length-temperature]

Roman symbols continued

L	axial flow length through matrix [length]
$\dot{m}$	mass flow rate of moist air [mass/time]
M	desiccant mass in dehumidifier matrix [mass]
n	power in Dubinin isotherm equation [dimensionless]
Ntu_t	number of heat transfer units [dimensionless]
Ntu_w	number of mass transfer units [dimensionless]
P	perimeter of flow passage [length]
q_r	regeneration heat [energy/mass]
R	ideal gas constant [energy/mass-temperature]
S	shock wave speed [dimensionless]
t	moist air temperature [temperature]
T	desiccant matrix temperature [temperature]
w	moist air humidity ratio [mass water/mass dry air]
w_{eq}	humidity ratio in equilibrium with T, W [mass water/mass dry air]
W	desiccant moisture content [mass water/mass dry desiccant]
W_{tot}	desiccant maximum moisture content [mass water/mass dry desiccant]
x	axial coordinate [length]
z	axial coordinate [dimensionless]

Greek symbols

Δ	half thickness of desiccant matrix [length]
λ	expansion wave speed [dimensionless]
λ_l	conduction parameter, $kA_m/\dot{m}c_aL$ [dimensionless]
ϕ	relative humidity of moist air [dimensionless]
θ	time [time]
τ	time coordinate [dimensionless]

Subscripts

a	air
d	dry desiccant
i	combined potential index
j	period index
m	matrix
P	process state or period
R	regeneration state or period
s	saturated
w	water
wv	water vapor

Appendix B

Bibliography

1. Abdel-Wahed, R.M., A.E. Attia, 1984, "Fully developed laminar flow and heat transfer in an arbitrarily shaped triangular duct," Wärme und Stoffübertragung, Vol. 18, pp. 83-88.

2. Acrivos, A., 1956, "Method of Characteristics Technique: Application to Heat and Mass Transfer Problems," Ind. Eng. Chem., Vol. 48, No. 4, pp. 703-710.

3. Banks, P.J., 1972, "Coupled Equilibrium Heat and Single Adsorbate Transfer in Fluid Flow through a Porous Medium—I. Characteristic Potentials and Specific Capacity Ratios," Chem. Engng. Sci., Vol. 27, pp. 1143-1156.

4. Banks, P.J., 1982, "Effect of Fluid Carryover on Regenerator Performance," Journal of Heat Transfer, Vol. 104, pp. 215-217.

5. Banks, P.J., 1985, "Prediction of Heat and Mass Regenerator Performance Using the Nonlinear Analogy Method: Part 1—Basis," Journal of Heat Transfer, Vol. 107, pp. 222-229.

6. Banks, P.J., 1985, "Prediction of Heat and Mass Regenerator Performance Using the Nonlinear Analogy Method: Part 2—Comparison of Methods," Journal of Heat Transfer, Vol. 107, pp. 230-238.

7. Brandemuehl, M.J., P.J. Banks, 1984, "Rotary Heat Exchangers with Time Varying or Non Uniform Inlet Temperatures," Journal of Heat Transfer, Vol. 106, pp. 750-758.

8. Belding, W.A., W.M. Worek, D. Novosel, W.D. Holeman, 1991, "Desiccant Development for Gas-Fired Desiccant Cooling Systems," NY-91-6-3.

9. Bullock, C.E., J.L. Threlkeld, 1966, "Dehumidification of Moist Airby Adiabatic Adsorption," ASHRAE Transactions, Vol. 72, No. 1, pp. 301-313.

10. Cai, Z.H., L. Li, Y.W. Wu, H.S. Ren, 1984, "A Modified Selected Point Matching Technique for Testing Compact Heat Exchanger Surfaces," International Journal of Heat and Mass Transfer, Vol. 27, No. 7, pp. 971-978.

11. Charoensupaya, D., W.M. Worek, 1988, "Parametric Study of an Open-Cycle Adiabatic, Solid, Desiccant Cooling System," Energy, Vol. 13, No. 9, pp. 739-747.

12. Charoensupaya, D., W.M. Worek, 1988, "Effect of Adsorbent Heat and Mass Transfer Resistances on Performance of an Open-Cycle Adiabatic Desiccant Cooling System," Heat Recovery Systems & CHP, Vol. 8, No. 6, pp. 537-548.

13. Chuah, Y.K., P. Norton, F. Kreith, 1989, "Transient Mass Transfer in Parallel Passage Dehumidifiers with and without Solid Side Resistance," Journal of Heat Transfer, Vol. 111, pp. 1038-1044.

14. Close, D.J., P.J. Banks, 1970, "Coupled Heat and Mass Convection and Diffusion—Analogies with Heat Transfer," CHEMECA '70, Session 6A, pp. 17-33.

15. Close, D.J., P.J. Banks, 1972, "Coupled Equilibrium Heat and Single Adsorbate Transfer in Fluid Flow through a Porous Medium—II. Predictions for a silica-gel-air-drier using Characteristic Charts," Chem. Engng. Sci., Vol. 27, pp. 1157-1169.

16. Close,. D.J., 1983, "Characteristic Potentials for Coupled Heat and Mass Transfer Processes," Int. J. Heat Mass Transfer, Vol. 26, No, 7, pp. 1098-1102.

17. Collier, R.K., 1986, "On the Theoretical Performance of Open Cycle Desiccant Cooing Systems," ASME Winter Annual Meeting.

18. Collier, R.K., D. Novosel, W.M. Worek, 1990, "Performance Analysis of Open-Cycle Desiccant Cooling Systems," AT 90-19-2.

19. Collier, R.K., B.M. Cohen, 1991, "An Analytical Examination of Methods for Improving the Performance of Desiccant Cooling Systems," Journal of Solar Energy Engineering, Vol. 113, pp. 157-163.

20. Cooney, D.O., 1974, "Numerical Investigation of Adiabatic Fixed-Bed Adsorption," Ind. Eng. Chem., Vol. 13, No. 4, pp. 368-373.

21. Dubinin, M.M., 1975, "Physical Adsorption of Gases and Vapors in Micropores," Prog. Surf. Membrane Sci., Vol. 9, pp. 1-70.

22. Epstein, M., M. Grolmes, K. Davidson, D. Kosar, 1985, "Desiccant Cooling System Performance: A Simple Approach," Journal of Solar Energy Engineering, Vol. 107, pp. 21-28.

23. Farooq, S., D.M. Ruthven, 1991, "Numerical Simulation of a Desiccant Bed for Solar Air Conditioning Applications," Journal of Solar Energy Engineering, Vol. 113, pp. 80-88.

24. Ghezelayagh, H., D. Gidaspow, 1982, "Micro-Macropore Model for Sorption of Water on Silica Gel in a Dehumidifier," Chem. Eng. Sci., Vol. 37, No. 8, pp. 1181-1197.

25. Hajji, A., W.M. Worek, 1991, "Simulation of Regenerative, Closed-Cycle Adsorption Cooling/Heating System," Energy, Vol. 16, No. 3, pp. 643-654.

26. Harwell, J.H., et al., 1980, "A Non-Equilibrium Model for Fixed-bed Multicomponent Adiabatic Adsorption," Che. Eng. Sci., Vol. 35, pp. 2287-2296.

27. Hougen, O.A., W.R. Marshall, Jr., 1947, "Adsorption from a Fluid Stream Flowing Through a Stationary Granular Bed," Chemical Engineering Progress, Vol. 43, No. 4, pp. 197-208.

28. Incropera, F.P., D.P. DeWitt, 1996, *Introduction to Heat Transfer*, 3rd edition, John Wiley & Sons, New York, New York.

29. Ingram, J.B., G.C. Vliet, 1982, "Solid Desiccant Rotary Dryer Performance Charts," Progress in Solar Energy, pp. 603-608.

30. John, F., 1971, Partial Differential Equations, Springer-Verlag, New York.

31. Jurinak, J.J., 1982, "Open Cycle Solid Desiccant Cooling—Component Models and System Simulations," Ph.D. Thesis, University of Wisconsin, Madison, WI.

32. Jurinak, J.J., J.W. Mitchell, W.A. Beckman, 1984, "Open-Cycle Desiccant Air Conditioning as an Alternative to Vapor Compression Cooling in Residential Applications," Journal of Heat Transfer, Vol. 106, pp. 252-260.

33. Jurinak, J.J., J.W. Mitchell, 1984, "Recirculation of Purged Flow in an Adiabatic Counterflow Rotary Dehumidifier," Journal of Heat Transfer, Vol. 106, pp. 369-375.

34. Kang, T.S., I.L. Maclaine-cross, 1989, "High Performance, Solid Desiccant, Open Cooling Cycles," Journal of Solar Energy Engineering, Vol. 111, pp. 176-183.

35. Klein, H., 1988, "Heat and Mass Transfer in Regenerative Enthalpy Exchangers," M.S. Thesis, University of Wisconsin, Madison, WI.

36. Knight, K.M., 1992, "Analysis and Design of adsorptive Processes for Air Quality Control," Ph.D. Thesis, University of Wisconsin, Madison, WI.

37. Krishna, S.M., S.S. Murthy, 1989, "Experiments on a Silica Gel Rotary Dehumidifier," Heat Recovery Systems & CHP, Vol. 9, No. 5, pp. 467-473.

38. Lavan, Z., J-B., Monnier, W.M. Worek, 1982, "Second Law Analysis of Desiccant Cooling Systems," Journal of Solar Energy Engineering, Vol. 104, pp. 229-236.

39. Lax, P., 1973, Hyperbolic Systems of Conservation Laws and the Mathematical Theory of Shock Waves, SIAM, Philadelphia.

40. Liang, C.Y., Wen-Jei Yang, 1975, "Modified Single-Blow Technique for Performance Evaluation on Heat Transfer Surfaces," Journal of Heat Transfer, No. 2, pp. 16-21.

41. Löf, G.O., G. Cler, T. Brisbane, 1988, "Performance of a Solar Desiccant Cooling System," Journal of Solar Energy Engineering, Vol. 110, pp. 165-171.

42. Maclaine-cross, I.L., P.J. Banks, 1972, "Coupled Heat and Mass Transfer in Regenerators—Prediction using an Analogy with Heat Transfer," Int. J. Heat Mass Transfer, Vol. 15, pp. 1225-1242.

43. Maclaine-cross, I.L., 1985, "High-Performance Adiabatic Desiccant Open-Cooling Cycles," Journal of Solar Energy Engineering, Vol. 107, pp. 102-104.

44. Majumdar, P., W.M. Worek, 1989, "Performance of an Open-Cycle Desiccant Cooling System using Advanced Desiccant Matrices," Heat Recovery Systems & CHP, Vol. 9, No. 4, pp. 299-311.

45. Majumdar, P., W.M. Worek, 1989, "Combined Heat and Mass Transfer in Porous Adsorbent," Energy, Vol. 14, No. 3, pp. 161-175.

46. Mathiprakasam, B., Z. Lavan, 1980, "Performance Predictions for Adiabatic Desiccant Dehumidifiers Using Linear Solutions," Journal of Solar Energy Engineering, Vol. 102, pp. 73-79.

47. Mei, V.C., Z. Lavan, 1983, "Performance of Cross-Cooled Desiccant Dehumidifiers," Journal of Solar Energy Engineering, Vol. 105, pp. 300-304.

48. Mei, V.C., F.C. Chen, Z. Lavan, R.K. Collier, Jr., G. Meckler, 1992, "An Assessment of the Desiccant Cooling and Dehumidification Technology," Oak Ridge National Laboratory, ORNL/CON-309, July.

49. Nelson, J.S., W.A. Beckman, J.W. Mitchell, D.J. Close, 1978, "Simulations of the Performance of Open Cycle Desiccant Systems using Solar Energy," Solar Energy, Vol. 21, pp. 273-278.

50. Nimmo, B.G., R.K. Collier, K. Rengarajan, 1993, "DEAC: Desiccant Enhancement of Cooing-Based Dehumidification," CD-93-4-4.

51. Pam, C.Y., D. Basmadjian, 1971, "An Analysis of Adiabatic Sorption of Single Solutes in Fixed Beds: Equilibrium Theory," Chem. Eng. Sci., Vol. 26, pp. 45-57.

52. Pennington, N.A., 1955, Humidity Changer for Air-Conditioning, U.S. Patent #2,700,537.

53. Pesaran, A.A., T.R. Penney, A.W. Czanderna, 1993, Desiccant Cooling: State-of-the-art Assessment, NREL/TP-254-4147.

54. Polanyi, M., 1932, "Section III—Theories of the Adsorption of Gases. A general survey and some additional remarks," Trans. Far. Soc., Vol. 28, pp. 316-333.

55. Prasad, M., P. Kumar, 1984, "An Experimental and Analytical Study of Non-Conventional Air Conditioning Systems," Energy Convers. Mgmt., Vol. 24, No. 3, pp. 165-170.

56. Ruthven, D.M., 1984, *Principles of Adsorption & Adsorption Processes*, John Wiley & Sons, New York, New York.

57. San, J.Y., 1993, "Heat and Mass Transfer in a Two-Dimensional Cross-Flow Regenerator with a Solid Conduction Effect," Int. J. Heat Mass Transfer, Vol. 36, No. 3, pp. 633-643.

58. San, J.Y., S.C. Hsiau, 1993, "Effect of axial solid heat conduction and mass diffusion in a rotary heat and mass regenerator," Int. J. Heat Mass Transfer, Vol. 36, No. 8, pp. 2051-2059.

59. San, J.Y., J-B. Monnier, Z. Lavan, W.M. Worek, 1982, "Exergy Analysis of Solar Powered Desiccant Cooling Systems," Progress in Solar Energy, pp. 567-572.

60. Suzuki, M., 1990, *Adsorption Engineering*, Elsevier Science Publishers B. V., Amsterdam, The Netherlands.

61. Tuve, G.L. L.C. Domholdt, 1966, *Engineering Experimentation*, McGraw-Hill, New York, NY.

62. Van Den Bulck, E., 1983, "Analysis of Solid Desiccant Rotary Dehumidifiers," M.S. Thesis, University of Wisconsin, Madison, WI.

63. Van Den Bulck, E., J.W. Mitchell, S.A. Klein, 1985, "Design Theory for Rotary Heat and Mass Exchangers—I. Wave Analysis of Rotary Heat and Mass Exchangers with Infinite Transfer Coefficients," Int. J. Heat Mass Transfer, Vol. 28, No. 8, pp. 1575-1586.

64. Van Den Bulck, E., J.W. Mitchell, S.A. Klein, 1985, "Design Theory for Rotary Heat and Mass Exchangers—II. Effectiveness-Number-of-Transfer-Units Method for Rotary Heat and Mass Exchangers," Int. J. Heat Mass Transfer, Vol. 28, No. 8, pp. 1587-1595.

65. Van Den Bulck, E., 1987, "Convective Heat and Mass Transfer in Compact Regenerative Dehumidifiers," Ph.D. Thesis, University of Wisconsin, Madison, WI.

66. Van Den Bulck, E., S.A. Klein, 1990, "Single-Blow Test Procedure for Compact Heat and Mass Exchangers," Int. J. Heat Mass Transfer, Vol. 112, pp. 317-322.

67. Van Den Bulck, E., 1991, "Transient Heat and Mass Transfer in Laminar Flow Forced Convection in Ducts," Int. J. Heat Mass Transfer, Vol. 34, No. 4/5, pp. 1249-1258.

68. Van Horn, K.R. ed., 1967, "Aluminum. Volume I. Properties, Physical Metallurgy and Phase Diagrams," American Society for Metals, Metals Park, Ohio.

69. Waugaman, D.G., A. Kini, C.F. Kettleborough, 1993, "A Review of Desiccant Cooling Systems," Journal of Energy Resources Technology, Vol. 115, pp. 1-8.

70. Weber, T.W., R.K. Chakravorti, 1974, "Pore and Solid Diffusion Models for Fixed-Bed Adsorbers," AIChE Journal, Vol. 20, No. 2, pp. 228-237.

71. Zheng, W., W.M. Worek, D. Novosel, 1993, "Control and Optimization of Rotational Speeds for Rotary Dehumidifiers," CH-93-4-2.

Appendix C

Finite Difference Equation Set

The governing equations for simulataneous heat and mass transfer in desiccant matrices are as follows:

$$\frac{\partial w}{\partial z} = Ntu_m \left(w_{eq} - w\right) \tag{C.1}$$

$$\frac{\partial W}{\partial \tau} = Ntu_m \left(w - w_{eq}\right) \tag{C.2}$$

$$\frac{\partial t}{\partial z} = Ntu_t \left(T - t\right) \tag{C.3}$$

$$\left.\frac{\partial I}{\partial T}\right|_W \frac{\partial T}{\partial \tau} = Ntu_m \left(\left.\frac{\partial i}{\partial w}\right|_t - \left.\frac{\partial I}{\partial W}\right|_T \right) \left(w - w_{eq}\right) + Ntu_t \left.\frac{\partial i}{\partial t}\right|_w \left(t - T\right) \tag{C.4}$$

The finite difference representations of the governing equations are as follows:

$$\frac{w_{i+1}^{n+1} - w_i^{n+1}}{\Delta z} = Ntu_m \left(w_{eq}{}_{i+1/2}^{n+1} - w_{i+1/2}^{n+1}\right) \tag{C.5}$$

$$\frac{W_{i+1}^{n+1} - W_{i+1}^{n}}{\Delta \tau} = Ntu_m \left(w_{i+1}^{n+1/2} - w_{eq}{}_{i+1}^{n+1/2}\right) \tag{C.6}$$

$$\frac{t_{i+1}^{n+1} - t_i^{n+1}}{\Delta z} = Ntu_t \left(T_{i+1/2}^{n+1} - t_{i+1/2}^{n+1}\right) \tag{C.7}$$

$$\begin{aligned} \left.\frac{\partial I}{\partial T}\right|_W \frac{T_{i+1}^{n+1} - T_{i+1}^{n}}{\Delta \tau} &= Ntu_m \left(\left.\frac{\partial i}{\partial w}\right|_t - \left.\frac{\partial I}{\partial W}\right|_T \right) \left(w_{i+1}^{n+1/2} - w_{eq}{}_{i+1}^{n+1/2}\right) \\ &\quad + Ntu_t \left.\frac{\partial i}{\partial t}\right|_w \left(t_{i+1}^{n+1/2} - T_{i+1}^{n+1/2}\right) \end{aligned} \tag{C.8}$$

where Ntu_t has been updated from the input value based on dry air specific heat to the moist air specific heat as follows

$$Ntu_t = Ntu_t^0 c_a / \left.\frac{\partial i}{\partial t}\right|_w \tag{C.9}$$

A first-order Taylor series expansion of the isotherm is used to linearize the above equations [Zheng, 1993].

$$dw_{eq} = \left.\frac{\partial w_{eq}}{\partial T}\right|_W dT + \left.\frac{\partial w_{eq}}{\partial W}\right|_T dW \tag{C.10}$$

or

$$w_{eq_{i+1}}^{n+1} = w_{eq_{i+1}}^{n} + \left.\frac{\partial w_{eq}}{\partial T}\right|_W \left(T_{i+1}^{n+1} - T_{i+1}^{n}\right) + \left.\frac{\partial w_{eq}}{\partial W}\right|_T \left(W_{i+1}^{n+1} - W_{i+1}^{n}\right) \tag{C.11}$$

Arranging all $n+1$ variables on the left hand side gives:

$$\begin{aligned}\left(1 + \frac{Ntu_m \Delta z}{2}\right) w_{i+1}^{n+1} - \frac{Ntu_m \Delta z}{2} \left.\frac{\partial w_{eq}}{\partial W}\right|_T W_{i+1}^{n+1} - \frac{Ntu_m \Delta z}{2} \left.\frac{\partial w_{eq}}{\partial T}\right|_W T_{i+1}^{n+1} \\ = \left(1 - \frac{Ntu_m \Delta z}{2}\right) w_i^{n+1} + \\ \frac{Ntu_m \Delta z}{2} \left(w_{eq_i}^{n+1} + w_{eq_{i+1}}^{n} - \left.\frac{\partial w_{eq}}{\partial T}\right|_W T_{i+1}^{n} - \left.\frac{\partial w_{eq}}{\partial W}\right|_T W_{i+1}^{n}\right)\end{aligned} \tag{C.12}$$

$$\begin{aligned}-\frac{Ntu_m \Delta \tau}{2} w_{i+1}^{n+1} + \left(1 + \frac{Ntu_m \Delta \tau}{2} \left.\frac{\partial w_{eq}}{\partial W}\right|_T\right) W_{i+1}^{n+1} + \frac{Ntu_m \Delta \tau}{2} \left.\frac{\partial w_{eq}}{\partial T}\right|_W T_{i+1}^{n+1} \\ = \left(1 + \frac{Ntu_m \Delta \tau}{2} \left.\frac{\partial w_{eq}}{\partial W}\right|_T\right) W_{i+1}^{n} + \\ \frac{Ntu_m \Delta \tau}{2} \left(w_{i+1}^{n} - 2 w_{eq_{i+1}}^{n} + \left.\frac{\partial w_{eq}}{\partial T}\right|_W T_{i+1}^{n}\right)\end{aligned} \tag{C.13}$$

$$\begin{aligned}\left(1 + \frac{Ntu_t \Delta z}{2}\right) t_{i+1}^{n+1} - \frac{Ntu_t \Delta z}{2} T_{i+1}^{n+1} = \\ \left(1 + \frac{Ntu_t \Delta z}{2}\right) t_i^{n+1} + \frac{Ntu_t \Delta z}{2} T_i^{n+1}\end{aligned} \tag{C.14}$$

$$
\begin{aligned}
&-\left(\left.\frac{\partial i}{\partial w}\right|_t - \left.\frac{\partial I}{\partial W}\right|_T\right)\frac{Ntu_m\Delta\tau}{2}w_{i+1}^{n+1} - \frac{Ntu_t\Delta\tau}{2}\left.\frac{\partial i}{\partial t}\right|_w t_{i+1}^{n+1} + \\
&\left(\left.\frac{\partial i}{\partial w}\right|_t - \left.\frac{\partial I}{\partial W}\right|_T\right)\frac{Ntu_m\Delta\tau}{2}\left.\frac{\partial w_{eq}}{\partial W}\right|_T W_{i+1}^{n+1} + \qquad \text{(C.15)} \\
&\left(\left.\frac{\partial I}{\partial T}\right|_W + \left(\left.\frac{\partial i}{\partial w}\right|_t - \left.\frac{\partial I}{\partial W}\right|_T\right)\frac{Ntu_m\Delta\tau}{2}\left.\frac{\partial w_{eq}}{\partial T}\right|_W + \frac{Ntu_t\Delta\tau}{2}\left.\frac{\partial i}{\partial t}\right|_w\right)T_{i+1}^{n+1} = \\
&\left(\left.\frac{\partial I}{\partial T}\right|_W + \frac{Ntu_m\Delta\tau}{2}\left.\frac{\partial w_{eq}}{\partial T}\right|_W - \frac{Ntu_t\Delta\tau}{2}\left.\frac{\partial i}{\partial t}\right|_w\right)T_{i+1}^{n} + \\
&\frac{Ntu_t\Delta\tau}{2}\left.\frac{\partial i}{\partial t}\right|_w t_{i+1}^{n} + \\
&\left(\left.\frac{\partial i}{\partial w}\right|_t - \left.\frac{\partial I}{\partial W}\right|_T\right)\frac{Ntu_m\Delta\tau}{2}\left(w_{i+1}^{n} - 2w_{eq}{}_{i+1}^{n} + \left.\frac{\partial w_{eq}}{\partial W}\right|_T W_{i+1}^{n}\right)
\end{aligned}
$$

Appendix D

Experimental Equipment List

Item	Description	Serial Number
Keithley 500A AMM1A AIM7	Measurement and Control Center 8 channels of single-ended analog input and 12-bit A/D 16 channel thermocouple input with isothermal block, noise reduction and cold junction reference sensor	526216
King Rotameter	Full Scale 20 scfm	*N/A*
Omega subminiature thermocouple probes	0.02 in sheath dia grounded Copper-Constantan thermocouple	TMQSS-020 G-6
Polyscience Refrigerated Recirculator	Model 575	913194
Solomat MPM 500e		222924
Staco Variable Autotransformer	Type 2PF-1010	*N/A*